# Riverbank protection removal to enhance bar formation for habitat diversity

Master of Science Thesis report

Anke Wetser

February 2017

TU Delft

Deltares
Enabling Delta Life

NUS National University of Singapore

Cover photo: Gravel bar in restored section after removal of bank protection, Thur river, Switzerland (Paillex et al., 2014)

*Boundaries don't protect rivers, people do.*

Brad Arrowsmith, Landowner along the Niobrara National Scenic River, Nebraska

# Riverbank protection removal to enhance bar formation for habitat diversity

by

Anke Wetser

Student number: 4159756

in partial fulfilment of the
requirements for the degree of

Master of Science
in Hydraulic Engineering and Water Resources Management

at

Delft University of Technology

and

National University of Singapore

To be defended on
February 6, 2017 at 9:00 AM in Delft, The Netherlands

| | | |
|---|---|---|
| Graduation committee: | Prof. dr. ir. W. S. J. Uijttewaal | Chairman, Delft University of Technology |
| | Dr. ir. E. Mosselman | Delft University of Technology / Deltares |
| | Dr. ir. R. J. Labeur | Delft University of Technology |
| | G. Duró, MSc | Delft University of Technology |
| | Dr. E. Penning | Deltares |
| | Dr. J. Yuan | National University of Singapore |

# Preface

Before you is the thesis 'Riverbank protection removal to enhance bar formation for habitat diversity.' The research for this thesis was carried out in cooperation with Deltares. This thesis was written as part of my graduation from the Double Degree Master in Hydraulic Engineering and Water Resources Management at the Delft University of Technology and the National University of Singapore. From June 2016 until February 2017 I have been engaged in the research and writing of the thesis report.

Together with my supervisor, dr. ir. E. Mosselman, I have figured out the research topic for this thesis. With my research, I wanted to give scientifically new insights and improve our environment. I came to a topic that combines hydraulic engineering and ecology. I think that it is important for proper river maintenance that these disciplines work closely together. My thesis committee mirrored this combination of disciplines.

First, I would like to thank my graduation committee for their wise input and good guidance. Professor dr. ir. W. S. J. Uijttewaal for keeping me on the right track, dr. ir. E. Mosselman for his excellent guidance and input, dr. E. Penning for her inspiring environmental discussions and dr. J. Juan and dr. ir. R. J. Labeur for supervision of my research. Special thanks go to my supervisor G. Duró, MSc for his intensive support, revisions of my work and Matlab lessons. My graduation committee helped me when necessary and gave me the freedom to define my own path within this research. The tips and comments during this research are greatly acknowledged.

Next, I want to thank my supervisors from Deltares, dr. ir. E. Mosselman and E. Penning, for offering me a work space and giving me the opportunity to work with Delft3D. Frank Platzek helped me intensively with improving a bank scour version of Delft3D for which I am very thankful. My colleagues and other graduation students at Deltares and the TU Delft provided a nice working environment and joyful events after work.

Furthermore, I also want to thank the employees of the Fluid Mechanics Laboratory at the Delft University of Technology. Their help with constructing the flume and laboratory work was crucial for successfully carrying out the laboratory experiments.

Last, I want to thank my boyfriend, family and friends for their unconditional support.

Anke Wetser

Delft, January 2017

# Abstract

Over the past centuries natural riverbanks have been transformed into banks with artificial revetments or sheet piles to protect them from erosion, which led to disappearance of important river features for flora and fauna. River restoration projects show that the removal of man-made bank protections may lead to the formation of bars (e.g. Van den Berghe et al., 2012; Schirmer et al., 2014). Habitat diversity in rivers may be enhanced through the formation of river bars with preferably diversity in bar height, size and location. This research aims at gaining knowledge into the effects of removing riverbank protections on bar formation to enhance habitat diversity.

Mobile-bed flume experiments were performed in the Fluid Mechanics Laboratory of Delft University of Technology. The experiments were focussed on bar formation related to three variables of a bank protection removal; length, location and flow asymmetry. Geometrical and morphodynamic characteristics were selected for the experiment having a bar mode of one to obtain a system with alternate bars (Crosato and Mosselman, 2009) and showed gravel-bed river similarity based on bankfull river characteristics of Parker (2004). The experimental flume consisted of a 6.2 metre long and 0.2 metre wide straight channel with 0.5 metre wide floodplains on the sides. On both sides of the channel, bank protection could be removed over a limited length with optionally a groyne upstream. After seven hours at the end of each test, photos of the bed topography were taken and the longitudinal bed profile was measured. Bar wavelengths and bar heights in each experimental test were determined from detrended bed profiles. The bar height was divided in two classes: low and high. The areas of low bars, high bars, floodplains and the deep channel were determined from photos of the final bed topographies. Bar types were indicated with terminology from Duró et al. (2015) as forced, free or hybrid.

Removal of bank protections resulted in lateral erosion of channel banks over a limited length. The eroded bank line moved in downstream direction, which agrees with the downstream meander migration observed in field and laboratory investigations by many authors (e.g. Odgaard, 1987). Scour holes developed downstream of the widened section, due to turbulent eddies forced by the channel geometry. In the widened reach, flow decelerated which resulted in a lower sediment transport. Consequently, sediment was deposited in the widened reach and caused rising of the mean bed level along with formation of bars. In areas with higher flow velocities an increased sediment transport deepened the channel.

When the riverbanks were fixed, relatively low, small, side bars were formed in the channel. In general, the total bar area and bar height increased for an increase in channel widening, due to the removal of bank protection. An increased bank protection removal length up to nine times the channel width or an upstream asymmetrical flow forcing, i.e. groyne, increased the total bar area, whereas a bank protection removal at three different locations with a total length of nine times the channel width did not significantly increased the total bar area.

It is recommended to remove riverbank protections over a length of at least nine times the river width on both sides of the river with optionally a groyne upstream as a measure to enhance habitat diversity. It is also valuable to remove the bank protection on one side of the river only. It is advised to construct a groyne upstream of the bank protection removal to increase habitat diversity. This research led to results that can be used in further research. It is advised to conduct larger scale experiments and eventually move to the field.

# Contents

Preface ..... i
Abstract ..... iii
Nomenclature ..... ix
1 Introduction ..... 1
1.1 Context ..... 1
1.2 Problem definition ..... 4
1.3 Objectives and research questions ..... 4
1.4 Scope ..... 4
1.5 Research methodology ..... 5
1.6 Thesis outline ..... 5
2 Theoretical background ..... 7
2.1 Spatial scales and river planform ..... 7
2.2 River bars ..... 8
2.2.1 Bar mode ..... 9
2.2.2 Bar wavelength and adaptation length ..... 10
2.3 Channel width adjustment ..... 11
2.3.1 Reach-scale river width variations ..... 11
2.3.2 The effect of river width variations on bars ..... 11
2.4 Bank erosion ..... 12
2.4.1 Erosion mechanisms ..... 13
2.4.2 Effects of bank erosion ..... 13
2.5 Consequences of removing riverbank protection ..... 15
3 Research methodology ..... 17
3.1 Experimental conditions ..... 17
3.1.1 Simplified experimental conditions ..... 19
3.2 Experimental setup ..... 20
3.2.1 Preliminary phase ..... 23
3.3 Experimental tests ..... 24
3.3.1 Fixed banks ..... 25
3.3.2 Length of bank protection removal ..... 25
3.3.3 Location of bank protection removal ..... 25

3.3.4 Asymmetrical flow forcing ... 25
3.3.5 Channel bank cohesion ... 25
3.3.6 Bank protection shape ... 26
3.4 Data collection ... 27
3.4.1 Hydraulic parameters ... 28
4 Results ... 30
4.1 General experimental observations ... 30
4.2 Lateral erosion ... 32
4.2.1 Spatial evolution ... 32
4.2.2 Temporal evolution ... 35
4.3 Mean bed level ... 37
4.4 Scour hole ... 38
4.4.1 Perpendicular bank protection ... 38
4.4.2 Curved bank protection ... 39
4.5 Bar formation ... 39
4.5.1 Fixed banks ... 40
4.5.2 Length of bank protection removal ... 42
4.5.3 Location of bank protection removal ... 45
4.5.4 Asymmetrical flow forcing ... 46
4.5.5 Channel bank cohesion ... 48
4.5.6 Bank protection shape ... 49
4.5.7 Channel widening related to bar formation ... 50
5 Discussion ... 53
5.1 Context of research ... 53
5.1.1 Meaning of research ... 53
5.1.2 Research related to present literature ... 53
5.1.3 Spatial and temporal scale ... 54
5.2 Interpretation of results ... 55
5.3 Example design of bank protection removal ... 57
5.3.1 Objectives ... 58
5.3.2 Considerations ... 58
5.3.3 Choice of design ... 59
6 Conclusions and recommendations ... 60

6.1 Conclusions ..... 60
6.2 Recommendations ..... 61
6.2.1 Recommendations to river restoration practice ..... 61
6.2.2 Recommendations for further research ..... 61
References ..... 64
List of figures ..... 70
List of tables ..... 75
Appendices ..... 76
Appendix A. Numerical modelling ..... 76
A.1. Numerical modelling in Delft3D ..... 76
A.2. Bank erosion in Delft3D-FLOW ..... 76
A.3. New approach of bank erosion in Delft3D-FLOW ..... 76
A.4. Scaling of flume experiment ..... 77
A.5. Setup numerical model ..... 78
A.6. Results ..... 79
A.7. Discussion ..... 80
A.8. Conclusions and recommendations ..... 81
Appendix B. Gravel-bed river similarity ..... 85
Appendix C. Widely graded sediment ..... 90
Appendix D. Setup experimental tests ..... 92
Appendix E. Bar formation in laboratory experiment ..... 94
Appendix F. Bar area quantification methods ..... 105
F.1. Bed topography ..... 105
F.2. Bed profile ..... 107
F.3. Comparison methods ..... 108
Appendix G. Bank erosion in laboratory experiment ..... 111
Appendix H. Photos of experimental setup ..... 117
H.1. Photos of experimental setup ..... 117
H.2. Photos of data collection in experiment ..... 126

# Nomenclature

| Symbol | Name | Unit |
|---|---|---|
| $b$ | Degree of nonlinearity of sediment transport versus depth-averaged flow velocity | - |
| $B$ | River width | m |
| $\hat{B}$ | Dimensionless river width | - |
| $B_{bf}$ | Bankfull river width | m |
| $C$ | Chézy coefficient | $m^{1/2}/s$ |
| $C_{bf}$ | Bankfull Chézy coefficient | $m^{1/2}/s$ |
| $D_{50}$ | Median sediment grain size | m |
| $E$ | Calibration coefficient for gravity effects on sediment transport direction over transverse bed slopes | - |
| $E$ | Lateral erosion rate | m/s |
| $Fr$ | Froude number | - |
| $f(\theta)$ | Function for gravity effects on sediment transport direction over transverse bed slopes | - |
| $g$ | Gravitational acceleration | $m/s^2$ |
| $h$ | Water depth | m |
| $h_0$ | Reach-averaged water depth | m |
| $\hat{H}$ | Dimensionless water depth | - |
| $h_{bf}$ | Bankfull water depth | |
| $i$ | Longitudinal gradient | - |
| $k$ | Erodibility coefficient | m/s |
| $L_p$ | Streamwise bar wavelength | m |
| $m$ | Number of bars in a cross-section | - |
| $\hat{Q}$ | Dimensionless discharge | - |
| $Q_{bf}$ | Bankfull discharge | $m^3/s$ |
| $Q_w$ | Water discharge | $m^3/s$ |
| $q_{s0}$ | Reach-averaged sediment transport per unit of river width | $m^2/s$ |
| $Re^*$ | Reynolds particle number | - |
| $S_0$ | Sediment transport rate | $m^3/s$ |
| $u$ | Flow velocity | m/s |
| $u_0$ | Reach-averaged flow velocity | m/s |
| $u_b$ | Flow velocity along the bank line | m/s |
| $u^*$ | Shear velocity | m/s |
| $w_s$ | Fall velocity | m/s |
| $\lambda_s$ | Streamwise adaptation length of cross-sectional bed topography | m |
| $\lambda_w$ | streamwise adaptation length of transverse distribution of streamwise flow velocity | m |
| $\mu$ | Ripple factor | - |
| $\theta$ | Shields parameter | - |
| $\theta_c$ | Critical Shields parameter | - |
| $\theta_0$ | Reach-averaged Shields parameter | - |
| $\Delta$ | Relative sediment density under water | - |
| $\nu$ | Kinematic viscosity | $m^2/s$ |
| $\tau$ | Shear stress | $N/m^2$ |

| | | |
|---|---|---|
| $\tau_c$ | Critical shear stress for entrainment | $N/m^2$ |
| $\tau_{bf}^*$ | Estimate of bankfull Shields number | - |
| $\rho$ | Mass density | $kg/m^3$ |
| $\rho_w$ | Mass density of water | $kg/m^3$ |

# 1 Introduction

## 1.1 Context

Over the past centuries the main channel of many rivers has been restricted for the purpose of navigation, flood protection, water supply, hydroelectricity and landscape development. Natural riverbanks have been transformed into banks with artificial revetments or sheet piles to protect them from erosion. Construction of bank protections resulted in reduction of the dynamics of the river system. Important river features for flora and fauna disappeared and the ecological quality of the river reduced dramatically.

Recently, the importance of the ecological function of rivers has been getting more attention. River restoration is the common term to indicate projects that are aimed at returning river systems closer to their natural state and functioning in support of biodiversity, recreation, flood safety and landscape development (ECRR, 2016). One river restoration measure is the removal of man-made bank protections to increase habitat diversity and biodiversity of riparian areas and the river basin. The river morphology may be changed due to the freely eroding banks in the restored section. Reference projects for the removal of the riverbank protection show that the removal of riverbank protection in rivers may lead to the formation of bars (e.g. Van den Berghe et al., 2012; Schirmer et al., 2014). Bars increase morphological diversity, providing specific habitats for flora and fauna (Kurth and Shirmer, 2014; Kail et al., 2014). Januschke et al. (2011) emphasised that pioneers of plant species benefit strongly from re-establishment of open sand and gravel bars. They concluded that restoring river hydromorphology will almost generally increase riparian habitats and biodiversity.

Crosato and Mosselman (2009) explained this phenomenon by considering that the ecological river condition depends partly on the morphological state. Important quantitative indicators of the river morphological state are the number of bars in a cross-section, their position either near the banks or in the middle of the channel and their extension (Toffolon and Crosato, 2007). It can be concluded that the bar wavelength, area, location and number in a river cross-section give an indication of the ecological rivers condition.

*Figure 1.1 - Degraded section of the Thur river (left) and restored section (right) after removal of bank protection in 2002 (Paillex et al., 2014)*

Penning (2016) says that the aim for a certain bar wavelength, area, location and number in a river cross-section in a restoration project is dependent on the river and the species one wants to return. When it comes to the ecological river condition, diversity is most important. For each species the need for a specific habitat is different. Some species are more valuable in terms of ecological value, e.g. rare species or key stone species. For example, when specific fish species are reintroduced, they may attract fish-eating birds. Fish need spawning habitats, like riffle-pool sequences which can be reintroduced by the formation of bars. These spawning habitats can be located far from each other, in the order of hundreds of kilometres, depending on the species. While habitats for fish cover hundred kilometres of stretch, habitats for macroinvertebrate are in the order of several metres.

The bar location, either on the side or in the middle of a river, is a factor that may influence habitat- and biodiversity. The bar location is more important in wide rivers, since mid-channel bars become more isolated in wide rivers. Especially for non-flying, non-swimming, terrestrial fauna and vegetation with low dispersal capabilities, mid-channel bars can be hard to reach. These species have more change to settle near the main land, i.e. on a side bar. Insects and birds can fly to mid-channel bars, thus can establish both on side or mid-channel bars. Seeds of plants may be taken by the wind or flow and are therefore able to reach mid-channel bars. For example, poplar seeds are taken with the flow when a flood occurs and are deposited on a bar around the flood line. When the water level decreases after the flood, some seeds may have enough water available to germinate and grow. These poplar trees may trap other seeds that can establish on the bar.

It usually takes approximately three years before a river bar is covered with vegetation. The bar may be flooded within these three years and the flow force may remove the established vegetation. Low bar areas will be flooded more frequently than high bar areas. Figure 1.2 shows a schematic cross-section of a river bar in which different elevations indicate specific habitats. A deep bar zone is always submerged, the intermediate zone is usually wet and only dry in dry summers, the shallow zone is usually dry and only wet when a flood occurs and the high zone is always dry. The shallow and intermediate zones are the most important zones of a bar to increase habitat diversity, since the deep zone is always there and the high zone has the same habitat as the riverbanks. The shallow and intermediate zones have a high dynamic ecosystem with pioneer vegetation, whereas the high bar zone has a low dynamic ecosystem where in the final stage forest will develop. A combination of both low and high bar areas is needed to enhance habitat diversity and thus biodiversity.

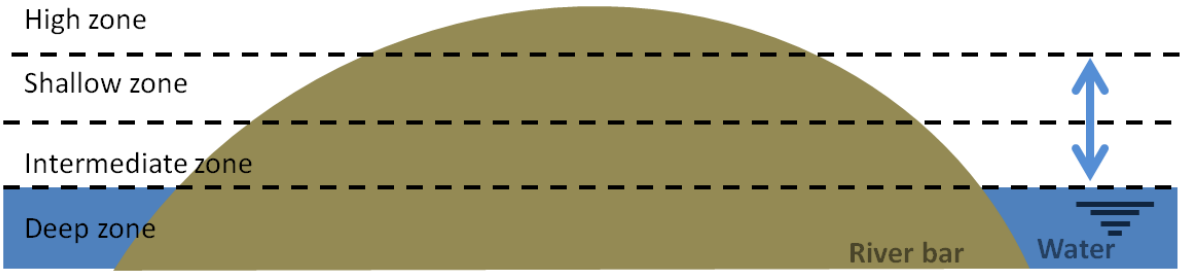


*Figure 1.2 – Cross-section of river bar. The high zone, shallow zone, deep zone and intermediate zone indicate different habitats of a bar.*

An example of a restoration project is the formerly braided Thur River in Switzerland that was channelized in the 1890s to protect the river valley against flooding (Schirmer et al., 2014). Since 1993, riverbank protection was removed at several 1 to 3 km long river sections. Freely eroding banks resulted in channel widening and formation of alternate gravel bars (Figure 1.1). The bars were first colonized by pioneer vegetation. Bird species which require gravel bars for nesting, returned to the restored Thur River reach after more than 100 years of absence. Furthermore, species richness of plants and soil organisms was higher in the restored section than in the channelized section upstream. Figure 1.3 shows the formation of alternating gravel bars in a restored section of the Thur river. The uncontrolled bank erosion resulted in large morphological changes and a large point bar as portrayed in Figure 1.3 gradually evolved. As bank line movement could create conflicts with land-owners and agricultural land use, further questions rise about ecosystem services and predictability of restoration-induced effects.

Human activities are performed in the areas along the riverbanks, such as agriculture and living. The length of removing riverbank protection and the channel widening is therefore usually limited. Furthermore, investment costs of a river restoration measure decrease for shorter lengths of removed riverbank protection. It is assumed that formation of bars is related to the length of the removal of bank protection and the widening due to the removal of bank protection. Therefore, guidance is needed for the design of riverbank protection removal to enhance bar formation for habitat diversity to make this a feasible river restoration method.

*Figure 1.3 - Restored section 'Schaffauli' of Thur river in 2009 (left) and 2012 (right) (Google Earth, 2015).*

## 1.2 Problem definition

Removing bank protections to develop river bars as a river restoration method is in its early stages. Only a laboratory experiment of Veldt (2015) can be found that scientifically explores the effects on the river bed topography of modifying a fixed river reach into a reach where the banks can erode freely for a limited reach. There is a lack of knowledge about the formation of bars related to the length and location of the removal of bank protection. Furthermore, guidance for river restoration practisers on the design of a bank protection removal to enhance bar formation for habitat diversity in rivers is not available. It is important to gain more knowledge about bar formation due to the removal of riverbank protection to promote this river restoration technique.

## 1.3 Objectives and research questions

This research aims at gaining knowledge with a scientific basis for the proper design of riverbank protection removal to enhance habitat diversity through bar formation. In addition, this research intends to contribute to the understanding of mechanisms that cause bar formation triggered by bank protection removal.

The main research question is defined as:

- What is the effect of removing riverbank protection on bar formation as a measure to enhance habitat diversity?

The main question is divided in sub questions. The sub questions addressed by this study are the following:

- What mechanisms contribute to the formation of bars when a limited length of bank protection is removed?
- What is the relation between the length and location of bank protection removal and the formation of bars?
- What is the effect of an asymmetrical flow forcing upstream of a bank protection removal on bar formation?

## 1.4 Scope

River restoration projects may be aimed at restoring river systems to their natural state and functioning in support of biodiversity, recreation, flood safety and landscape development (ECRR, 2016). This research focuses on restoring river systems to support the river ecological system from a morphological perspective. Restoring river systems may, however, involve changes in multiple riverine functionalities and not just affect the river ecological system. The river restoration measure discussed in this research, namely the removal of bank protection, may affect other riverine functions than the ecological system, such as navigation, flood management, recreation, agriculture, landscape development, hydropower, water supply, etc. These riverine functions are outside the scope of this research.

In the present study, river morphological changes due to the removal of bank protection are of interest. More specifically this research focuses on changes in river bedforms with cross-sectional scale, i.e. river bar development. Smaller bedforms, such as ripples and dunes, are not taken into direct consideration. These smaller scale bedforms have an effect on the bed roughness, thus they are taken into consideration indirectly, but not from an ecological perspective.

## 1.5 Research methodology

The research methodology includes a laboratory experiment that is carried out in the Fluid Mechanics Laboratory of Delft University of Technology. A small scale experiment has been conducted in a flume of 7 metres long and 1.2 metres wide to gain insight in the hydromorphological effects of removing riverbank protections. Small scale laboratory experiments have the advantage of fast evolution, so different experimental setups can be tested. In laboratory experiments it is possible to record and witness hydromorphological conditions and to control initial and boundary conditions. The experiment is focussed on the relation between the length of bank protection removal and the formation of bars. The bank protections of the channel banks are removed with a length of zero, three, six, nine and ten times the channel width on either one or both sides. Furthermore, the experiment is aimed at finding geometrical changes in the setup that lead to a change in bar formation. The bank protection is removed at different locations along the channel side or with an asymmetrical flow forcing upstream of the bank protection removal. In all experiments, the number, location and size of bars are measured, since these give an indication of the ecological river condition.

Numerical modelling is a research methodology that may be used to predict hydromorphological effects of riverbank protection removal. The modelling software Delft3D can be used to investigate hydrodynamics, sediment transport and morphology in rivers (Deltares, 2016a). The FLOW module of Delft3D is a multidimensional (2D or 3D) hydrodynamic and transport simulation programme. Currently, Delft3D-FLOW includes lateral erosion with a very simplistic method and is therefore mainly suited in studies with fixed riverbanks. In this research, however, due to removal of riverbank protection the banks are not fixed and may erode. Canestrelli (2016) developed a new approach to reproduce movable banks in Delft3D-FLOW, in a way that the hydraulic geometry of a channel can then be varied both vertically and laterally. This research included further development of the new approach of bank erosion in Delft3D-FLOW and modelling of an upscaled version of the laboratory experiment in this software. The flume experiment is upscaled to a natural river size and modelled in the new approach of bank erosion in Delft3D-FLOW. No conclusions for this research can be drawn from this numerical model, since the model is still in its initial stages. The numerical modelling section is therefore not included in the main report, but is reported in Appendix A.

## 1.6 Thesis outline

The structure of the report is described to guide readers through this report.

In Chapter 2, a theoretical background is given. The aim of this theoretical background is to discuss morphological consequences of removal of bank protection. First, spatial scales and river planform are considered to understand to what category river bars belong in a broader hydromorphodynamic context. Second, river bar types, bar mode and bar wavelength are discussed to gain a better understanding of bars. Third, an explanation of reach-scale river width variations and their effect on bars is given, which might be a result of the bank protection removal. Fourth, bank erosion mechanisms and effects of bank erosion are presented, since the banks can erode freely due to the removal of bank protections. The chapter concludes with an overview of the morphological consequences of removal of bank protection.

Chapter 3 describes the methodology that is used to conduct the research. Laboratory experiments have been carried out in the Fluid Mechanics Laboratory of Delft University of Technology. Systematically, this chapter gives a description of the experimental conditions, experimental setup, experimental tests and data collection. First, the choice of the experimental conditions and what they imply is explained. Second, a description of the general experimental

setup is given and it is explained why this setup is chosen. Third, the choice for the different experimental tests and their setup are given. Finally, the chapter concludes with the data collection of the experiment.

In Chapter 4, results of the laboratory experiments are presented. This chapter starts with describing experimental observations that could be generalised for all tests in order to provide an overview of the main processes that occurred during the tests. Afterwards, this chapter is subdivided in bar formation, lateral erosion and scour hole formation, since these are the main morphological processes due to the removal of bank protections.

In Chapter 5 the discussion is presented. The context of this researchis given and interpretation of the results are discussed. Furthermore, an example design of a bank protection removal is given to put the results into perspective.

Chapter 6 gives the conclusion and recommendations of this research. The conclusion provides an answer to the research questions based on the results from the experiment. In the recommendations an advice is given on how to make a proper design for the removal of bank protections on bar formation as a measure to enhance habitat diversity. Furthermore, recommendations are given for further research.

Finally, the references and appendices conclude this report.

# 2 Theoretical background

## 2.1 Spatial scales and river planform

River morphodynamics deals with the shape of the river bed that can be divided into different spatial scales (Wright and Crosato, 2011). In decreasing order the spatial scales are basin scale, reach scale, corridor scale, cross-section scale, depth scale and process scale. At the largest spatial scale, the entire river basin or single sub-basins are considered. Zooming in on the river system, each river reach is characterised by planform style and sinuosity. Human interventions, such as river training, and natural evolution of the river on the long term, such as bed aggradation and degradation, planform changes and sinuosity changes, pertain to reach scale morphodynamics. Generally, river planforms are classified as either meandering or braiding. A meandering river is usually referred to as a planform of repeated bends which create a large sinuosity of the river channel, whereas braided rivers have little sinuosity and a mainly straight channel (Friend and Sinha, 1993). Meandering rivers have point bars and a single channel, whereas braided river have mid-channel or central bars and multiple channels in a cross-section. In between these two planforms a transitional stage with both point and central bars characterizes the river. Figure 2 shows images of these river planforms: meandering river, transitional stage and braiding river.

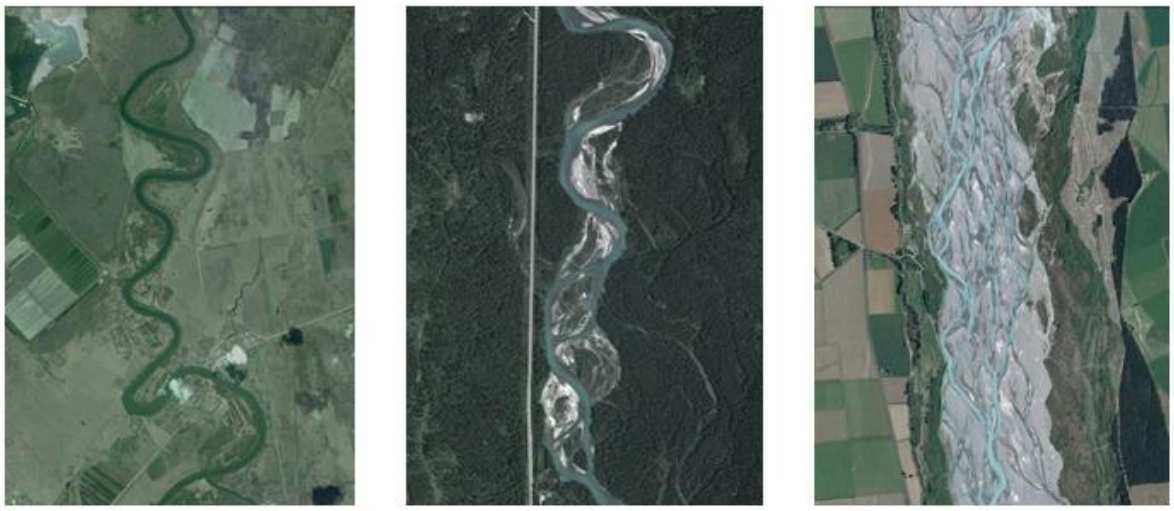

*Figure 2.1 – River planform stages (from left to right): meandering Cauto River in Cuba, transitional Fraser River in Canada and braiding Waimakariri River in New Zealand (Google Earth, 2015)*

Zooming in further on the river, the area including main river channel and floodplains, with recognizable morphological features such as point bars, pertains to the corridor scale. At a cross-section scale, central and multiple bars are the characteristic geomorphological features to be studied. Effects of human interventions or natural developments at cross-section scale are bar formation, bar migration, channel widening and narrowing. Depth-scale studies move from observation above the river to observation inside the river and deal with local deposits and scours, dunes, bank erosion and bank accretion. At the smallest spatial scale, processes such as entrainment and deposition of sediment grains play a role and ripples are the typical geomorphological forms to be studied.

Temporal and spatial scales are strongly linked in morphodynamics and the link is formed by sediment transport. For larger geomorphological forms, larger amounts of sediment need to be displaced. Phenomena interact dynamically when they occur on the same scale, but can appear as noise or produce residual effects on larger scales. Small-scale phenomena, such as ripples, can appear as noise in the interactions with phenomena on larger scales, such as bar migration, but they can also change the bed roughness.

## 2.2 River bars

Bars in rivers are large sediment deposits of which the length scales with the channel width and the height with the water depth (Duró et al., 2015). The width-to-depth ratio of the river is an important parameter for the development of bars. When a river is deep and narrow, having a small width-to-depth ratio, there is usually no formation of bars (Struiksma et al., 1985). One bar is developed in a cross-section for small with-to-depth ratios and multiple bars are developed in the river cross-section for large width-to-depth ratios (Crosato and Mosselman, 2009).

Bars can propagate in longitudinal direction of the river, i.e. migrating, or bar are fixed at a certain location along the river axis, i.e. non-migrating. Non-migrating bars are usually longer than migrating bars (Eekhout et al, 2013). Non-migrating bars present wavelengths that are two to three times larger than the most commonly observed migrating bars (Olesen, 1983).

According to stability analyses of bars in the 1970s and 1980s (e.g. Parker, 1976; Fredsøe, 1978; Struiksma et al., 1985; Blondeaux and Seminara, 1985; Colombini et al., 1987; Tubino et al., 1999) there are two types of bars: free bars and forced bars (e.g. Seminara, 1988). Duró et al. (2015) defined a new terminology that describes both the appearance and the mechanism of formation and growth of bars. They defined three types of bars: forced bars, free bars and hybrid bars. Each of these bar types belong to the appearance category of either local or periodic bars. A local bar is one single bar and periodic bars are recurring.

Local bars are defined as sediment deposits forced by a permanent finite deformation of the water flow, e.g. caused by a natural bend, a channel width variation or a structure. Forced bars belong to this category and are non-migrating.

Periodic bars are defined as sediment deposits with a formation that depends on morphodynamic instability. They only arise if the system is in the morphodynamic instability range. Free bars fall into this category and arise within the morphodynamic instability range of the system when an infinitesimally small perturbation of the flow or bed level is present. Free bars are usually migrating.

Hybrid bars also belong to the category of periodic bars and arise from morphodynamic instability and the presence of forcing (Duró et al., 2015). They are non-migrating and usually take longer than free bars to grow to their final amplitude. The term “hybrid” expresses that these bars have both free and forced aspects, since they require a certain forcing and morphodynamic instability.

*Table 2.1 – Definition of bars according to the new terminology of Duró et al. (2015)*

| Bar type | Appearance | Mechanism |
|---|---|---|
| Forced | Local | Permanent forcing |
| Free | Periodic | Morphodynamic instability |
| Hybrid | Periodic | Permanent forcing + morphodynamic instability |

### 2.2.1 Bar mode

Crosato and Mosselman (2009) defined a physics-based predictor that estimates the number of hybrid bars in a river cross-section, i.e. bar mode m. A bar mode equal to one indicates alternate bars, a bar mode equal to two indicates central bars and larger bar modes indicate multiple bars (Figure 2.2). Furthermore, the number of bars in a cross-section indicates the river planform by assuming that meandering is characterized by at most one bar per cross-section ($m \leq 1.5$), braiding by at least two bars per cross-section ($m \geq 2.5$) and a transitional stage in between those planforms ($1.5 < m < 2.5$).

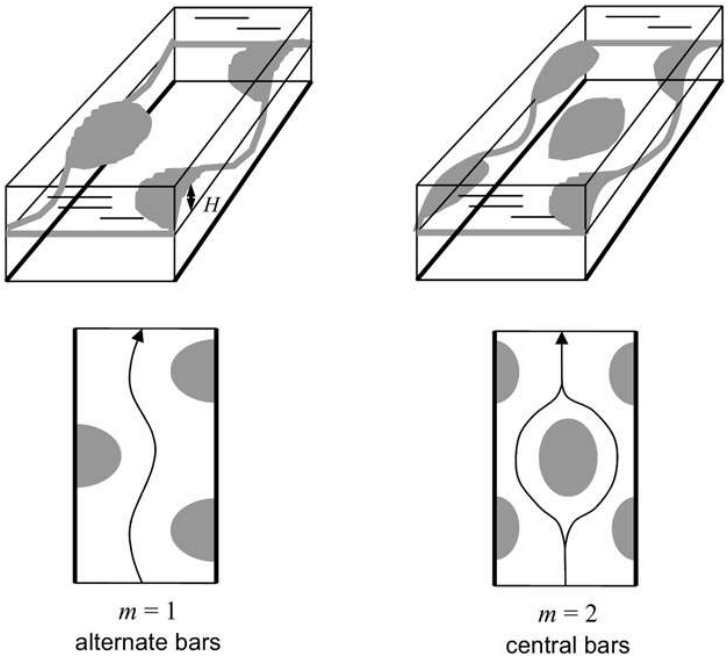


*Figure 2.2 – Bars located in straight channel: (left) first bar mode (alternate bars) and (right) second bar mode (central bars) (Crosato and Mosselman, 2009).*

The theory behind the physics-based predictor for river bars is a second-order linear model for hydrid bars derived by Struiksma et al (1985). A simplified version, valid for uniform flow conditions, is defined as (Crosato and Mosselman, 2009):

$$m^2 = 0.17g \frac{(b-3)}{\sqrt{\Delta D_{50}}} \frac{B^3 i}{C Q_w} \tag{1}$$

where the nearest integer of bar mode m relates to the most probable number of hybrid bars per cross-section. The parameters in equation (1) are defined as river width $B$, Chézy coefficient $C$, longitudinal gradient $i$, median sediment grain size $D_{50}$, gravitational acceleration $g$, relative sediment density under water $\Delta$, degree of nonlinearity of sediment transport versus depth-averaged flow velocity $b$ and water discharge $Q_w$. A value of $b = 4$ is assumed for sand bed rivers and $b = 10$ for gravel bed rivers (Crosato and Mosselman, 2009). At experimental scale, however, sediment mobility will be lower due to downscaling and the assumed values for sand and gravel bed river do not hold. The degree of nonlinearity of sediment transport versus depth-averaged flow velocity $b$ can be calculated with:

$$b = \frac{u_0}{q_{s0}} \frac{dq_{s0}}{du_0} \tag{2}$$

where the parameters are defined as reach-averaged flow velocity $u_0$ and reach-averaged sediment transport per unit of river width $q_{s0}$.

Substituting the sediment transport formula of Meyer-Peter-Müller (1948) into equation (2) gives the expression:

$$b = \frac{3}{1 - \frac{\theta_c}{\mu\theta}} \tag{3}$$

In which the parameters are defined as Shields parameter $\theta$, critical Shields parameter $\theta_c$ and ripple factor $\mu$.

Important indicators in this predictor are the width-to-depth ratio, longitudinal slope, bed roughness and sediment characteristics at bankfull conditions. Bankfull conditions are used, because in most rivers the largest amounts of sediments are transported during the highest flows. During low-flows the transport rates are much lower than during high-flows. Reaching the morphological final stage during low-flow conditions may take a long period. Within this period, usually a high-flow has already occurred and therefore these bankfull conditions are decisive.

### 2.2.2 Bar wavelength and adaptation length

The length of a bar can be indicated with the streamwise wavelength. Struiksma et al. (1985) derived a formula for the streamwise wavelength $L_p$ of non-migrating bars:

$$\frac{2\pi}{L_p} = \frac{1}{2\lambda_w} \left( (b+1) \frac{\lambda_w}{\lambda_s} - \left( \frac{\lambda_w}{\lambda_s} \right)^2 - \frac{(b-3)^2}{4} \right)^{\frac{1}{2}} \tag{4}$$

In which $\lambda_s$ = adaptation length of the bed topography development; $\lambda_w$ = adaptation length of the main flow:

$$\lambda_w = \frac{hC^2}{2g} \tag{5}$$

$$\lambda_s = \frac{1}{\pi^2} h \left( \frac{B}{h} \right)^2 f(\theta_0) \tag{6}$$

where parameter $h$ is the reach-averaged water depth and the function for gravity effects on sediment transport direction over transverse bed slopes is defined as:

$$f(\theta_0) = \frac{0.85}{E} \sqrt{\theta_0} \tag{7}$$

where $E$ = calibration coefficient having values between 0.5 and 1.0; $\theta_0$ = reach-averaged value of the Shields parameter.

The adaptation length of alternate or central bars in narrowed or widened channel reach can be observed in the model results of Duró et al. (2015). For most simulations, central bars are formed immediately at the start of the widened reach. For example, a simulation showing the final development stage is characterized by fading non-migrating central bars in the upper part and slowly migrating alternate bars in the lower part, starting at a location of approximately 40 times the width of the widened reach.

## 2.3 Channel width adjustment

Fluvial erosion, fluvial deposition and mass bank failure are the fundamental processes responsible for channel width adjustment (Thorne et al., 1998). Thorne et al. (1998) described the following seven topics concerned with the mechanisms of bank line movement: bank erosion, weakening of resistance to erosion, bank stability with respect to mass failure, basal endpoint control, effects of vegetation, seepage effects and bank advance. In this section the morphological effects of channel width adjustments are discussed.

### 2.3.1 Reach-scale river width variations

The long-term reach-scale response of rivers to channel width variations can be assessed through the theory of reach-scale equilibrium described in e.g. Jansen et al. (1979) and De Vries (1975). The short and long term effects on bed aggradation and degradation processes of widening of the main channel due to bank erosion are shown in Figure 2.3 (Van der Mark et al., 2012).

The effects of spatial variations of river width on bed aggradation and degradation processes were analysed by Siviglia et al. (2008) using a 1D numerical model. Results show that a single channel expansion resulted in bed aggradation both in the upstream and downstream channels. For higher Froude numbers (near critical/super-critical conditions), deposition in the upstream channel occurs faster and attains higher values (Siviglia et al., 2008). The depositional phenomenon is more intense when the difference between the upstream and downstream channels is larger.

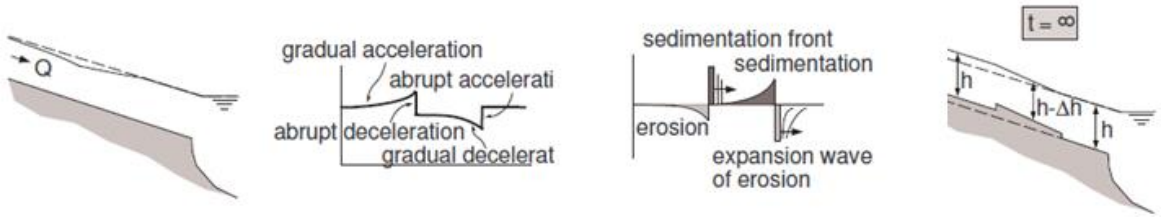


*Figure 2.3 – Morphological response on the short and long term due to widening of the main channel due to bank erosion (Van der Mark et al., 2012)*

### 2.3.2 The effect of river width variations on bars

There are several works analysing morphodynamic effects of spatial river width variations analytically (e.g. Luchi et al., 2011; Zolezzi et al., 2012; Frascati and Lanzoni, 2013), numerically (Eke et al., 2014; Duró et al., 2015; Siviglia et al., 2008; Luchi et al., 2010), experimentally (Repetto et al., 2002; Wu and Yeh, 2005) or with field observations (Hooke, 1986; Knighton, 1972; Luchi et al., 2010a).

Repetto et al. (2002) and Wu and Yeh (2005) theoretically demonstrated and experimentally verified the importance of width variations for the development of mid-channel bars in a straight channel configuration. This relation between the bedform dynamics and

channel width variation was also observed through a field survey for a reach of the River Bollin in NW England (Luchi et al., 2010a). Frascati and Lanzoni (2013) developed an analytical model that described this process of central bars induced by width variations. Crosato and Mosselman (2009) stated that river widening may usually lead to the formation of bars, while river narrowing usually results in their disappearance. Field observations of Knighton (1972) and Hooke (1986) give strength to the concept that cross-sectional widening is an important mechanism responsible for the presence and development of mid-channel bars.

Central bars tend to divert the flow against two banks, which may be a cause of cross-sectional widening and give rise to a mutual feedback mechanism that characterizes interactions between mid-channel bars and width variations in river meanders (Luchi et al., 2010, Zolezzi et al., 2012, Klaassen et al. 1993). Zolezzi et al. (2012) suggest that in meanders with initially constant width, curvature nonlinearly forces mid-channel bar growth, enhancing bank erosion downstream and possibly triggering width oscillations.

Duró et al. (2015) addressed effects of relatively large channel widening and narrowing of infinite length on the formation of periodic bars. They modelled a case where upstream of the widening no bars were present and in the widened reach regular central bars were formed. The first bar showed a more complex geometry than the following bars, which Duró et al. (2015) related to the imposed channel geometry at the widened area (local geometrical forcing). Several channel reaches with a widening were modelled and the results showed that the location where bars form and their final shape depend on the symmetry-asymmetry of the inflow with respect to the symmetric-asymmetric character of the bars. For example, regular central bars appeared only at the initial stages of the river bed development if starting from a flat bed or close to a symmetric flow forcing. Based on the bar mode expression of Crosato and Mosselman (2009), certain geometric and flow conditions of the widened reach were chosen by Duró et al. (2015) that predicted the formation of alternate or central bars. Duró et al. (2015) concluded that narrowing the river width for a distance equal to 10 times the river width may be sufficient to free an area from bars equal to two to three times the original channel width.

Duró et al (2015) explain how relatively large narrowing and widening cause the long-term reach-scale river parameters to adapt to the new width to get to a morphodynamic equilibrium. The bed level and water level will gradually adjust and therefore the width-to-depth ratio changes during the adaptation period. The bar mode is affected by this change in width-to-depth ratio in the narrowed or widened river reach. The bar mode just after the intervention may therefore be different from the bar mode after a long time. For example, Parker et al. (1976) observed that aggradation can lead a meandering river planform to become a braided planform.

Hunzinger (1998) investigated morphological effects of a local widening of the river bed of finite length by means of laboratory experiments and numerical simulations. He performed experiments in a flume of 25 metre long and constant discharge and varied the dimensions of the widening. Hunzinger (1998) found that if the length of the widened reach is chosen too short, the flow cannot expand to the total width and no braiding will occur.

## 2.4 Bank erosion

Riverbank erosion is a complex phenomenon, since it can result from a variety of mechanisms in which many factors can play a role. Bank erosion can result from flow and sediment transport, but also from processes beyond the basic system of river morphology (Mosselman, 1998). Banks erode mainly by either the entrainment of individual particles, i.e. fluvial erosion, or mass failures (Mosselman, 1989).

### 2.4.1 Erosion mechanisms

Two main erosion processes will be discussed in this section: fluvial erosion and mass failure.

*Fluvial erosion*

Fluvial erosion is the removal of bank sediments by the direct action of the flow. Water flowing in an alluvial channel exerts drag and lift forces on the boundaries that may detach and entrain grain particles (Thorne et al., 1998; Mosselman, 1989). The boundary sediment must be able to supply an internally derived force that can resist the erosive forces applied by the flow to remain in place. These resisting forces are determined by the bank material.

Non-cohesive bank material is usually detached and entrained grain by grain through fluvial erosion, whereas cohesive bank material is usually eroded by the entrainment of aggregates or crumbs (Thorne and Osman, 1988). For non-cohesive soils, resistance to entrainment depends on inter-particle forces due to friction and interlocking, whereas for cohesive soils physo-chemical properties of the soil, pore and eroding fluids tend to be more decisive (Thorne and Osman, 1988; Mosselman, 1989). Erosion rates are generally lower for cohesive banks than for non-cohesive banks, since critical boundary shear stresses tend to be higher for cohesive bank materials (Thorne et al., 1998; Thorne and Osman, 1988). Another limiting property of fluvial bank erosion is vegetation (Thorne and Osman, 1988). Vegetation may reduce the shear stresses on the soil by protecting the soil surface directly and also the roots and rhizomes of plants reinforce the soil and introduce extra cohesion (Weaver, 1976).

*Mass failure*

Mass failure is the collapse and movement of bank material under the action of gravity (Rinaldi and Nardi, 2013). Mass failures generally result from bank destabilization due to a combination of weakening factors and a variety of erosion processes (Lawler et al., 1997). According to Thorne and Osman (1988) instability of cohesive banks is most commonly caused by two processes: bed degradation and lateral erosion. They describe that when the channel bed is widened due to lateral erosion, whereby the banks are steepened, its stability is reduced. Bed degradation increases the bank height, which also decreases the bank stability (Osman and Thorne, 1988). Rinaldi and Nardi (2013) mentioned that interacting processes of soil hydrology, seepage erosion, and fluvial erosion can result in mass failure.

Fluvial erosion may result in mass failure when the bank slope is increased, which promotes the occurrence of slides or other types of mechanisms (Rinaldi and Nardi, 2013; Thorne et al., 1998). Seepage erosion can result in bank deformation by the movement of groundwater, in addition to changing the pore water pressure or the generation of the seepage gradient forces that may result in mass failure (Rinaldi and Nardi, 2013). Vegetation has effects on bank hydrology and thus on bank stability and mass failure. The river bank stability can be decreased or increased, dependent on the type, age, health and density of the vegetation.

### 2.4.2 Effects of bank erosion

Bank erosion has many effects on the hydromorphodynamics of the river. In this section effects of bank erosion that may lead to the formation of bars will be described.

*Channel widening and bed aggradation*

Erosion of the riverbank of one or both sides can increase the river width - Figure 2.4a (Thorne et al., 1998). When the riverbank is eroding at the same rate as the opposite bank is accreting, however, the river width will remain constant and a meandering river pattern may develop. Widening in a river bend may occur when the outer bank erosion rate exceeds the rate of advance of the inner bank, due to alternate or point bar growth - Figure 2.4b. In braided rivers, bank erosion by flows deflected around growing braid bars cause the river to widen - Figure

2.4c. When the banks become unstable due to bed degradation, mass failure may cause the banks to erode and the channel to widen – Figure 2.4d. Bank erosion may cause the channel to widen when the channel is aggrading and flow accelerates due to a decreasing cross-sectional area, coupled with current deflection around growing bars - Figure 2.4e. Widening changes the width-to-depth ratio of the river, which is a key parameter in river morphology (Mosselman, 1992).

Laboratory tests of Friedkin (1945) showed that the rate of bank erosion determines the shape of the cross sections of a meandering river. Based on the tests, he stated that slowly eroding banks result in deep narrow cross-sections and rapidly eroding banks result in wide shallow cross-sections. For extremely easily erodible banks, a braided channel developed.

Mosselman (1992) concluded from an analytical and numerical model that bank erosion makes rivers shallower and steeper in general. He stated that bank erosion is a positive feedback mechanism, since the shallowing and steepening make flow velocities larger and enhance bank erosion.

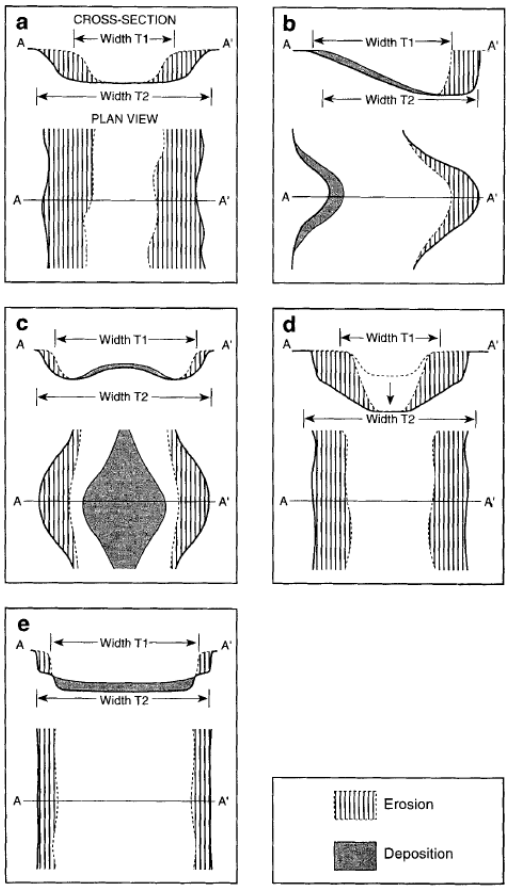


*Figure 2.4- Geomorphology of channel widening: (a) channel enlargement by bank erosion without incision; (b) erosion of outer bank in sinuous channel at faster rate than accretion on bar opposite; (c) deflection of flows by growing braid bar; (d) bank failure and retreat due to mass instability following channel incision; (e) bank erosion due to flow acceleration and deflection in coarse-bedded, aggrading river (Thorne et al., 1998)*

*Sediment balance*

Exner (1920, 1925) derived a sediment balance equation for bed load from the conservation of sediment mass over a river reach. Sediment input equals sediment output for a river reach in equilibrium state. Sediment from the eroding banks may increase the bed load transport and force the river reach out of its morphological equilibrium. This may increase sediment deposition and river bars may develop.

The amount of additional bed load material due to bank erosion depends on the erosion rate, bank height and bank composition. Obviously, for larger erosion rates and higher bank heights more sediment may be added to the flow. Another important variable determining the influence of bank erosion on the river bed is the composition of the bank. When the sediment eroded from the bank is transported by the flow a distinction can be made between bed load transport and suspended load transport (Jansen et al., 1979). Wash load is part of the suspended load transport that involves very fine sediments, such as silt and clay, and does not exchange with the bed. River bars are therefore not affected by wash load and are composed by bed material such as sand and gravel. As a conclusion, additional bed material may be added to the flow when the banks erode and this may affect bar formation.

From a linear analysis Mosselman (1992) showed that sediment input from bank erosion due to excess flow shear stress leads to smaller wave lengths of hybrid alternate bars, but does not affect the damping lengths of those bars. For bank erosion due to excess near-bank water depth in his linear analysis, hybrid alternate bars become shorter at higher values of the interaction parameter and longer at lower values (Mosselman, 1989). The damping lengths of the bars increased then.

## 2.5 Consequences of removing riverbank protection

Several mechanisms can trigger the formation of bars in rivers. In Figure 2.5 the potential effect of the removal of riverbank protection and mechanisms that might trigger bar formation are shown in a conceptual framework.

Natural banks, when there is no protection applied, are able to erode freely due to fluvial erosion and mass failure (Thorne et al., 1998). Bank erosion can perturb the flow and morphology locally at the bank line when viewed at a cross-section scale and provide the bed load and the suspended load with additional sediment from the eroded bank. The local perturbation in the riverbank line may induce morphological changes in the bed such as a scour hole or sediment deposit. When the flow velocity and direction are changed due to a scour hole or sediment deposit it induces further bank erosion. Furthermore, the scour hole, sediment deposit and local perturbation in the bank line can be a trigger for the formation of bars, due to changes in the flow and sediment transport. When viewed at a cross-section scale, the sediment input from the bank may add to a sediment deposit and influence the wave lengths and damping of bars (Mosselman, 1992).

Cross-section scale hydromorphodynamic changes may result in reach-scale effects if the bank protection is removed over a reach-scale length. The local bank erosion may eventually result in a reach-scale channel widening, under the condition that both banks are eroding or the bank erosion rate exceeds the accretion rate of the opposite bank (Thorne et al., 1998). The sediment of the eroded bank may be deposited in the widened reach and lead to reach-scale bed aggradation. Furthermore, channel widening may on the long term result in aggradation of the channel bed to establish reach-scale equilibrium (e.g. Siviglia et al. 2008, Jansen et al., 1979; De Vries, 1975). Parker et al. (1976) observed that aggradation can lead from a meandering to braided state and therefore may influence bar development. Channel widening increases the

width-to-depth ratio of the river and hence may influence the number of bars in a river cross-section (Crosato and Mosselman, 2009).

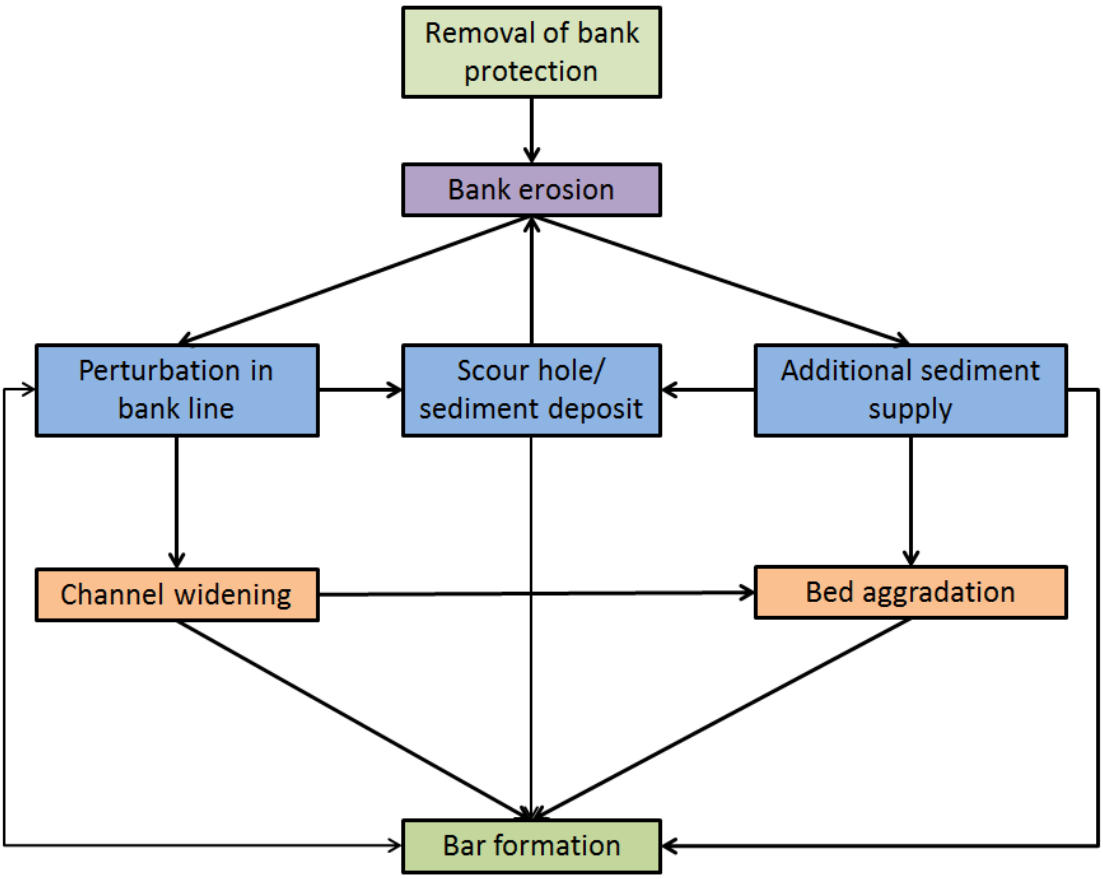


*Figure 2.5 – Conceptual framework of the effects of removing riverbank protection*

# 3 Research methodology

## 3.1 Experimental conditions

The aim of the experiment was to find a relation between the length of a bank protection removal and the formation of bars. Furthermore, the experiment was aimed at finding geometrical changes in the setup that led to a difference in bar formation. The experiment was aimed at representing hydromorphological conditions as close as possible to natural rivers, such that the results of the experiment would be meaningful for natural rivers.
The experimental conditions were therefore aimed at sediment mobility, formation of bars, minimisation of ripples and (anti) dunes in the channel bed and a turbulent flow regime. These conditions resulted in a hydraulically rough channel bed, gravel-bed river similarity and a bed load dominated transport.

*Sediment mobility*

Sediment is in motion when the Shields number is larger than the critical Shields number. Shields parameter $\theta$ is the balance between the bed shear stress and gravity and is defined as (Shields, 1936):

$$\theta = \frac{\tau}{(\rho_s - \rho_f) g D_{50}} \tag{8}$$

where $\rho_s$ is the sediment density, $\rho_f$ the fluid density, $D_{50}$ the median sediment diameter and $g$ the gravitational acceleration. The total shear stress $\tau$ in steady uniform flow is defined as:

$$\tau = \rho_f g \left( \frac{u^2}{C^2} \right) \tag{9}$$

Down scaling the sediment size can impose problems in experiments (Kleinhans, 2014). For very small particles like clay or silt, threshold mobility and cohesion are significantly different from sand or gravel. Therefore, the sediments cannot be much smaller than those in nature. A problem in morphological experiments is that despite the larger bed slopes than in nature, the shear stress is much lower due to small water depths. The sediment mobility may be lower than the threshold of sediment motion in the experiment. From the Shields diagram for incipient motion could be determined whether the sediment was in motion under certain conditions.

A method to increase the sediment mobility at an experimental scale is to use low-density model sediment. When low-density model sediment is used at an experimental scale, the transport is suspended load dominated. Sand-bed rivers have suspended load dominated transport. When natural sediment is used at an experimental scale, the transport is bed load dominated. Gravel-bed rivers have bed load dominated transport. Low-density model sediment allows both the Reynolds number and the densimetric Froude number to maintain the same value in the prototype and in the model. Despite this advantage, geometric length, fall speed and relative density scales are not satisfied and scale effects are introduced (Frostick, 2011). In this research is therefore chosen to conduct experiments with natural sediment. The transport is therefore bed load dominated in the experiment and gravel-bed river similarity is obtained.

*Bed load dominated transport*
The sediment transport is bed load dominated in the experiment, due to downscaling the hydrodynamics from a river scale to a small scale experiment and using natural sediment. The sediment in the flume channel is transported along the bed by rolling, sliding and hopping. The sediment transport formula of Meyer-Peter and Muller (1948) is suitable to calculate the bed load dominated transport capacity of the flow. The formula is valid for situations in which $\mu\theta < 0.2$, $D_{50} > 0.4\ mm$ and $\frac{w_s}{u^*} > 1$, where the parameters are defined as ripple factor $\mu$, Shields parameter $\theta$, median sediment grain size $D_{50}$, fall velocity $w_s$ and shear velocity $u^*$.

*Gravel-bed river similarity*
The experiment has been conducted with natural sediment and therefore the dimensionless parameters characterizing channel bankfull geometry of the experiment fall in the range of gravel-bed rivers. Dimensionless plots of bankfull characteristics from Parker (2004) show that alluvial rivers have a considerable degree of commonality. In Appendix B several sets of data from gravel bed and sand bed rivers are plotted to find relations between parameters characterizing channel bankfull geometry. Gravel-bed river similarity causes the flow condition to be close to critical.

*Hydraulically rough channel bed*
For hydraulically smooth conditions, ripples form if there is enough water depth or scour holes form in shallow flow. In experiments, ripples or scour holes make it hard to observe bars. A hydraulically rough channel bed remains planar or dunes form, which is therefore a suitable condition to observe bars.

The channel bed is hydraulically rough or smooth when particles are respectively emerged or submerged in the laminar sublayer (Kleinhans et al., 2014). The Reynolds particle number is the balance between inertial and viscous forces at the bed and defined as

$$Re^* = \frac{u^* D_{50}}{\nu} \tag{10}$$

Where $u^* = \sqrt{\tau/\rho}$ is the shear velocity. The transition from hydraulicaly smooth to rough conditions is gradual ($Re^* = 3{,}5 - 70$), however, from comparison to empirical bedform stability diagrams the transition may be defined at $Re^* \approx 5$.

The Reynolds particle number has a value of 15 in the experiments and therefore represents a hydraulically rough channel bed.

*Turbulent flow regime*
The dimensionless Reynolds number expresses the ratio of inertial forces to viscous forces in a fluid. The Reynolds number is defined as

$$Re = \frac{uh}{\nu} \tag{11}$$

where $\nu \approx 1 * 10^{-6}$ is the dynamic viscosity for water at 20°C. The Reynolds number is utilised to determine similar flow patterns in different fluid flow situations. The Reynolds number charactarizes different flow regimes such as laminar or turbulent flow. Laminar flow (Re< 2000) occurs when viscous forces are dominant and a smooth, constant fluid motion prevails.

Turbulent flow (Re> 2000) is dominated by inertial forces and chaotic eddies, vortices and other flow instabilites occur. The experiment is aimed at having a turbulent flow regime, since the flow regime of rivers is generally turbulent.

*Bar mode*
The aim of the experiment was to find a relation between the length of a bank protection removal and the formation of bars. Therefore, formation of bars in case the bank protections were removed was an experimental condition. The bar mode given by Equation (1) of Crosato and Mosselman (2009) defined a physics-based predictor that estimates the number of hybrid bars in a river cross-section. The experiment is aimed at a bar mode of one in a channel with fixed banks, which means that in theory there is one bar in a channel cross-section. The bar mode may increase when the channel widens.

### 3.1.1 Simplified experimental conditions

Some hydromorphological river conditions or natural river geometries were simplified in the experiment. The conditions of the laboratory experiment were limited, generally due to practical reasons which are described in this section.

*Smooth wall roughness*
The sides of the channel were smooth, since the fixed walls were constructed from wood and steel plates. The wall roughness was therefore smaller than would occur in a river. The effect of the wall roughness on hydromorphodynamics was, however, small in the laboratory experiment, since the water depth was relatively small in the flume channel.

*Steady, bankfull discharge*
A constant, bankfull discharge in time was used during the laboratory experiments for practical reasons and to simplify river conditions. River discharges show much variation during a year and in the short term. In most rivers the largest amounts of sediments are transported during the highest flows. During low flows the transport rates are much lower than during high flows. Reaching the morphological final stage during low-flow conditions may take a long period. Within this period, usually a high flow has already occurred and therefore the bankfull conditions are decisive.

*Water surface curve*
A drawdown curve is generated with a free overfall over the downstream weir in the flume. Drawdown curves are characterized by flow depth that decrease in the flow direction ($\frac{dh}{dx} < 0$). Morphological development might be affected by this drawdown curve in the downstream part of the laboratory flume. The adaptation length $\lambda$ is the characteristic length scale over which a water level curve with exponential shape approaches the asymptote of steady uniform flow depth. An estimation of the adaptation length for the drawdown curve is given with $\lambda = \frac{3h}{S}$ in which parameter S is the energy slope.

*Straight channel geometry*
Rivers are usually not straight and a straight channel flume is therefore a simplification. It is practical to construct a straight channel geometry. The flow in a straight channel is symmetrical, but bends will force asymmetrical flow. Asymmetrical flow was forced in the straight channel by constructing a groyne upstream in the channel in several tests.

*Bank height and cohesiveness*

Riverbanks can have different bank heights in longitudinal and transversal direction. In the laboratory experiment, the erodible bank had a constant bank height, since this was most practical for constructing the channel banks. Furthermore, the channel banks were in most tests non-cohesive, since they were composed of the same material as the channel bed. In rivers, however, the banks are usually more cohesive than the river bed, due to vegetation for example. One experimental test was therefore performed with cohesive banks to determine whether bank cohesiveness had an influence on the final bank erosion shape and the formation of bars.

## 3.2 Experimental setup

The experiments were performed in a wooden flume that was 7 metre long and 1.2 metre wide. A schematisation of the longitudinal profile of the experimental setup is shown in Figure 3.3. Within this flume a channel of 6.2 metre long and 0.2 metre wide was constructed. In the middle of this channel, both bank protections could be removed over a distance of 2 metre in three sections of 0.6 metre and one section of 0.2 metre, which are made from 1.5 mm thick stainless steel.

A frequency controller attached to a discharge pump controlled the water discharge. The frequency controller was calibrated for a discharge ranging from 0.42 L/s to 0.85 L/s (Figure 3.1).

Dry sediment was introduced at the head of the flume by a sediment feeder. A tap at the bottom of the feeder controlled the sediment-feeding rate. Under the tap a wooden plank with an angle of 45 degrees was positioned to ensure that the sediment was evenly spread over the width of the main channel. Sediment output at the downstream end of the flume was collected in a sieve. The upstream and downstream weir of the main channel were constructed at a height matching the equilibrium bed slope from 11 cm to 6 cm over the length of the flume. The erodible bank was constructed 2 cm higher than the bed level. The sediment on the channel bed was shaped manually with a chip into a smooth slope. A well-sorted sediment with $D_{50} = 0.52$ mm, $D_{90} = 0.63$ mm and $D_{15} = 0.44$ mm was used in this study (Figure 3.2).

Lasers installed on a platform on rails surveyed the bed topography. A digital camera was installed above the flume to monitor the morphological dynamics of the experiment. Appendix H.1 shows photos of the laser platform, digital camera and other details of the experimental setup.

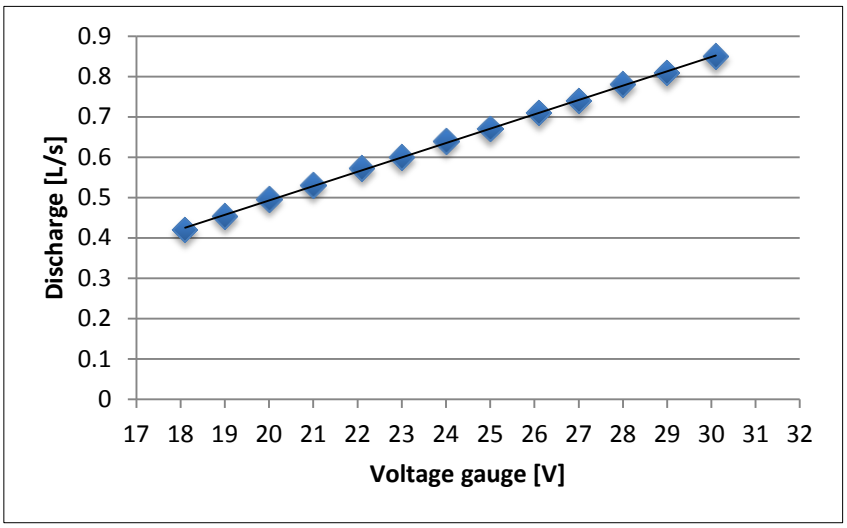


*Figure 3.1 - Discharge pump calibration*

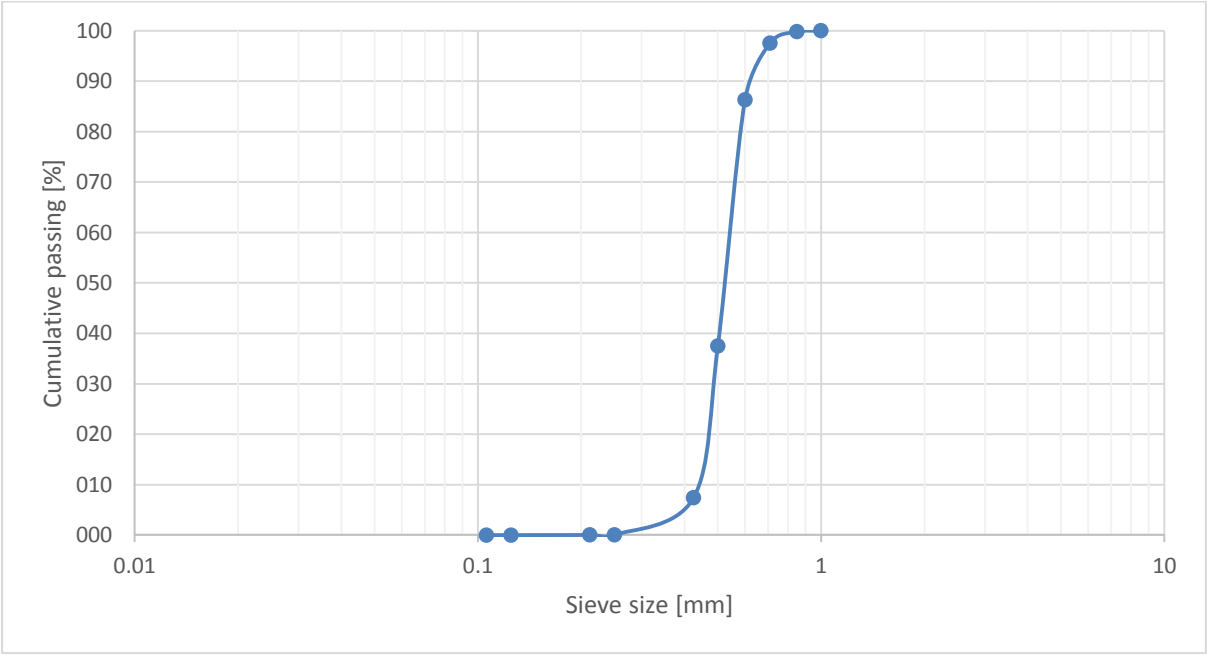


*Figure 3.2 – Sieve curve of well-sorted sediment*

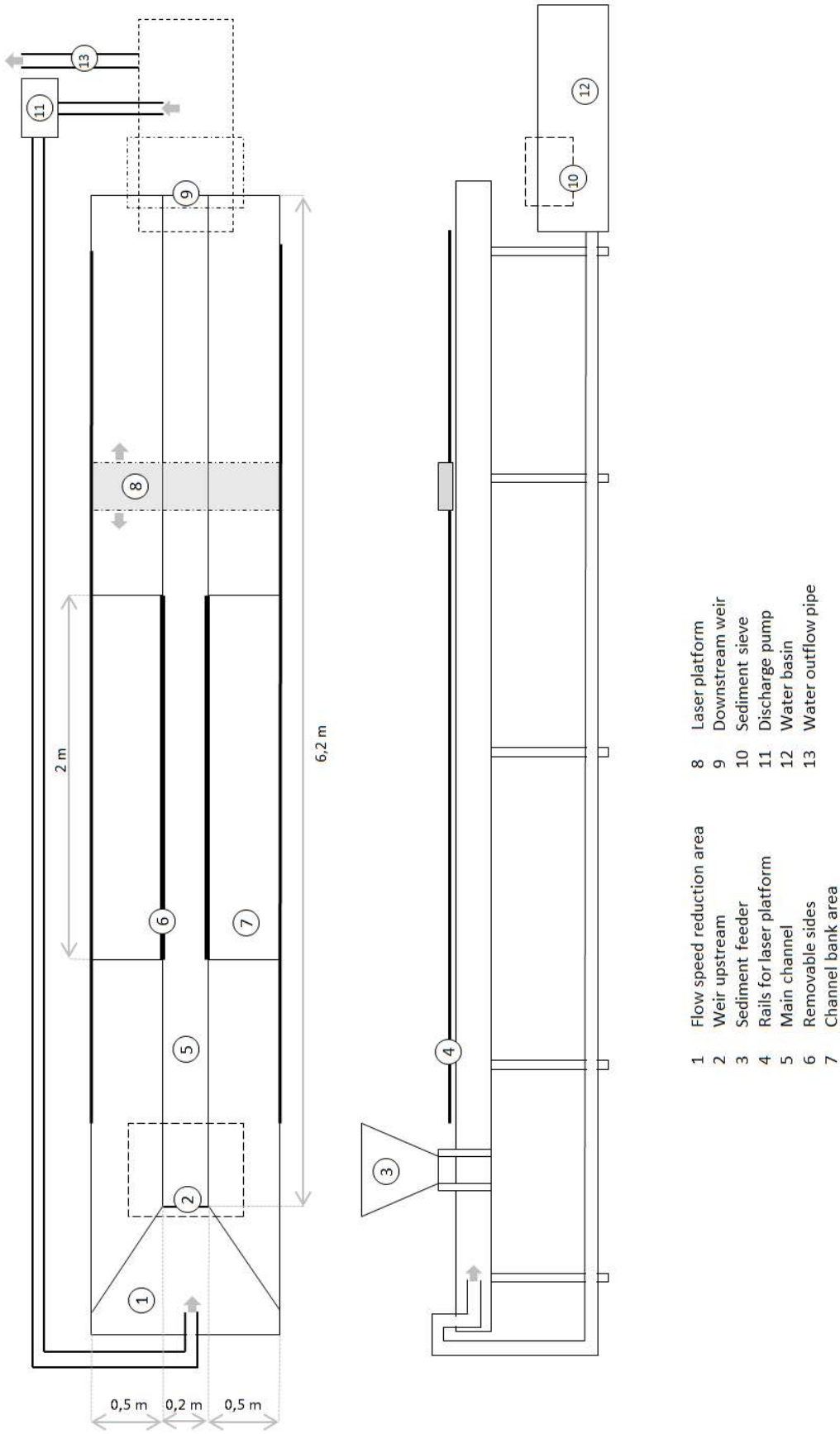


*Figure 3.3 – Longitudinal profile of experimental setup: top view (left) and side view (right). Not to scale.*

### 3.2.1 Preliminary phase

In the preliminary phase fixed bank protections over the entire length of the flume ensured that no lateral erosion occurred. The aim of this phase was to find a combination of water discharge, initial bed slope and sediment mixture that could be used for all experimental tests. The experiments in the preliminary phase were aimed at achieving conditions for which there was sediment mobility, formation of bars, minimisation of ripples and (anti) dunes in the channel bed and a turbulent flow regime as described in Section 3.1.

For a specific combination of parameters, i.e. water discharge, channel width and bed load rate, an equilibrium state had to be reached. An equilibrium state was reached when the sediment output equalled the sediment input for steady state conditions, so that the mean bed slope would remain constant during the considered time interval (Requena et al., 2006). The duration of reaching an equilibrium stage was reduced by building an initial channel bed slope, which approximately matched the expected equilibrium bed slope.

The first combination of water discharge, initial bed slope and sediment mixture was chosen based on experimental conditions of Tewolde (2015). The expected equilibrium bed slope was therefore determined based on the final bed slope in experiments of Tewolde (2015). Tewolde did laboratory experiments to investigate the effects of suspended sediments on gravel bars. The experimental setup was similar in geometry and sediment feeding. One of the conditions that Tewolde used for his experiment was a discharge of 0.6 L/s, channel bed slope of 0,008 and a median sediment diameter of 0,00058 m. Two bars were formed when a groyne at the upstream end of the flume was used as an asymmetric forcing.

The preliminary test Pr01 with conditions based on experiments of Tewolde (2015) is shown in Table 3.1. The channel bed was covered with (anti)dunes and it was tried to minimise these dunes by decreasing the bed slope (test Pr02), increasing the discharge (test Pr03) and/or using a more widely graded sediment mixture (test Pr04). A steeper bed slope and increased discharge resulted in more (anti)dunes in the bed and a wider graded sediment mixture resulted in clogging of the sediment feeder. Preliminary test Pr01 fulfilled the conditions described in Section 3.1 best and was chosen as a starting point for the experimental tests.

*Table 3.1 – Conditions of tests Pr01 to Pr05 in the preliminary phase. Figure 3.2 shows the sieve curve of the sediment used in test Pr01 to Pr03 and Figure C.1 in Appendix C shows the sieve curve of the sediment used in test Pr04.*

| Experimental test | Discharge Q | Initial bed slope i | Median sediment diameter D50 |
|---|---|---|---|
| | m3/s | - | m |
| Test Pr01 | 0,0006 | 0,008 | 0,00052 |
| Test Pr02 | 0,0006 | 0,004 | 0,00052 |
| Test Pr03 | 0,0008 | 0,004 | 0,00052 |
| Test Pr04 | 0,0008 | 0,008 | 0,00063 |

The reach-averaged water depth was estimated in test Pr01 and used to calculate the reach-averaged flow velocity, Chézy coefficient, Reynolds number, Reynolds particle number, Froude number, Shields number, degree of nonlinearity and bar mode (Table 3.2). The equations that were used to calculate the parameters are as follows; reach-averaged flow velocity $u_0 = \frac{Q}{Bh_0}$, Chézy coefficient $C = \frac{u_0}{\sqrt{h_0 i}}$, Froude number $Fr = \frac{u_0}{\sqrt{g h_0}}$ and Shields number $\theta = \frac{u_0^2}{C^2 \Delta D_{50}}$. The

Reynolds number has a value larger than 2000 and therefore the flow regime is turbulent. The channel bed is hydraulically rough, since the Reynolds particle number is large than 5 in the experiment. The degree of nonlinearity $b = 10$ in the experiment that was calculated with Equation (3) has the same value as Crosato and Mosselman (2009) predict for natural gravel-bed rivers. The bar mode of $m = 1$ calculated with Equation (1) corresponds with alternating bars.

The measured surface flow velocity was 0.35 m/s in the main channel with the method described in Section 3.4 using a paper and stopwatch. Based on the $8/10^{th}$ rule from Whipple (2004) the depth- and reach-averaged flow velocity was estimated as $u_0 = 0.35 * 8/10 = 0.28$ m/s. This value of this estimated flow velocity is close to the flow velocity of 0.3 m/s in Table 3.2 calculated with the discharge, width and estimated reach-averaged water depth. Calculating the water depth with the estimated flow velocity gives $h_0 = \frac{Q}{u_0 B} = \frac{0.0006}{0.28*0.2} = 0.01$ m. Since this water depth is similar to the estimated reach-average water depth shown in Table 3.2, it can be a good approximation of the real reach-averaged water depth.

The sediment input rate and sediment output rate were measured every hour during test Pr01. An equilibrium state was reached after six hours when the sediment input rate equalled the sediment output rate for steady state conditions, so that the mean bed slope would remain constant. This sediment transport rate is the transport capacity of the flow. The formula of Meyer-Peter and Muller (1948) is valid for the experimental conditions, since $\mu\theta < 0.2$, $D_{50} > 0.4$ mm and $\frac{w_s}{u^*} > 1$. The theoretical bed load transport capacity calculated this formula gives $S_0 = 8.47 * 10^{-5}$ g/min and underestimates the transport capacity in the experiment.

*Table 3.2 – Conditions in preliminary test Pr01*

| | | |
|---|---|---|
| Discharge Q | $m^3/s$ | 0.0006 |
| Bed slope i | - | 0.008 |
| Median sediment diameter $D_{50}$ | m | 0.00052 |
| Reach-average water depth $h_0$ | m | 0.01 |
| Reach-average flow velocity $u_0$ | m/s | 0.30 |
| Chézy coefficient C | $m^{1/2}/s$ | 33 |
| Sediment transport rate | g/min | 94 |
| Reynolds number Re | - | 3000 |
| Reynolds particle number Re* | - | 15 |
| Froude number Fr | - | 0.94 |
| Shields parameter θ | - | 0.09 |
| Degree of nonlinearity b | - | 10 |
| Bar mode m | - | 1.14 |

## 3.3 Experimental tests

Several experimental tests were performed to find a relation between a bank protection removal and the formation of bars. The choice and setup of the tests are given in this section. The conditions of the experimental tests are similar as the conditions of preliminary test Pr01.

Figure D.1 and Figure D.2 in Appendix D show the setup of the experimental tests. The setup of the tests is summarized in Table 3.3. In all figures in this report, the bank protection at the top of the figure is indicated as the left bank protection and the bank protection at the bottom of the figure is indicated as the right bank protection. Furthermore, the flow is in all figures from left to right.

### 3.3.1 Fixed banks

The reference case was an experimental test without removal of bank protection, such that no lateral erosion was allowed. The banks were fixed and the flow was forced to remain in a straight channel. This setup could be related to a river with fixed banks, before the river reach is restored. This setup was tested in order to compare the formation of bars in a test with no bank protection removal with tests where the bank protection was removed.

Test P01 with a symmetrical flow forcing and test P02 with an asymmetrical flow forcing were performed with fixed banks. Test P01 could be compared with tests which had a symmetrical flow forcing and test P02 could be compared with tests which had an asymmetrical flow forcing.

### 3.3.2 Length of bank protection removal

Experimental tests R01 to R06 were focussed on the relation between the length of bank protection removal and the formation of bars. Veldt (2014) found that removing a length of one or two times the width of the main channel did not result in formation of bars. The bank protections were therefore removed in sections of three times the width of the main channel. The bank protection was removed on either one or both sides of the main channel, since one of these measures can be chosen in river restoration projects. On which side the bank protection is removed in river restoration projects may depend on the available space for lateral erosion. The bank protections of the channel banks in the experimental tests were removed with a length of three, six and nine times the channel width on either one or both sides.

### 3.3.3 Location of bank protection removal

The aim of test R07 was to find a relation between the location of bank protection removal and the formation of bars. In river restoration projects, the decision for the location of the bank protection removal may depend on infrastructure or houses located along the river. In test R07 is therefore chosen to remove the bank protection at different locations in smaller sections at both sides of the channel. Three sections of bank protection with a total length of three times the channel width were removed at different locations.

### 3.3.4 Asymmetrical flow forcing

Rivers have bends and perturbations that cause asymmetric flow patterns. Therefore, a groyne upstream in the channel forced an symmetrical flow in experimental tests R08, R09 and R10 to simulate a natural river flow. The length of the groyne was half the channel width and was located upstream of the bank protection removal at a distance of five times the channel width. Furthermore, a groyne could be used to change the bar formation in river restoration projects. The bank protection was removed in the experiment on different sides of the channel, to find a relation between the location of the groyne and the formation of bars. In test R08 the bank protection was removed on the right side and in test R09 the bank protection was removed on the left side. In test R10 on both sides of the channel the bank protections were removed.

### 3.3.5 Channel bank cohesion

Riverbanks are usually cohesive. The erodible bank in test R11 was therefore constructed of cohesive material, unlike in the other tests which had a non-cohesive banks. The aim of this experiment was to compare the shape of the eroded bank line in test R11 with the shape of the eroded bank line in the tests with non-cohesive banks. This was done in order to determine if the bar formation and channel widening in the tests with non-cohesive banks would be representative for a natural riverbank.

Kleinhans et al. (2014) found that silt-sized silica flour was the most suitable material to be added to the well-sorted sand in order to increase bank cohesiveness. It is not fully understood

how this silt affects the morphodynamics, but it increases critical shear stress and therefore the threshold for bank erosion. The advantage of silt is that it is not as cohesive as clay, since clay may lead to non-erodible banks in these experimental conditions. Furthermore, silt smaller than a certain cut-off size does not contribute to bed level changes and roughness. The silica flour had a particle size distribution where $D10$ is 0.003 mm, $D50$ is 0.017 mm and $D90$ is 0.04 mm. It was mixed into the bank to represent a heterogeneous bank with many thin layers of cohesive sediment. Dry silica flour and well-sorted sand were mixed followed by wetting in proportions of 20% silica flour versus 80% sand (Kleinhans et al., 2014).

### 3.3.6 Bank protection shape

From experiments of Veldt (2015) it can be seen that large erosion holes developed at the downstream end of the widened reach. In river restoration projects, it is important to know whether and how these scour holes can be reduced in size. Different bank protection shapes from the widened reach to the main channel were therefore tested in tests R12, R13 and R14. In test R12 and R13 the bank protection was removed over a length of ten times the river width, such that the remaining bank protection on the downstream end was perpendicular to the flow direction. In test R12 a groyne was located upstream of the reach where the bank protection was removed. In test R14 the bank protection was removed with a length of three times the channel width. At the downstream end of the reach without bank protection, a curved bank was located to streamline the flow from the widened reach towards the main channel. The radius of the curved bank protection was approximately the width of the channel.

*Table 3.3 – Setup of experimental tests. B=width of the main channel.*

| Test | Length of bank protection removal on right side of the channel | Length of bank protection removal on left side of the channel | Details |
|---|---|---|---|
| P01 | - | - | |
| P02 | - | - | Groyne |
| R01 | 3*B | - | |
| R02 | 6*B | - | |
| R03 | 9*B | - | |
| R04 | 3*B | 3*B | |
| R05 | 6*B | 6*B | |
| R06 | 9*B | 9*B | |
| R07 | 3*B | 6*B | Three locations removal |
| R08 | 9*B | - | Groyne |
| R09 | - | 9*B | Groyne |
| R10 | 9*B | 9*B | Groyne |
| R11 | 6*B | - | Cohesive bank |
| R12 | 10*B | 10*B | Groyne, perpendicular bank protection |
| R13 | 10*B | 10*B | Perpendicular bank protection |
| R14 | 3*B | - | Curved bank protection |

## 3.4 Data collection

This section describes what data is collected in the experiment and how this data is collected. In Appendix H.2, photos of collecting the data during the experiments are shown.

*Bed profile*

Four lasers were used to measure the bed profile in the flume. Three lasers were attached to a platform that moved in longitudinal direction on rails. When moving the platform over the rails, a wheel connected to the platform that also moved over the rails automatically collected 5000 data points per wheel rotation. The periphery of the wheel was 50 cm, so the distance in longitudinal direction between the bed profile measurements with the lasers was 0.1 mm. One laser was located in the middle of the main channel of 0.2 m width and the other two lasers were located 3 cm inward from the sides of the main channel. The lasers could measure over a longitudinal distance of 4.2 metres starting from a point 6 cm upstream of the removable sides. The bed level upstream of the widened reach could not be measured by the lasers, since the rails was not extended to this section.

During the experiment the water surface was covered with small waves that reflected the laser light in many directions. The lasers could therefore only measure the bed profile when there was no water in the flume at the end of the experiment. The development of the bed profile during the experiment could not be measured.

A fourth laser could slide over the platform in transverse direction. This laser had to be moved manually. The laser could be used to measure the bed profile in longitudinal or transverse direction outside of the main channel. When moving the laser in transverse direction each data point had to be computed manually, since the wheel only rotated in longitudinal direction. Measuring the bed profile manually was unpractical and time consuming and therefore this laser was not used. The bed profile outside of the main channel was therefore not measured with the lasers.

The lasers were connected to a computer where the icon-based software DASYLab 13.0 was used for the data acquisition, graphics, control and analysis (Figure H.19). Data that the four lasers obtained were in unit voltage. In MATLAB R2016a a script was written to convert the data from DASYLab 13.0 to the bed elevation of the flume . This MATLAB script created charts of measured bed profiles.

The lasers could only measure the bed profile in dry flume conditions, i.e. no layer of water on the sandy bed. Therefore, at the end of each experiment the discharge pump was turned off. To ensure a dry bed, two stoppers in the bottom on each side of the flume were removed until the channel was sufficiently drained.

*Sediment rate*

The sediment rate added at the upstream end of the flume by the sediment feeder was measured several times during each experiment. A small bowl was placed under the tap of the sediment feeder during one minute and weighted afterwards to get the incoming sediment rate in grams per minute (Figure H.20).

The sediment rate at the downstream end of the flume was measured several times during each experiment. Just above the sieve in the water basin a small sieve caught the sediment during one minute (Figure H.21). This sediment was put in an oven for at least one hour at a temperature of

100 degrees Celsius to let it dry. When the sediment was dry, it was weighted to obtain the outgoing sediment rate in grams per minute.

*Erosion rate*

At the section where the bank protections were removed, the banks eroded freely. This erosion rate was measured both manually with a tapeline and automatically by camera (Figure H.22). The camera was set to take pictures at an interval capture of 15 minutes. The camera was located at a height of 5 metres in a crane and positioned above the middle of the flume. The erosion rate of the scour holes was also measured.

*Bedforms*

The dimensions and location of bedforms in the channel bed, such as bars, ripples and dunes, were measured both during wet and dry conditions in the flume. The bedforms were analysed using three tools: a camera, lasers and dye. Four methods were executed with these tools to analyse bedforms.

The first method was performed during wet conditions in the flume, i.e. when the discharge pump was on and water was flowing in the channel. The method consisted of visual observation and camera photo analysis of emerged and submerged bedforms. The dimensions of bedforms were measured with a tapeline.

In the second method the discharge was decreased significantly such that water was flowing in lower regions. Dye was added to the flowing water at the upstream end of the flume that coloured troughs in the channel bed (Figure H.23). The dye is a mix of water and potassium permanganate and disappears after a couple of minutes when it is added to the water in the flume.

The discharge was set to zero for the third method to observe bedforms. In the first couple of minutes afterwards troughs in the channel bed were filled with water whereas peaks emerged. The 'pools' reflected light on the flume, which made the difference between troughs and peaks visible on camera.

The last method concerned measuring bedforms with lasers that measured the bed elevation. As stated before, this could only be done in dry flume conditions. Analysing the difference in bed elevation was a method to quantify the dimensions of the bedforms.

### 3.4.1 Hydraulic parameters

Water depth was measured with a paper ruler that was fixed to the bank protections of the main channel at four locations in the flume. The water depth at four different locations was read from the rulers and averaged to get an estimate of the reach-averaged water depth.

A fifth laser was attached to the platform that was supposed to measure the water level automatically in longitudinal direction. The water level fluctuated too much to get a good measure, since there were small waves present on the water surface. The water depth had to be estimated from the rulers at the sides of the channel, which was less accurate.

Flow velocity in the main channel was calculated using two methods. The first method used the reach-averaged water depth $h_0$ as an input value for the depth- and reach-averaged flow velocity $u_0$ that was calculated with $u_0 = \frac{Q}{Bh_0}$. For the second method, surface flow velocity was estimated and converted to a depth-averaged flow velocity with a rule of thumb. A paper was

placed upstream and the time to travel a certain distance was clocked with a stop watch. This was done three times and the average value of the time $t$ it took to travel distance $x$ was used to calculate the surface flow $u_s = x/t$. Whipple (2004) states as a rule of thumb to calculate the depth-averaged flow velocity that $u_0 = \frac{8}{10} * u_s$. This second method was used to validate the first method.

The Chézy coefficient was calculated with a rewritten formula for normal flow conditions $C = u_0/\sqrt{h_0 i}$. The estimated water depth and flow velocity were used as input values.

# 4 Results

## 4.1 General experimental observations

In the experimental tests, similar events and processes took place. In each experimental test, however, different setups of the experiment results in a different outcome that are described in the next sections. The sequential events and processes in the experiments will be described, but it has to be noted that each experiment can have its own processes that are not regarded here.

In the first hour of each test the bank protection was still in place and the bed profile was smoothed with a chip into a slope of 0.008. The water was flowing in the channel for one hour to obtain a smooth slope and some initial bedforms. The purpose of this first hour was to have similar conditions in the flume as in a natural river. Figure 4.1A shows that the bed profile was not smooth and the bed slope could differ over the length of the channel. The discharge pump was turned on to a frequency of 23.0 V which resulted in a water discharge in the main channel of 0.6 L/s. A flood wave travelled through the main channel of the flume and smoothed the bed profile.

Empty compartments next to the main channel were slowly filled with water up to the same water level as in the channel. Large perturbations in the channel bed had a depositing front that moved downstream with a speed of approximately 0.56 cm/min. The water depth varied slightly along the channel and at locations with larger water depth bedforms in the order of 2 cm length appeared in the bed. This caused the water to be disturbed, showing small waves in the water surface with a height of approximately 0.5 cm. The waves were in phase with the bed elevation, which indicated that the bedforms were antidunes. The bedforms were, however, travelling downstream, which indicated that the bedforms were dunes. This phenomenon might be due to a transcritical flow regime being in a state between sub- and supercritical.

Just downstream of the upstream weir the bed immediately started to erode. The sediment feeder was turned on by twisting the tap to a rate of approximately 94 grams/minute. This sediment rate was measured and adjusted according to this outcome. Another way to obtain an equilibrium slope of 0.008 was by observing if the bed was eroding or accreting downstream of the upstream weir. In case of an eroding bed, the tap was opened slightly more and the extra sediment available would fill the erosion hole. The tap of the sediment feeder was closed slightly more in case of an accreting bed where the flow would transport the surplus of sediment downstream.

The discharge pump and sediment feeder were turned off after one hour and the bed profile was measured. This bed profile had a single slope and might show some dunes and free bars. It is shown in Figure 4.1B that irregularities in the bed were smoothed. A certain length of bank protection was removed according to the experimental test. The discharge pump and sediment feeder were turned on at the same rates as in the first hour of the test.

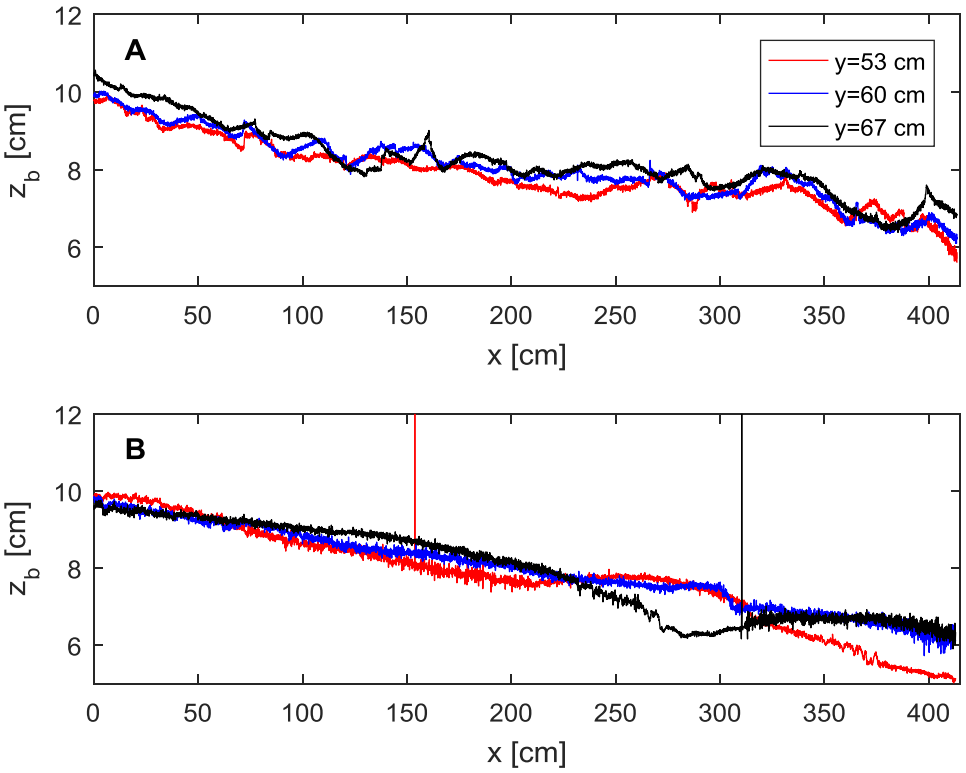


*Figure 4.1 – Bed profile of test R04: A) Before test when bed profile is smoothened with a chip and B) after one hour testing without removal of bank protections. Vertical lines in the graphs are distortions in the laser measurements caused by a small layer of water that reflect the laser in different directions.*

Again, the smallest bedforms were smoothed by the flood wave moving downstream in the main channel. The sandy banks had a height of approximately 2 cm above the main channel and a vertical slope. When the flood wave caused the bank to become unstable, mass failure caused the collapse and movement of bank material and this resulted in a bank slope of about 45 degrees. Fluvial erosion detached and entrained grain particles below the water level and thus steepened the banks. This resulted occasionally in mass failure, but the main eroding mechanism was fluvial erosion by the direct action of the flow. The bank erosion rate decreased in time.

The channel widened due to this bank erosion. Figure 4.2 shows that the widening started upstream and moved in downstream direction. A scour hole developed downstream of the erodible bank, due to turbulent flow patterns around the transition to the bank protection. The dimensions of the scour hole increased in time.

In most tests forced bars developed in the widened reach of the channel. If the width of the channel increases, the flow will decelerate when the discharge remains constant, since $u = Q/A$. Sediment transport will decrease, since the transport capacity and flow velocity are related by $S \sim u^b$ where b is the degree of nonlinearity of sediment transport versus depth-averaged flow velocity. Sediment is therefore deposited in the widened reach with lower flow velocities. This results in bed aggradation in the widened reach and in the formation of forced bars. In areas with higher flow velocities is more sediment transport, which results in deepening of the

channel. One or more hybrid bars formed downstream of the widened reach, due to the curvature of the flow around the bars in the widened reach and curvature of the flow by the scour hole. These bars had usually lower heights, smaller wavelengths and smaller bar areas than the bars formed in the widened reach, since width-to-depth ratio was smaller. Sometimes free bars formed downstream of the bar in the widened reach or hybrid bars, which could be recognized by their shape and non-steady position.

After six hours the discharge was decreased to a rate of approximately 0.0002 L/s. Water would only flow in the lowest bed elevations. Dye was added to the flow upstream in the main channel. Bar troughs and scour holes were coloured and photos were taken with the camera above the flume. The discharge pump and sediment feeder were turned off and photos of the flume were taken with a hand camera. Bar troughs and tops could be distinguished, due to the reflection of the light by the water present in the lowest bottom elevations. Holes in the downstream compartments filled with water could be opened to drain the water from the flume. The sandy bed was drained slowly, where after the bed profile was measured

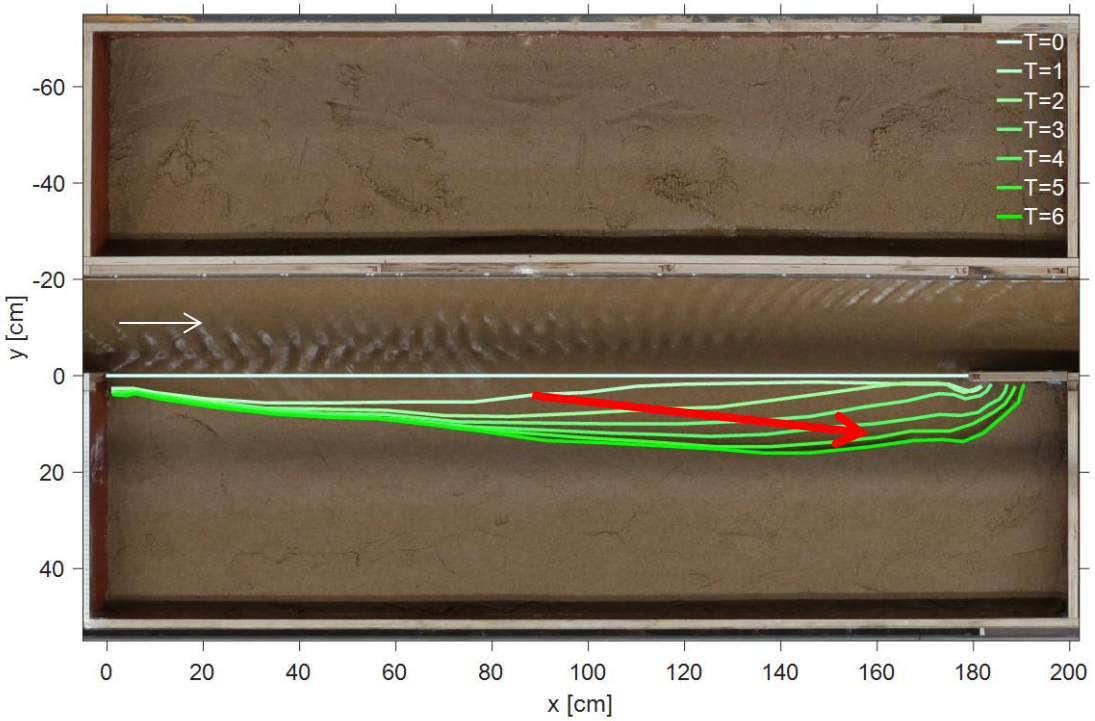


*Figure 4.2 – Evolution of bank erosion of test R03 with time T in hours. Red arrow indicates channel widening in downstream direction.*

## 4.2 Lateral erosion

The channel banks eroded at the sections where the bank protections were removed. In Section 4.1 the general process of the eroding banks are described. In this section, lateral erosion of the channel banks is analysed in detail.

### 4.2.1 Spatial evolution

The progress of the lateral erosion was analysed manually by drawing the bank line in photos taken from above the flume. Figure G.1 to Figure G.10 in Appendix G show the evolution of the bank line for tests R01, R02, R03, R05, R08, R09, R10, R11, R13, R14. The evolution of the bank line is shown at an interval of one hour. From the figures can be seen that the eroded bank line

moves downstream. This development was observed in most experiments and agrees with the downstream meander migration observed in field and laboratory investigations by many authors (e.g. Odgaard, 1987). The bank line shapes and erosion mechanisms in the experimental tests are described in this section. Furthermore, the effects of an asymmetrical flow forcing, bar formation and different downstream bank elements on the bank erosion shape are given.

Table G.1 shows in Appendix G shows the maximum channel width in the widened reach at the end of each test.

*Bank erosion mechanism*
The spatial evolution of the lateral erosion shows similar bank line shapes and erosion mechanisms in the experimental tests.

First, the vertical bank is eroded by the flood wave travelling through the main channel when the discharge pump is turned on and a sloped bank of about 45 degrees remains. Erosion of the bank is the results of an instable vertical bank on which the flow exerts its force. This lateral erosion results in a slightly wider channel section where the bank protection is removed.

Second, the upstream part of the section without bank protection is eroded. At the transition from the bank protection towards the unprotected bank protection the streamlines of the flow are slightly curved, due to the change in channel width. The flow at this transition is locally directed towards the unprotected bank. Sediment particles from this bank are entrained grain by grain by the flow and transported along the bed as bed load. This results in lateral erosion of the bank. The erosion rate at the upstream part decreases in time and is almost zero when the bank line made an angle of approximately 7 degrees with the main channel. The erosion rate increases in downstream direction and decreases again when the bank line has an angle of 7 degrees with the main channel. The flow will finally be parallel to the bank, due to the movement of the bank line and direct action of the flow on the bank is decreased. The bank line will therefore remain under a constant angle. A longer length of unprotected bank therefore results in a wider channel bank protection.

Third, the bank erodes at the downstream end of the unprotected bank protection. This erosion is both caused by turbulent eddies and by undermining of the bank. The flow is perpendicular to the bank protection downstream that divides the flow both to the main channel and the floodplain. The part of the flow to the floodplain side of the bank protection flows parallel to the bank protection. The flow is blocked by the bank line and forced back into the main channel, which causes turbulent eddies. The flow has to turn with an angle of 180 degrees when it arrives at the floodplain side of the bank protection. This curvature of the streamlines is from the bank protection towards the bank line and then back to the main channel. In Figure G.3, this means that the flow is clockwise in the downstream eroded part. The turbulent eddies entrain sediment particles from the bank and bed. Scouring of the bed causes undermining of the bank.

Lateral erosion of the downstream bank erosion occurs simultaneously with the upstream bank erosion. The upstream eroded bank line and the downstream eroded bank line meet at a location in the downstream half of the widened reach.

The maximum channel width in the widened reach at the end of test R01, R02 and R03 with a bank protection removal on one side of the channel were 1.5*B, 1.7*B and 1.8*B, respectively. The maximum channel width in the widened reach at the end of test R04, R05, R06 and R07

with a bank protection removal on two sides of the channel were 2.1*B, 2.3*B, 3.2*B and 1.5*B, respectively.

*Asymmetrical flow forcing*
In the tests with a groyne upstream, the flow was curved such that the main flow was not parallel to the banks anymore. In test R08 the right bank protection was removed, so it could erode laterally. A groyne was located on the right side of the flume and asymmetrically forced the flow to the right bank at the location of the bank protection removal. Due to this curvature of the flow the erodible bank was subject to a larger flow force compared to test R03 with a symmetrical flow forcing. In test R08 therefore a larger bank volume was eroded compared to test R03. The final bank line angle of test R08 was approximately 14 degrees with the main channel.

In test R09 the left bank protection was removed, so it could erode laterally. The flow was forced asymmetric to the right bank protection and the main flow remained on the right side of the channel. The flow force on the left bank was therefore smaller which resulted in less bank erosion compared to test R03 with symmetrical flow forcing. The final bank line angle was 4 degrees with the main channel.

In test R10, on both sides of the main channel the bank protection was removed, so both banks could erode laterally. The flow was curved to the right bank due to the upstream asymmetrical flow forcing. Due to the higher flow force on the right bank compared to the left bank, the right bank eroded more than the left bank.

The maximum channel width in the widened reach at the end of test R08, R09 and R10 were 2.4 *B, 1.5*B and 3.3*B, respectively.

*Bar formation*
Figure G.5, Figure G.7 and Figure G.9 of test R08, R10 and R13 show that the spatial evolution of the lateral erosion is irregular compared to the other tests. In test R06, R08, R10, R12, R13 a relatively large bar developed in the widened reach. In these experiments, the flow is forced around the bar and therefore pushed to the banks. The lateral erosion is locally increased due to this flow force. The bank line shape is therefore changed according to the shape of the bar in the widened reach.

*Bank protection shape*
The shape of the bank protection on the downstream end of the widened reach determined to a great extent the spatial evolution of the lateral erosion. The bank protection on the downstream end of the widened reach was constructed parallel to the main channel in most tests. This caused the formation of a scour hole and turbulent eddies behind the bank protection downstream, which in turn caused lateral erosion of the bank. After some time, the bank line was converging from the widened towards the main channel in an angle of about 45 degrees, but disturbed by the bank protection downstream.

In test R12 and R13, the downstream bank protection was constructed parallel to the main channel. The bank line could, however, not move further downstream than the starting location of bank protection, since a wooden wall was located perpendicular to the bank protection. Lateral erosion in the beginning of the test caused the channel to widen slightly. The flow at the downstream end of the widened reach was directed perpendicular to the wooden wall. When the flow reached the wall, it was reflected into different directions creating turbulent eddies.

The flow force on the bank downstream was increased due to the eddies and lateral erosion of the bank occurred. Figure G.9 of test R13 shows large widening of the channel in the downstream half of the widened reach.

Figure G.10 shows that the downstream bank protection was constructed in a curved shape in test R14. When lateral erosion caused the channel to widen, the flow was converged towards the main channel. The streamlined design of the bank protection resulted in a smooth transition from the widened reach to the main channel. This reduced the turbulent eddies and the formation of a scour hole. The lateral erosion was therefore reduced in the downstream half of the widened reach compared to test R01 with a straight bank protection. The bank line angle of approximately 7 degrees with the main channel in the upstream half of the widened reach was similar in test R14 an R01. In test R14 the bank line was under this angle over the entire widened reach, whereas in test R01 the bank line was under this angle only in the upstream half of the widened reach.

The maximum channel width in the widened reach at the end of test R12, R13 and R14 were 4.9 *B, 4.0*B and 1.6*B, respectively. In test R12 the widening was so large that one eroded bank reach the boundary of the flume, so that the bank could not erode further.

*Cohesive bank*

The bank in test R11 was cohesive, unlike in the other tests which had non-cohesive banks. The boundary sediments in cohesive banks have greater internally derived forces. The critical boundary shear stress was therefore higher in the cohesive bank material and resisted the erosive forces applied by the flow better. The cohesive bank material was detached and entrained grain by grain. The erosion rate was therefore lower compared to non-cohesive banks as described in Section 4.2.2. The final shape of the cohesive bank in test R11 had similar characteristics as the final bank shapes of non-cohesive banks. The bank line started to erode upstream and moved in downstream direction which resulted in an angle of approximately 1 degree of the final bank line with the main channel. Furthermore, the scour hole downstream of the widened section created a similar bank shape as in the tests with non-cohesive banks.

The maximum channel width in the widened reach at the end of test R11 was 1.4*B.

### 4.2.2 Temporal evolution

The temporal evolution of the lateral erosion was described generally for all tests and in detail for test R11, which had a cohesive bank. The lateral erosion rate is defined as the velocity of bank erosion at a considered time increment and measured perpendicular to the initial bank line of the main channel.

*General erosion rate*

In general, the tests showed that the erosion rate decreased exponentially in time. This reduction of the erosion rate is caused by the widening of the channel. When the channel widens, the flow surface is increased and with the same discharge the flow velocity will decrease. The erosive flow force is therefore decreased and lateral erosion reduced.

Figure 4.3 shows an example of the exponentially decreasing erosion rate. When the tests were ended after 6 hours, the erosion rate was in most tests reduced to zero. Tests R06, R08, R10, R12, R13 were an exception, since the formation of a large bar pushed the flow towards the banks and resulted in locally increased erosion rates, even at the end of the tests. The erosion

rate at the start of the tests differed between 4 to 10 cm/hour in the middle of the widened reach.

The erosion rates of the left and right bank were sometimes slightly different in the experiments with a symmetrical forcing. This is also shown in Figure 4.3 of test R04 where the erosion rate of the right bank was higher in the first 2 hours. This might be caused by a small disturbance of the bed which causes the flow asymmetrically or a different constructed bank height. In the tests with an asymmetrical flow forcing, the flow applied higher erosive forces at the bank towards which the flow is curved. This resulted in a higher erosion rate on this bank.

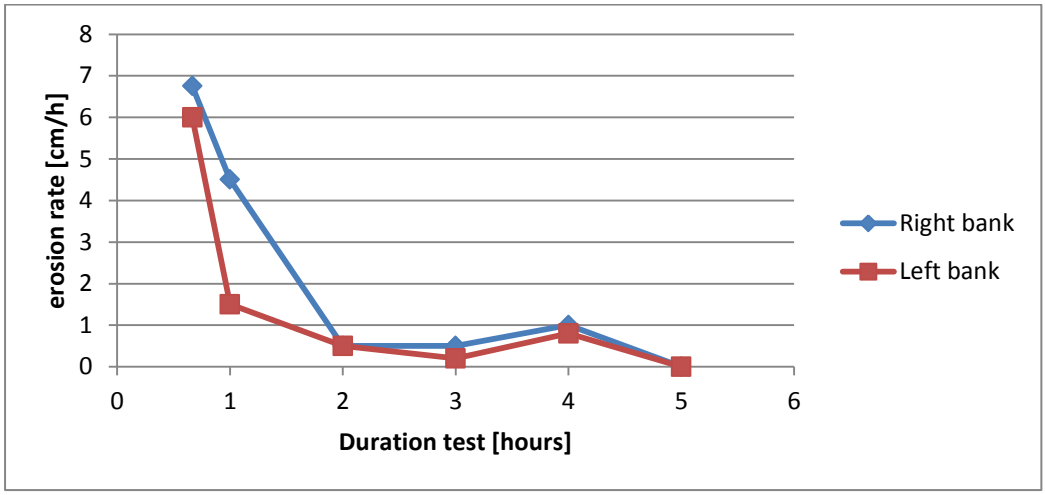


*Figure 4.3 – Erosion rate of test R04 in the middle of the widened reach.*

*Cohesive bank*

Test R11 could be compared to test R02 in which the same length of bank protection was removed. The erosion rate differed per location in longitudinal direction of the channel and therefore Figure 4.4 shows the eroded area per hour of test R11 and R02. The erosion rate of the cohesive bank in test R11 was significantly lower than the erosion rate of the non-cohesive bank in test R02 at the start of the tests. While the erosion rate was reduced exponentially in test R02, the erosion rate did not reduce as much in test R11. The cohesive bank needed more time to get to an equilibrium channel width, because the channel widening went slower.

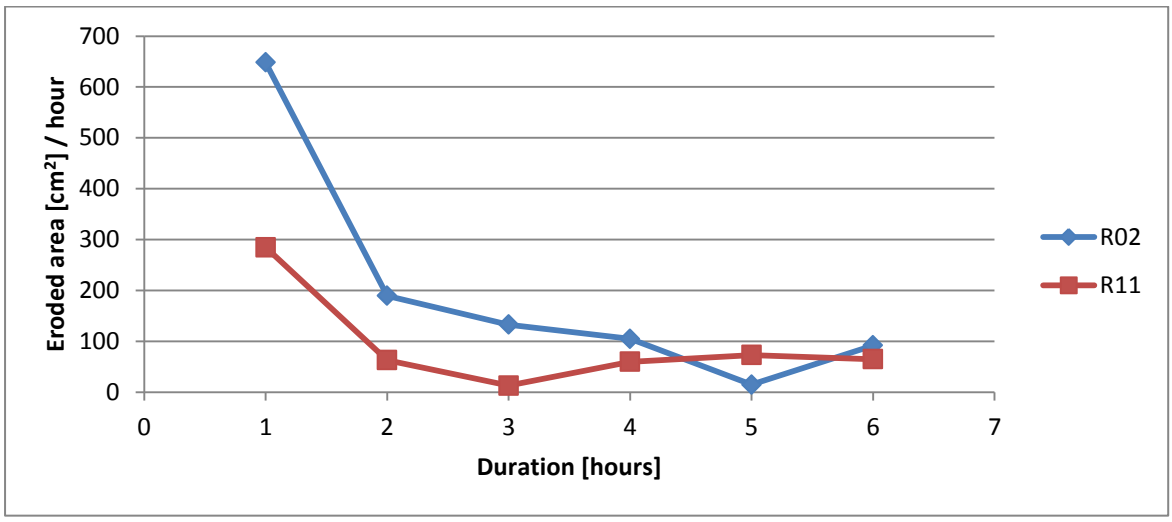


*Figure 4.4 – Eroded area per hour of tests R02 and R11.*

## 4.3 Mean bed level

The mean bed slope of the channel in the tests was 0.8 %. This was the initially constructed bed slope. The aim was that this bed slope was maintained on average over the entire channel length. The bed level upstream of the widened reach was not measured by the lasers and is therefore not included in the analysis.

Test R04 is used as an example to explain morphological responses due to widening of the main channel for all tests. When bars are formed in the widened reach it is harder to observe bed aggradation. Test R04 is therefore used as an example, since no bars formed in the widened reach of this test. Figure E.6 shows a detrended bed level of test R04. This figure shows that the bed level in the widened reach was higher elevated than the bed level downstream of the widened reach. This is a typical long term effect of a channel widening which is described in Section 2.3.1. If the width of the channel increases, the flow will decelerate when the discharge remains constant, since $u = Q/A$. Sediment transport will decrease, since the transport capacity and flow velocity are related by $S \sim u^b$. Sedimentation of the bed in the widened reach occurs, since more sediment is transported into this section than out of this section. This sedimentation will result in a higher elevated bed, compared to the non-widened reachs.

Furthermore, sedimentation of the bed in the widening resulted in different bed slopes in the channel. From the longitudinal bed profile in Figure E.6 the bed slope was estimated by linear regression. The final bed slope in the widened reach of test R04 was 0.44 % and downstream of the widened reach the bed slope was 0.96 %. Another example is test R06, in which the final bed slope in the widened reach was 0.62 % and downstream of the widened reach the bed slope was 0.91 %. In general could be seen from all tests that the final bed slope was decreased in the widened reach. This morphological response due to widening of the main channel is a short term response according to the theory presented in Section 2.3.1. It is expected that the bed slope in the widened reach will be eventually larger than the bed slope downstream of this section. Furthermore, the morphological response described in the theory in Section 2.3.1 is caused by an abrupt widening, whereas in the tests the widening was gradual. This gradual widening may cause a decreased bed slope, since the sedimentation will increase in downstream direction.

## 4.4 Scour hole

A scour hole developed at the downstream end of the widened reach in the tests where the bank protection was removed. The bank protection on the downstream end of the widened reach was constructed parallel to the main channel in most tests. The side of the bank protection was blocking the flow, thus forcing the flow to change its course locally. The flow was diverted in different directions and turbulent eddies were created near the bank protections side. This flow forced entrainment of sediment particles from the bed and bank. The bed was locally deepened and the bank eroded. This change in channel geometry induced even more turbulent eddies and particle entrainment that resulted in a positive feedback mechanism creating a scour hole. The dimensions of the scour hole increased quickly when the main flow force was directed on the downstream bank protection side. In most experiments this occurred when the channel widening, which moved in downstream direction, reached the downstream bank protection side of the widening. Afterwards, the scouring rate decreased in time.

The shape of the bank protection on the downstream end of the widened reach determined to a great extent the evolution of the scour hole. In test R12, R13 and R14 a different shape of the bank protection on the downstream end of the widened reach was constructed, which changed the scour hole evolution.

*Figure 4.5 – Scour hole in final bed topography of test R01 at the downstream end of the widened section. Red dye indicates deep bed profile.*

### 4.4.1 Perpendicular bank protection

In test R12 and R13, the maximum length of bank protection was removed such that the wooden walls that were perpendicular to the main channel marked the end of the widened reach (Figure 4.6). The bank line could therefore not move further downstream than this wall and no erosion was allowed behind the downstream bank protection. The flow at the downstream end of the widened reach was directed perpendicular to the wooden wall and was reflected into different directions creating turbulent eddies. These strong turbulent eddies entrained particles from the bed and bank and caused relatively large scour holes. Figure E.14 and Figure E.12 of test R12 and test R10 with an asymmetrical flow forcing show that the perpendicular bank protection forced a larger scour hole that resulted in a wider channel in the downstream half of the widened reach. A similar conclusion can be drawn from Figure E.15 and Figure E.8 when comparing test R13 with test R06 with a symmetrical flow forcing.

*Figure 4.6 – Scour holes in test R13 after 1.5 hours. The flow is from bottom to top of the figure.*

### 4.4.2 Curved bank protection


*Figure 4.7 –Scour hole in test R01 (left) at the straight bank protection with a diameter of 12 cm and a depth of 3,5 cm (flow from left to right). Scour hole in test R14 (right) at the curved bank protection with a width of 4 cm and a depth of 3 cm (flow from right to left).*

Figure D.2 shows that the downstream bank protection was constructed in a curved shape in test R14. The streamlined design of the bank protection resulted in a smooth transition from the widened reach to the main channel. This reduced turbulent eddies near the bank protection side and thus entrainment of sediment particles from the bed and bank. The dimensions of the scour hole in test R14 were therefore smaller in comparison with tests R01, which had a straight bank protection and a similar bank protection removal length (Figure 4.7). The scour hole size in test R01 increased in time, but the scour hole size decreased in test R14 in time. In test R01, turbulent eddies increased due to scouring of the bed and bank, thus creating a positive feedback mechanism that maintained the scour hole deepening and widening. In test R14, scouring of the bed and bank did not significantly increase turbulent eddies due to the streamlines shape of the bank protection that smoothens the flow patterns. The sediment transported from upstream could settle in the scour hole, since the flow velocity decrease due to deepening of the bed was larger than the flow velocity increase due to turbulent eddies in the scour hole. This resulted in a decreasing scour hole size in test R14 after two hours.

## 4.5 Bar formation

Bars were formed in the channel during the experimental tests. In Section 4.1, general experimental observations including bar formation were described. In this section, the

mechanisms leading to bar formation and the bars in the final bed topography are analysed per experimental test.

Bar formation is analysed on the basis of the final bed profiles and photos of bed topographies collected during the experiment. Detrended bed profiles of each experimental test are shown in Appendix E in Figure E.1 to Figure E.16. The bed profiles were detrended, since than the bar height is easier to read from the figure. Photos of the final bed topographies are also shown in these figures. The bar areas are drawn in these figures for which the bar height is indicated in two classes: high and low. Table E.1 shows the height classes for each bar that formed in the experimental tests.

The relative area of high bars, low bars, deep channel and floodplain are determined with a method explained in Appendix F. The area and height of bars that formed in the entire channel is an indicator to quantify the formation of bars. Characteristics of the individual bar(s) that formed in the widened reach are an indicator for diversity in bar height, size and location. In Section 4.5.1 to 4.5.6, the total area of low and high bars in the entire channel and individual bar heights, areas and locations in the widened reach are compared between the tests. Bar area is a better indicator for the size of the bars than bar wavelength thus in the description is focussed on bar area. The bar wavelength, bar areas, bar location and maximum bar height of the bars that formed in the channel are given in Table E.1 in Appendix E for each experimental test.

In Table E.1 the bar type is indicated with the terminology from Duró et al. (2015) as forced, free or hybrid. The temporal evolution of the bars to determine the bar type was analysed with the images taken at an interval of 15 minutes from the camera above the flume. In areas with large water depths indicating a deep channel, dunes covered the bed and could be observed as small waves in the water level. The shallow areas indicating bars were not covered with these waves. Furthermore, the bar wave length and shape was analysed in the final photos taken of the bed profile, since free bars have a different wave length and shape than forced bars. Migrating bars have smaller wavelengths than non-migrating bars (Olesen, 1983; Eekhout et al., 2013). The shape of migrating bars is different from non-migrating bars as can be seen in numerical models from Duró et al., 2015.

Figure D.1 and Figure D.2 in Appendix D show the setup of each test in which the length and location of bank protection removal is shown.

### 4.5.1 Fixed banks

In test P01 and P02 was no bank protection removed, so no lateral erosion was allowed. Test P01 and P02 both had fixed banks, but test P01 had a symmetrical flow forcing upstream and test P02 an asymmetrical flow forcing since a groyne was located upstream.

*Bar formation mechanism and bar area*

According to the bar theory of Crosato and Mosselman (2009), the channel conditions in test P01 and P02 corresponded with the first hybrid bar mode that would result in alternate bars. The system is in therefore in the morphodynamic instability range in both tests. In test P01 free, migrating bars were formed. Free bars arise within the morphodynamic instability range of the system when an infinitesimally small perturbation of the flow or bed level is present. In the final bed topography low alternating bars were present. The deep channel area was not at a fixed position during the test, which indicated migrating bars.

In test P02 a forced bar and hybrid bars were formed. The groyne in test P02 locally reduced the channel width. If the width of the channel is reduced, the flow will accelerate when the discharge and water depth remain constant, since $u = Q/Bh$. Sediment transport will increase, since the transport capacity and flow velocity are related by $S \sim u^2$. The channel bed was deepened in the narrow reach next to the groyne, since more sediment is transported out of this section than into this section. On the downstream side of the groyne, was a stagnant zone created. The streamlines were forced around the groyne and reached the right wall again at a location of about 1.5 metres downstream of the groyne. Due to the reduction in flow velocity, sedimentation occurred downstream of the groyne. A forced bar was formed downstream of the groyne and the bar wavelength increased in time. Hybrid bars were formed downstream of the forced bar, since they arise from morphodynamic instability and the presence of forcing. The main flow was directed towards the right wall downstream of the forced bar. The flow velocity on the right side was larger than on the left side of the channel. The channel was deepened on the right side of the channel, since more sediment was transported on this side due to the higher flow velocity. On the left side of the channel a hybrid bar developed, due to deposition of sediment in this lower flow velocity area. In a similar way was a second hybrid bar was formed on the right side of the channel downstream of the first hybrid bar.

Table F.1 shows that the relative low bar area for test P01 and P02 was respectively 6.8 % and 11.8 %.

*Comparison theoretical bar wavelength*

The average wavelength of hybrid bars in test P02 is 1.7 metres. The theoretical hybrid bar wavelength calculated with equation (4) is 1.6 metres (Crosato and Mosselman, 2009). It can therefore be concluded that the hybrid bar wavelength in the experiment corresponds well with the theory.

Figure 4.8 shows that the choice of the degree of nonlinearity of sediment transport versus depth-averaged flow velocity b = 10 recommended by Crosato and Mosselman (2009) for gravel-bed rivers agrees well with the experimental results.

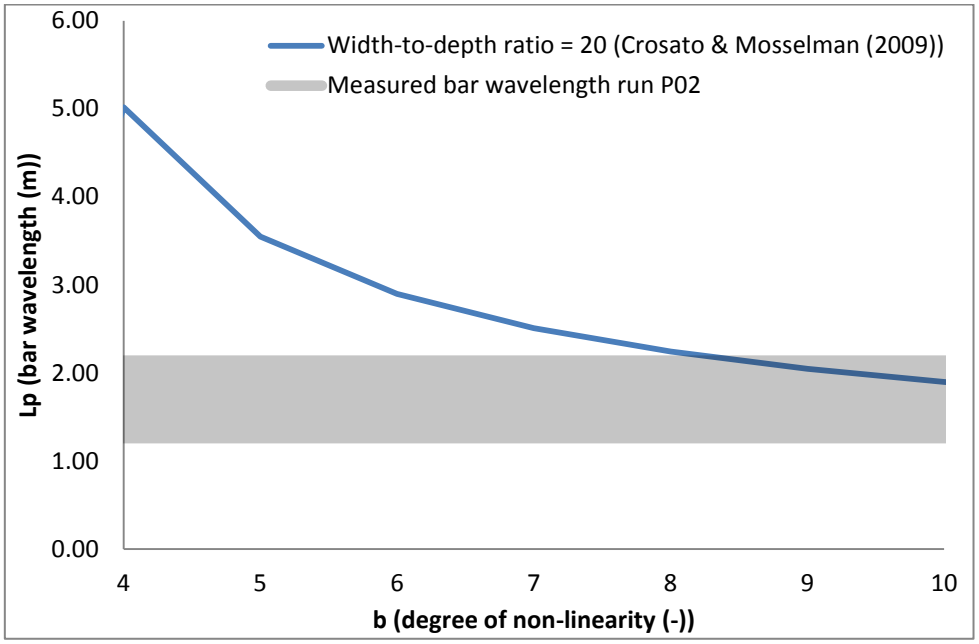


*Figure 4.8 - Comparison of measured hybrid bar wavelength in test P02 (Table E.1) and predicted hybrid bar wavelength (equation (4)) related to the degree of non-linearity b.*

### 4.5.2 Length of bank protection removal

In tests R01 to R06 the length of the bank protection removal length varied between three to nine times the width of the main channel. In R01, R02 and R03 the bank protection was removed on one side of the channel with a length of three, six and nine times the channel width respectively. In test R04, R05 and R06 the bank protection was removed on both sides of the channel with a length of three, six and nine times the channel width respectively.

*One side removal of bank protection*

Bar formation mechanism

When the bank protection was removed on one side of the channel, lateral erosion moved the bank line to the right. The streamlines of the flow curved to the right side of the channel, due to the moved bank line. The streamlines were converted on the right side of the channel and diverted on the left side of the channel that resulted in an increased flow velocity on the right side compared to the left side. Sediment transport was therefore increased on the right side of which caused deepening of the channel, whereas sediment transport was decreased on the left side which caused deposition of sediment. This resulted in the formation of a forced bar on the left side of the channel. The flow is curved around this bar and thus the flow velocity downstream of the bar on the left side of the channel increased and flow velocity decreased on the right side of the channel. In a similar way as the first bar, a decreased sediment transport resulted in the formation of a bar on the right side of the channel. This process was repeated until the downstream end of the flume and resulted in the formation of three to four bars. In test R02 and R03 with a removed bank protection length of respectively six and nine times the channel width, the second bar from upstream was formed in the channel widening. These channel widenings were of sufficient length and width to significantly decrease the flow velocity, such that a high bar formed in the widened reach. In test R01, the widened reach was smaller than in test R02 and R03, which resulted in flow velocities that transported enough sediment such that no bar was formed.

Final bar formation in widened reach

Table E.1 shows that a bar with a relative bar area of 2.9 % and a maximum bar height of $0.35*h_0$ was formed upstream of the widened reach when a bank protection length of three times the channel width was removed. A bar with a relative bar area of 5.9 % and a maximum height of $0.65*h_0$ was formed in the widened reach on the right side of the channel when a bank protection with a length of six times the channel width was removed. A bar with a relative bar area of 9.6 % and a maximum height of $0.8*h_0$ was formed in the widened reach on the right side of the channel when a bank protection with a length of nine times the channel width was removed. The relative bar area and maximum bar height thus increased in the widened reach when a longer length of bank protection was removed.

Final bar formation in entire channel

Table F.1 shows that the relative low bar area for a removed bank protection length of three, six and nine times the channel width is 9.9 %, 5.2 % and 6.4 %, respectively. From Table F.1 can be obtained that the relative high bar area for a removed bank protection length of three, six and nine times the channel width is 0.0 %, 7.2 % and 9.6 %, respectively. Figure 4.9 shows the relative size of the floodplain area, deep channel area, high bar area and low bar area for a length of bank protection removal of zero, three, six and nine times the channel width. From this figure can be seen that the removal of a bank protection on one side of the channel with a length of three, six or nine times the channel width increases the bar area compared to no removal of bank protection. The total bar area increased when a longer length of bank protection was removed on one side of the channel up to nine times the channel width.

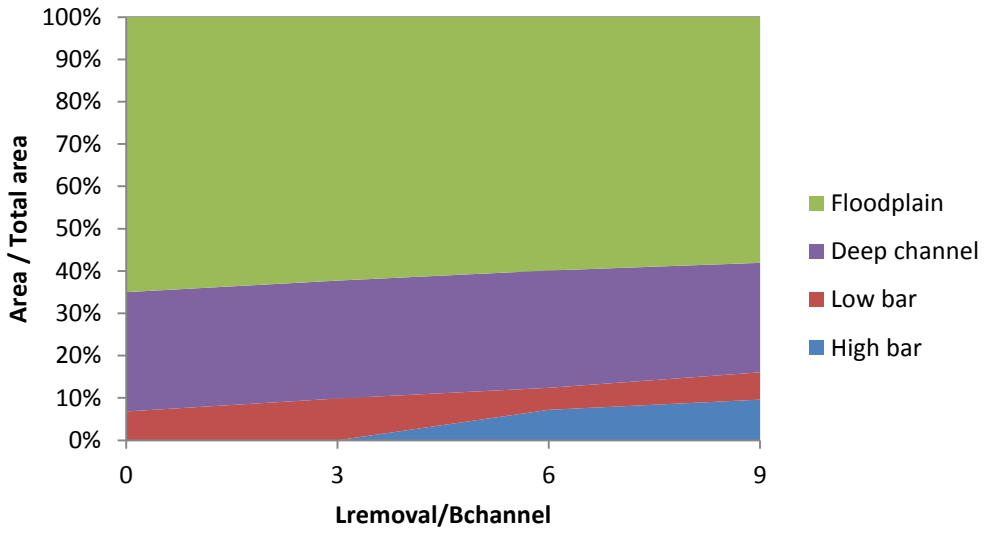


*Figure 4.9 – One side removal of bank protection: dimensionless area of the floodplain, deep channel, low bars and high bars in tests P01, R01, R02 and R03 related to the dimensionless length of bank protection removal.*

*Two sides removal of bank protection*

Bar formation mechanism

When the bank protection was removed on two sides of the channel, lateral erosion caused the channel to widen in this reach. The streamlines of the flow were diverted in the widened reach, which resulted in a decrease of the flow velocity. Sediment transport was therefore decreased in the widening. This caused deposition of sediment in the widened reach at a location where the

flow velocity was reduced most. Since the highest flow velocities were in the main channel, bars formed on one or two sides of the main channel in the widened reach. The flow was curved around the bar(s) and flow velocity increased due to the converged streamlines. This cause an increase in sediment transport and deepening of the channel. The deeper channel was curved around the largest bar in the widened reach an on the opposite side of the channel the flow velocity was decreased. This reduced sediment transport which resulted in the formation of a bar. This process was repeated until the downstream end of the flume and resulted in the formation of three to four bars.

Final bar formation in widened reach

Table E.1 shows that a bar with a relative bar area of 2.9 % and a maximum height of $0.15*h_0$ was formed in the widened reach when a bank protection length of three times the channel width was removed. A bar with a relative bar area of 6.5 % and a maximum height of $0.6*h_0$ was formed in the widened reach on the right side of the channel when a bank protection with a length of six times the channel width was removed. Two bars with a relative bar area of 7 % and 7.7 % with both a maximum height of $0.9*h_0$ were formed in the widened reach on both sides of the channel when a bank protection with a length of nine times the channel width was removed. The relative bar area, maximum bar height and number of bars in the cross-section thus increased in the widened reach when a longer length of bank protection was removed.

Final bar formation in entire channel

Table F.1 shows that the relative low bar area for a removed bank protection length of three, six and nine times the channel width is 5.8 %, 7.1 % and 3.9 %, respectively. Table F.1 shows that the relative high bar area for a removed bank protection length of three, six and nine times the channel width is 2.2 %, 6.5 % and 15.9 %, respectively. Figure 4.10 shows the relative size of the floodplain area, deep channel area, high bar area and low bar area for a length of bank protection removal of zero, three, six and nine times the channel width. From this figure can be seen that the removal of a bank protection on two sides of the channel with a length of three, six or nine times the channel width increases the bar area compared to no removal of bank protection. The total bar area increased when a longer length of bank protection was removed on both sides of the channel up to nine times the channel width.

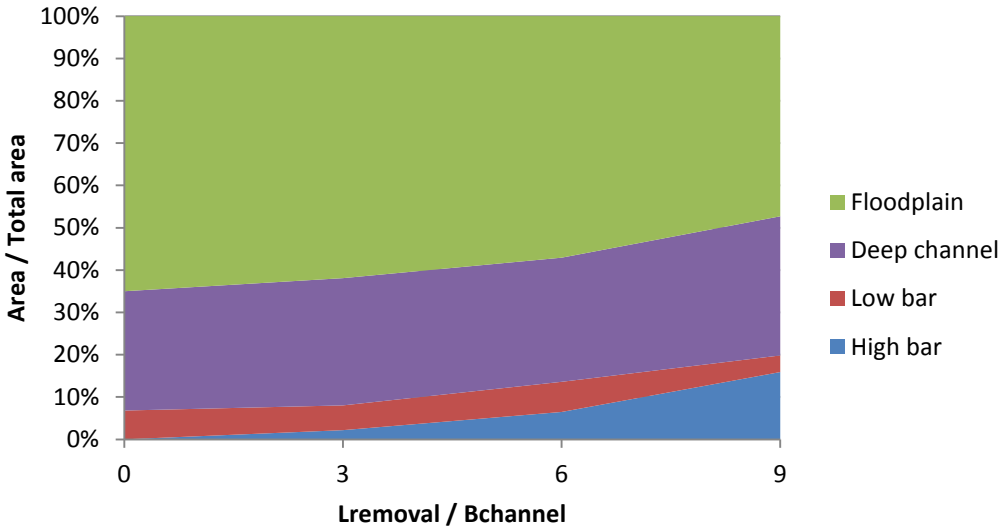


*Figure 4.10 – Two sides removal of bank protection: dimensionless area of the floodplain, deep channel, low bars and high bars in tests P01, R04, R05 and R06 related to the dimensionless length of bank protection removal.*

### 4.5.3 Location of bank protection removal

In test R03 and test R07 the same lengths of bank protections were removed, but at different locations. In test R03 the bank protections were removed on the right side of the channel and in test R07 the bank protections were removed in three different sections on both sides of the channel.

*Bar formation mechanism*

The mechanisms contributing to the formation of bars in test R03 are described in Section 4.5.2. In test R07, the channel widened in the sections where the bank protection was removed due to lateral erosion of the bank. The widening caused the streamlines to divert and the flow velocity decreased. Due to a decreased sediment transport on the left side of the channel where the flow velocity was reduced most, sediment was deposited and a bar formed. The flow was forced around the bar and convergence of the streamlines increased the flow velocity. More sediment was transported and the channel deepened. The deep channel was located in the widened section on the right side of the channel, since the bar on the left side forced the flow around the bar. The flow curved to the left bank downstream of the bar, since the bank line shape moved the flow to the left side. The flow velocity was therefore increased on the left side of the channel in the downstream widened section compared to the right side of the channel. The left side of the widened section deepened, whereas on the right side a bar was formed. This bar forced curvature of the flow and in a similar way two more bars were formed downstream in the channel.

*Final bar formation in widened reach*

Table E.1 shows that a bar with a relative bar area of 3.5 % and a maximum height of $0.5*h_0$ was formed in the upstream widened reach of test R07 on the left side of the channel. A second bar with a relative bar area of 1.6 % and a maximum height of $0.7*h_0$ was formed in the downstream widened reach of test R07 on the right side of the channel. In test R03, a bar with a relative bar area of 9.6 % and a maximum height of $0.8*h_0$ was formed in the widened reach on the right side of the channel. In test R03, the relative bar area was thus longer and the maximum

bar height was higher compared to the bars formed in test R07. The smaller bar areas in test R07 might be related with the smaller length of the widened reach that cause curvature of the flow over a shorter lengths. Two bars formed in the widened reach in test R07, whereas only one bar formed in the widened reach in test R03.

*Final bar formation in entire channel*

Table F.1 shows that the relative area of low bars for test R03 and R07 is respectively 6.4 % and 3.1 %. The relative area of high bars for test R03 and R07 is respectively 9.6 % and 6.6 %. Figure 4.11 shows the relative size of the floodplain area, deep channel area, high bar area and low bar area for test R03 and R07. The total bar area in test R03 is larger than in test R07.

Test R08 and R09 are included in Figure 4.11, since the same length of bank protection is removed. The formation of bars in test R08 and R09 is described in Section 4.5.4.

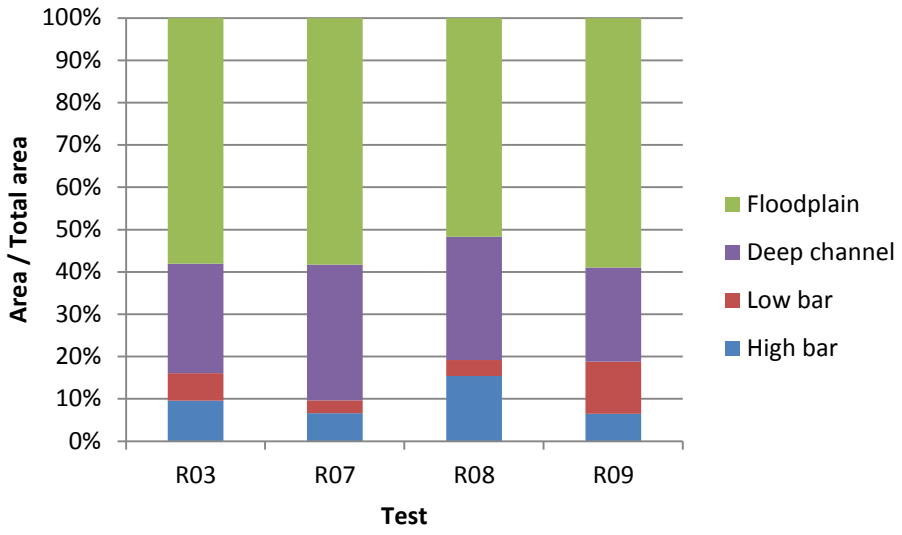


*Figure 4.11 – One side bank protection removal with length L/B=9: dimensionless area of the floodplain, deep channel, low bars and high bars in tests R03, R07, R08 and R09.*

### 4.5.4 Asymmetrical flow forcing

In test R08, R09 and R10, a groyne is located one metre upstream of the widened reach on the right side of the channel. This groyne forces the flow asymmetrically into the channel. In test R08 and R09, a bank protection length of nine times the channel width is removed on respectively the right and left side of the channel. In test R10, a bank protection length of nine times the channel width is removed on both sides of the channel.

*Bar formation mechanism*

At the location of the groyne the streamlines were converged and the flow was accelerated. Sediment transport was increased and the channel was deepened on the left side of the groyne. Sediment was deposited downstream of the groyne on the right side of the channel, due to a decrease in flow velocity and thus sediment transport. This resulted in the formation of a forced bar downstream of the groyne. The flow was curved around the forced bar such that the highest flow velocities were at the right side of the channel where the flow force erodes the bank in test R08 and R10. Due to widening of the channel in test R08 and R10, the streamlines were diverted

and the flow was decelerated in the middle of the widened reach. This resulted in a decreased sediment transport and a bar was formed in the middle of the channel in test R08 and R10.
In test R09, the curved flow around the forced bar was directed to the bank protection, so the highest flow velocities remained at the right side of the channel. On the left side the bank was slightly eroded by the lower flow velocities. The reach was widened and the flow decelerated more on the left side of the channel. Due to the decrease in flow velocity on this side, a bar was formed on the left side in the widened reach. The bar in the widened reach forced the curvature of the flow and the formation of a bar downstream.

*Final bar formation in widened reach*
Table E.1 shows that a bar with a relative bar area of 11.6 % and a maximum height of $0.8*h_0$ was formed in the widened reach of test R08 on the right side of the channel. In test R09, a bar with a relative bar area of 6.7 % and a maximum height of $0.75*h_0$ was formed in the widened reach on the left side of the channel. The maximum bar heights in tests R08 and R09 were approximately similar, but the relative bar area is larger in test R08 than in test R09. Figure E.10 and Figure E.11 show that the bar in test R08 is wider than the bar in R09.

In test R10, a bar with a relative bar area of 12.6 % and a maximum height of $0.9*h_0$ was formed in the widened reach in the middle of the channel. The bar wavelength in test R10 is smaller than the bar wavelengths in test R08 and R09. A reason might be that large erosion holes on both sides of the channel in test R10 disturbed the morphology (Figure E.12).
Test R10 was compared with test R06 in which the same length of bank protection was removed. Test R10 had an asymmetrical flow forcing and test R06 a symmetrical flow forcing. In test R10, one bar was formed in the widened reach with a relative bar area of 12.6 % and in test R06, two narrower bars with relative bar areas of 7 % and 7.7 % were formed in the widened reach. The maximum bar heights were similar in both test. In test R10, the groyne forced the flow asymmetrically into the widened reach and in the middle of the widened reach a bar was formed. In test R06, the symmetrical flow went straight through the widened reach and therefore bars formed on the sides of the channel where the flow velocity was reduced.

*Final bar formation in entire channel*
Table F.1 shows that the relative area of low bars for test R08, R09 and R10 were respectively 3.7 %, 12.8 % and 4.0 %. The relative area of high bars for R08, R09 and R10 were respectively 15.4 %, 6.7 % and 17.0 %. Figure 4.12 shows the relative size of the floodplain area, deep channel area, high bar area and low bar area for test P02, R08, R09 and R10 with an asymmetrical flow forcing. From this figure can be seen that the removal of a bank protection on one or both sides of the channel with a length of nine times the channel width increases the total bar area compared to no removal of bank protection. The total bar area was approximately equal for a bank protection removal on the right side, left side or both sides of the channel. The high bar area was, however, smaller when the bank protection was removed on the left side of the channel.

The bar areas of test R08, R09 with an asymmetrical flow forcing was compared to the bar area of R03 with a symmetrical flow forcing and the same length of bank protection removal. Figure 4.11 shows that the total bar area is larger when the flow forcing is asymmetrical than when the flow forcing is symmetrical. The high bar area is, however, smaller in test R09 with an asymmetrical flow forcing compared to the high bar area in test R03 with a symmetrical flow forcing.

Test R10 was compared with test R06 in which the same length of bank protection was removed. Test R10 had an asymmetrical flow forcing and test R06 a symmetrical flow forcing. The total bar area in test R06 and R10 was approximately similar.

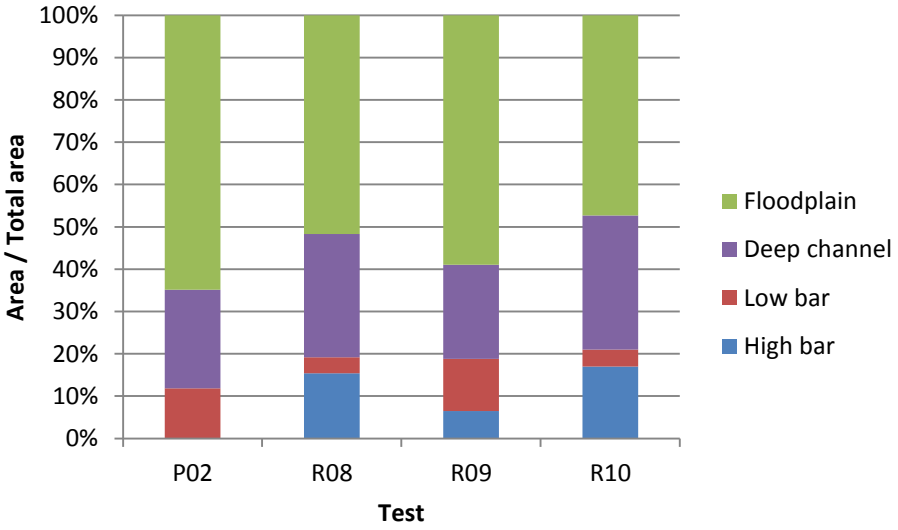


*Figure 4.12 –Bank protection removal with asymmetrical flow forcing: dimensionless area of the floodplain, deep channel, low bars and high bars in tests P02, R08, R09 and R10.*

### 4.5.5 Channel bank cohesion

In tests R02 and R11 the same length of bank protections were removed on the right side of the channel, but the erodible banks had a different cohesiveness. In test R02 the erodible bank was non-cohesive and consisted of bed material as in all other tests. The erodible bank in test R11 consisted of 80% from bed material and of 20% from silica flour, which led to a cohesive bank.

*Bar formation mechanism*

In section 4.5.2 was described how bars were formed in test R02. In test R11, bars were formed in a similar way.

*Final bar formation in widened reach*

Table E.1 shows that a bar with a relative bar area of 4.7 % and a maximum height of $0.4*h_0$ was formed in of the widened reach of test R11 on the right side of the channel. In test R02, a bar with a relative bar area of 5.9 % and a maximum height of $0.65*h_0$ was formed in the widened reach on the right side of the channel. In test R02, the relative bar area was larger and the maximum bar height was higher compared to test R11. Figure E.4 and Figure E.13 show that the bar is wider in test R02 than in test R11. This might be due to a larger widened reach in test R02 compared to test R11. The flow deceleration in the widened section in test R02 was therefore larger than in the widened reach of test R11. This resulted in a lower sediment transport and thus increased sediment deposition in the widened section of test R02 compared to test R11.

*Final bar formation in entire channel*

Table F.1 shows that the relative area of low bars for test R02 and R11 were respectively 5.2 % and 12.6 %. The relative area of high bars for R02 and R11 were respectively 7.2 % and 0.0 %. Figure 4.13 shows the relative size of the floodplain area, deep channel area, high bar area and low bar area for test R02 and R11. The total bar area is approximately equal in both tests, but the high bar area is larger in test R02 than in test R11.

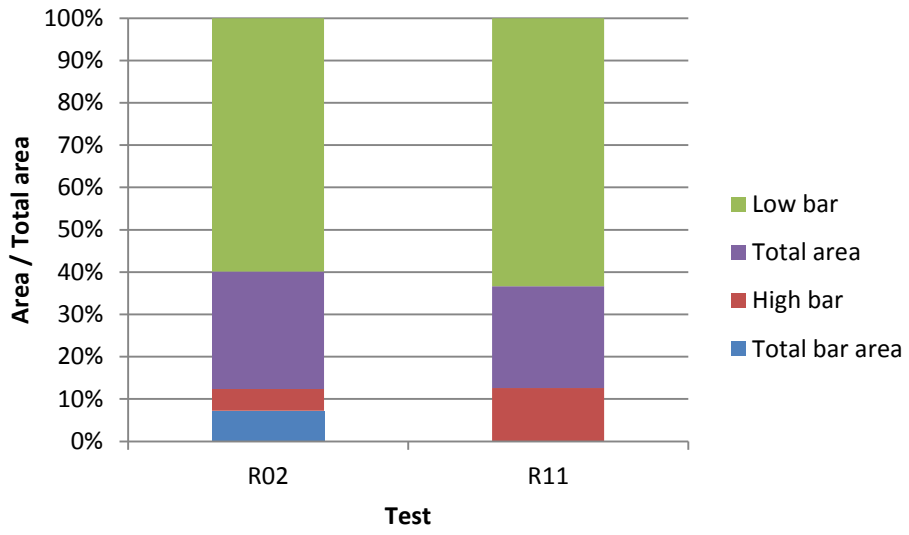


*Figure 4.13 - Dimensionless area of the floodplain, deep channel, low bars and high bars in tests R02 and R11 with respectively a non-cohesive and cohesive bank.*

### 4.5.6 Bank protection shape

The shape of the bank protection at the downstream end of the widened reach was parallel to the main channel in the tests except from test R12, R13 and R14. In test R12 and R13, the bank protection at the downstream end of the widened reach was perpendicular to the main channel and in test R14 the bank protection was curved. In test R12 and R13, on both sides of the channel a bank protection length of nine times the channel width was removed. Test R12 had an asymmetrical flow forcing and test R13 had a symmetrical flow forcing. In test R14, the flow was symmetrical upstream and a bank protection length of three times the channel width was removed.

*Bar formation mechanism*

The mechanisms contributing to the formation of bars in test R12 were similar to test R10. In test R12 the channel widening was larger than in test R10, due to the perpendicular bank protection at the downstream end of the widened reach and the longer removal of bank protection. This resulted in a low sediment transport in a wider area, due to a flow deceleration. The bar that formed in the widened reach in test R12 was therefore larger than in test R10.

In test R13, the deep channel was initially straight and on both sides the flow velocity was decreased in the widened reach. The bank eroded faster on the left side of the channel than on the right side, due to a small perturbation in the flow or bed. The flow velocity was most reduced on the left side of the channel and therefore a bar was formed. The flow velocity increased on the right side of the channel when the bar formed on the left side in the widened reach. This resulted in an increased sediment transport on the right side of the channel which deepened the channel. In test R06, the channel widening was more symmetrical than in test R13 and therefore on both sides of the channel bars were formed.

The mechanisms contributing to the formation of bars in test R14 were similar to test R01. The experimental setup was similar except from the bank protection shape downstream of the widening. The curved bank protection in test R14 decreased the scour hole in the bed, but did not significantly change the flow or morphology in the remaining part of the channel.

*Final bar formation in widened reach*

Table E.1 shows that a bar with a relative bar area of 16.1 % and a maximum height of $0.9*h_0$ was formed in the widened reach of test R12 in the middle of the channel. In test R13, a bar with a relative bar area of 11.4 % and a maximum height of $0.95*h_0$ was formed in the widened reach in the middle of the channel. The maximum bar height was approximately similar in test R12 and R13, but the relative bar area was larger in test R12. Figure E.14 and Figure E.15 show that the bar in test R12 is wider than in test R13.

Table E.1 shows that a bar with a relative bar area of 1.9 % and a maximum height of $0.3*h_0$ was formed upstream of the widened reach of test R14 on the left side of the channel. Test R14 can be compared with test R01, for which the same length of bank protection was removed. The relative bar area and maximum bar height of the bar formed upstream of the widened reach were slightly larger in test R01 compared to test R14.

*Final bar formation in entire channel*

Table F.1 shows that the relative area of low bars for test R12, R13 and R14 was respectively 3.6 %, 3.3 % and 8.1 %. The relative area of high bars for R12, R13 and R14 was respectively 19.7 %, 11.4 % and 0.0 %. Figure 4.13 shows the relative size of the floodplain area, deep channel area, high bar area and low bar area for test R12, R13 and R14. The total bar area is larger in test R12 than in test R13. The total bar area is approximately similar in test R14 and test R01.

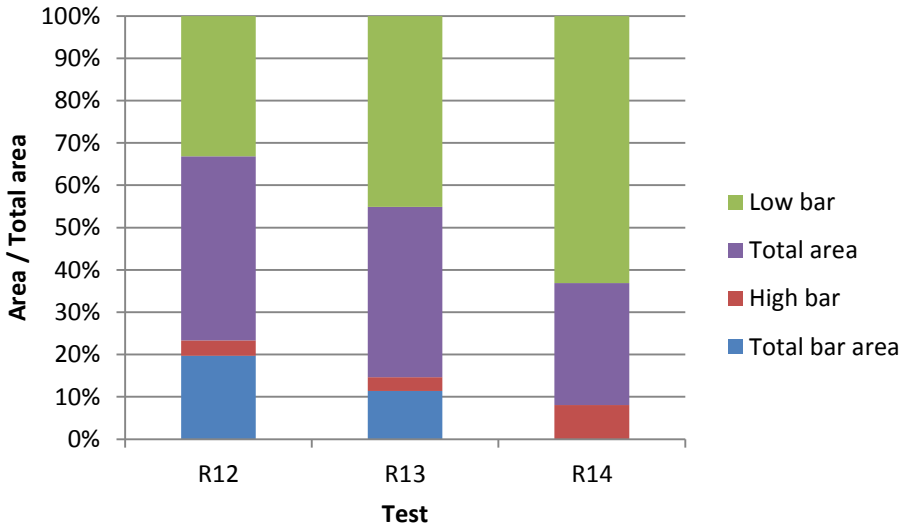


*Figure 4.14 - Dimensionless area of the floodplain, deep channel, low bars and high bars in tests R12, R13 and R14 with a different bank protection shape at the downstream end of the widened reach.*

### 4.5.7 Channel widening related to bar formation

A relation between the channel widening and bar formation in the widened reach was determined from the experimental tests. In general, it was observed that the bar area increased for a larger channel widening. Furthermore, it was observed that in general the maximum bar height in the widened reach increased for a larger channel widening. The channel widening could be quantified for each experimental test by calculating the eroded bank area with a method described in Appendix F. Table F.2 shows the eroded bank area for each test.

*Bar formation in widened reach*

Figure 4.15 shows a scatter plot of the bar area in the widened reach and the eroded bank area, i.e. area of the channel widening, that was determined for each test individually. No distinction is made between a low bar and a high bar. The bar areas were summed up in case more than one bar was formed in the widened reach. The total area of the bar was used when the bar was formed partly in the widened reach and partly downstream or upstream of this reach. Figure 4.15 shows an increase in bar area in the widened reach for an increase in eroded bank area.

Furthermore, the channel widening was related to the maximum bar height in the widened reach. Figure 4.16 shows a scatter plot of the maximum bar height in the widened reach and the eroded bank area that was determined for each test individually. Figure 4.16 shows an increase of the maximum bar height in the widened reach for an increase in the eroded bank area.

The increase in bar area and maximum bar height is caused by the increase in channel widening. Channel widening results in a decrease in flow velocity. Consequently, sediment transport is decreased in the widened reach. This increases sediment deposition in the widened reach and this results in an increased bar area and maximum bar height.

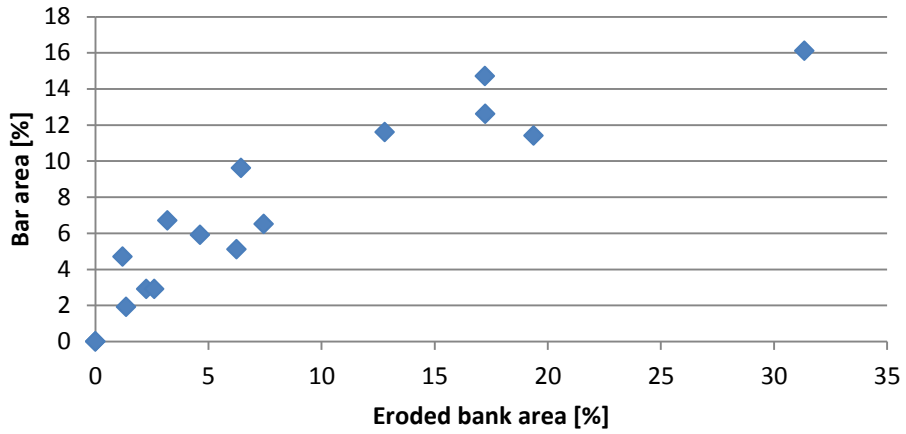


*Figure 4.15 - Scatter plot of bar area in widened reach and eroded bank area, i.e. area of channel widening, based on all experimental tests. No distinction is made between a low bar and a high bar.*

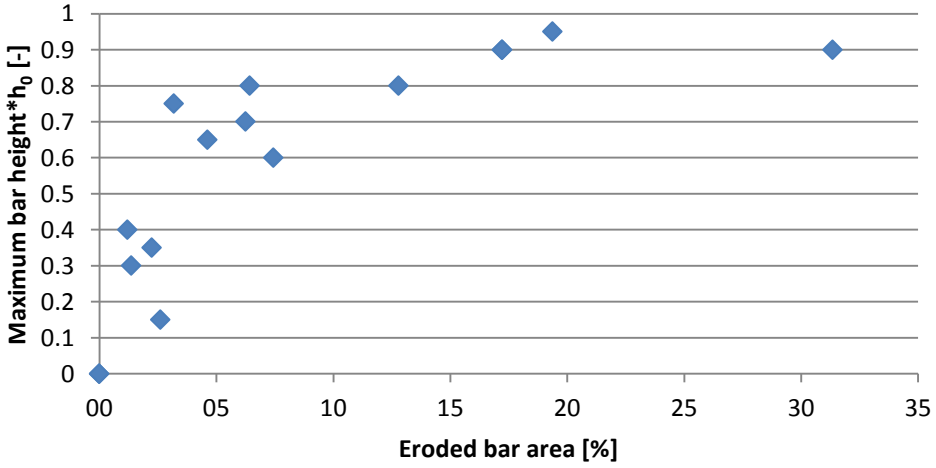


*Figure 4.16 - Scatter plot of maximum bar height in widened reach and eroded bank area, i.e. area of channel widening, based on all experimental tests.*

*Bar formation in entire channel*

Figure 4.17 shows a scatter plot of the bar area in the entire channel and the eroded bank area, i.e. area of the channel widening, that was determined for each test individually. The bar area is subdivided in low bar area, high bar area and total bar area. The total bar area is the sum of the low bar area and high bar area.

Figure 4.17 shows that total bar area and high bar increases for an increase in eroded bank area. Low bar area decreases for an increase in eroded bank area. The decrease in low bar area might be due to the increase in bar area for an increase in eroded bank area, which causes bars to be categorized as a high bar instead of low bar.

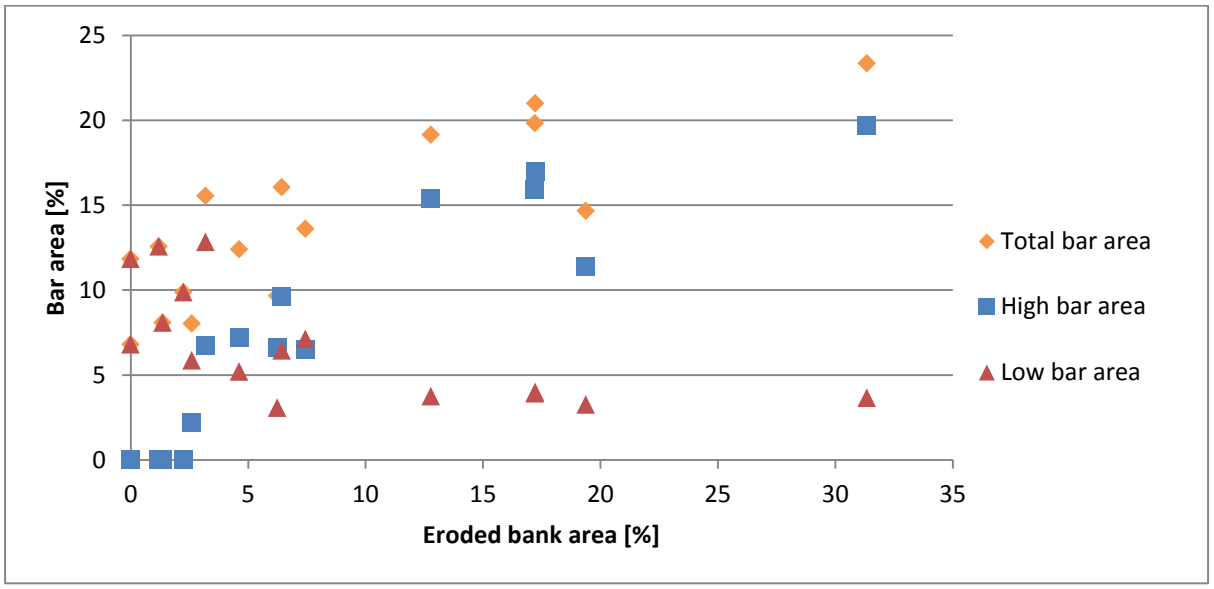


*Figure 4.17 –Scatter plot of bar area and eroded bank area, i.e. area of channel widening, based on all experimental tests. The bar area is divided in low bar area and high bar area and the sum is the total bar area.*

# 5 Discussion

## 5.1 Context of research

### 5.1.1 Meaning of research

There is a lack of knowledge about bar formation related to the length and location of the removal of bank protection and the effect of an asymmetrical forcing. The method of this research to gain more knowledge on bar formation related to bank protection removal included laboratory mobile-bed experiments in a flume at the Fluid Mechanics Laboratory of Delft University of Technology. The results of the experiment showed that the unprotected banks laterally eroded, the mean bed level raised in the widened reach, scour holes developed at the downstream end of the widened reach and bars formed in the channel. It was found that different geometrical variables of a bank protection removal, such as the length, location and asymmetrical flow forcing, resulted in a different bar formation. These findings are an important addition to the present literature on bar formation. Section 5.1.2 further elaborates on the new findings from this study that can be added to the present literature.

Construction of riverbank protections in the past centuries resulted in disappearance of important river features for flora and fauna and reduction of the ecological river quality. To improve the ecological river condition, river reaches should be restored. Piégay et al. (2005) state that river manager demands exist to recreate meanders, to remove bank protection to re-establish the channel movement and the consequential complex riparian vegetation patches. They provided an overview of the erodible corridor concept, focusing on the provision of guidelines for applying the concept in practice. This research is a valuable addition to these guidelines for applying the erodible corridor concept in practice, since it provides river restoration practisers a guidance on how to design a bank protection removal such that it enhances bar formation for habitat diversity. This study specifically addresses what length of bank protection should be removed, at what location the bank protection should be removed and whether to construct a groyne upstream to enhance bar formation for habitat diversity.

### 5.1.2 Research related to present literature

Only a laboratory experiment of Veldt (2015) can be found that scientifically explores the effects on the river bed topography of modifying a fixed river reach into a reach where the banks can erode freely for a limited reach. This laboratory experiment had experimental conditions that were different from the experiments in this research. The experiment of Veldt (2015) focused on bank protection removals on one side of the channel with a symmetrical and asymmetrical flow forcing. The number and location of bars in the experiment of Veldt (2015) were different from the final formation of bars in the experiment in this research, which might be due to the difference in experimental conditions. The shape of the eroded bank and formation of scour holes at the downstream end of the widened reach was approximately similar in the experiment of Veldt (2015) and in the experiment of this research. This research included experiments to investigate formation of bars with bank protection removal on both sides of the channel with a limited length, which has not been investigated by Veldt (2015). Another new experiment to investigate formation of bars was a bank protection removal with limited lengths at three different locations.

Duró et al. (2015) addressed effects of relatively large channel widening and narrowing of infinite length on the formation of bars with a numerical model in Delft3D. The model results of

Duró et al. (2015) showed for most simulations that central bars were formed immediately at the start of the widened reach. This formation of central bars in the widened reach was also observed in the experiments of this research. Duró et al. (2015) found that the location where bars form and their final shape depend on the symmetry-asymmetry of the inflow with respect to the symmetric-asymmetric character of the bars. In this research, it was found that the height, location and shape of the bars in the widened reach depended on the symmetry-asymmetry of the inflow as well.

One bar in each cross-section was formed in the main channel of the flume which agrees with the bar mode of one that was calculated with the physics based predictor of Crosato and Mosselman (2009). In the widened reach, however, the physics based predictor overestimated the number of bars. Maximum two bars formed in a cross-section, while according to the theory the bar mode was larger than two in some experimental tests due to widening of the channel.

The results showed that the bed level in the widened reach was higher elevated than the bed level downstream of the widened reach. This typical long term effect of a channel widening is shown in Figure 2.3 (Van der Mark et al., 2012) and is described in Jansen (1979) and De Vries (1975). Furthermore, the results showed that the final bed slope was decreased in the widened reach. This is a short term morphological response of a river reach, due to widening of the main channel and agrees with Figure 2.3 of Van der Mark et al., 2012.

The non-cohesive bank material was detached and entrained grain by grain through fluvial erosion, which agrees with the theory for non-cohesive banks of Thorne and Osman (1988). According to Thorne and Osman (1988) cohesive bank material is usually entrained by aggregates or crumbs or the bank is eroded by mass failure. In the experiment in this research, however, it was observed that the grains were entrained grain by grain through fluvial erosion. The results of most experimental tests showed that the eroded bank line moved downstream. This development agrees with the downstream meander migration observed in field and laboratory investigations by many authors (e.g. Odgaard, 1987).

### 5.1.3 Spatial and temporal scale

This study focussed mainly on the spatial scales of the morphological processes due to the removal of bank protection. In this section, the temporal scale of the morphological processes due to the removal of bank protection is discussed as well.

The timescale of bar formation in the small scale flume was in the order of several hours and depended mainly on the morphological development of the longitudinal profile. In rivers, however, timescale for the development of bars will be larger due to the larger spatial scale in a river. In rivers are two main processes that determine the timescale of the formation of (stable) river bars (Mosselman, 2017); morphological development of the longitudinal river profile and establishment of bar vegetation.

The river reach is the key spatial scale, since river features responds to influences from larger spatial scales and interactions and feedback between geomorphic and hydraulic units and smaller river elements such as plants, large wood and sediment particles within the reach (REFORM, 2015). The removal of bank protection in a river reach causes bank erosion and thereby widening of the river reach. The longitudinal river profile will adapt to the new river width with on a certain temporal scale. Figure 5.1 shows that a reach scale riverbank protection removal (length > 20*B) is likely to persist over an indicative timescale of ten to hundred years. A river bar is a geomorphic unit (length 0.1 – 20*B) with an indicative timescale of one to ten

years. The formation of bars depend on the width-to-depth ratio which changes due to adaptation of the longitudinal bed profile to the river widening.

Establishment of vegetation is dependent on the development time of the vegetation. Pioneer vegetation will establish on bare bars and promote the colonization by other species later on. The colonization by plants will stabilize bars and consequently the threshold for erosion of the bars increases in time. It usually takes approximately three years before a river bar is covered with vegetation (Penning, 2016). The established vegetation may, however, be removed within this period when a bar is flooded. The river spatial dynamics becomes less predictable after this period of approximately three years, since vegetation plays a role in stabilization of river bars and it is unknown where each plant species establishes.

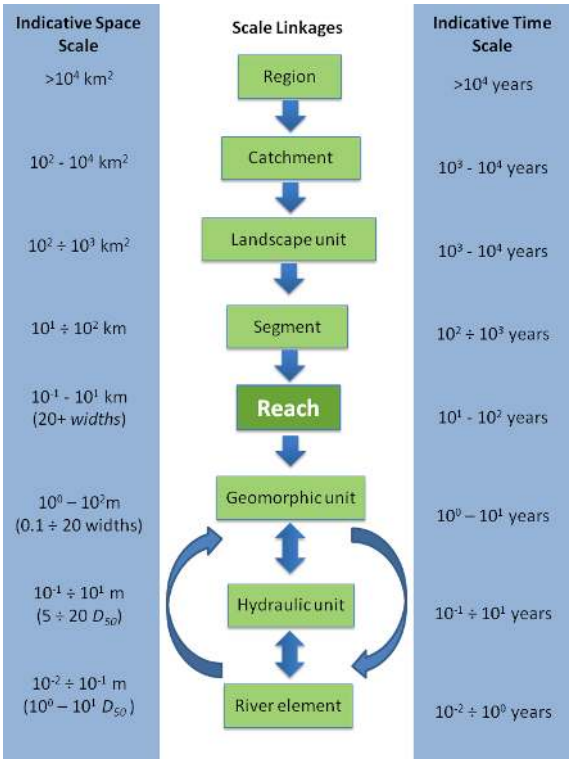


*Figure 5.1 – Hierarchy of spatial scales of rivers, including indicative spatial dimensions and timescales over which these units are likely to persist (REFORM, 2015).*

## 5.2 Interpretation of results

Some hydromorphological river conditions and river geometries could not be represented in the conditions of the laboratory experiment, generally due to practical reasons described in Section 3.1. This section discusses what these limitations of the experimental conditions imply for the interpretation of the results of this research.

*Reliability and accuracy*

The results from the experimental tests were reliable after repetition of some experimental tests which showed similar results. It is therefore expected that the experimental tests that were not repeated would also give similar results if they were repeated.

The accuracy of the results in this research depends on the accuracy of the measurement and the accuracy of the method to analyze the results. The method to quantify bar areas is based on

drawn areas of bars on photos taken above the flume. These drawn areas are an estimation of the actual bar area, which are based on bed profiles measured in the main channel and photos of the bed topography indicated with deep channel areas that became visible when dye was added to the flow. The inaccuracy is expected to be relatively small such that the bar formation analysis gives representative results of the experiment.

*Steady, bankfull discharge*

In the experimental tests, bars were formed during a steady, bankfull discharge in the channel. In Section 3.1 is described why it is legit to use bankfull conditions in the experiment, while rivers show a variable discharge regime. Bars may emerge during low-flow conditions in rivers. In the experiment, the bar area was determined during low flow conditions, since then it was easier to observe bars. During low-flow conditions at the end of the experimental tests, dye was added to the flow which indicated deep channel areas. Bars became therefore visible to the eye and photos of the bed topographies were taken.

Low-flow conditions were, however, not exactly the same in every experiment and therefore deep channel areas and bar areas in the photos might not be comparable between the experimental tests. For example, low-flow conditions that are too high result in bar areas that are flooded and thus wrongly indicated as deep channel area.

The bar areas drawn in Figure E.1 to Figure E.16 in Appendix E were also based on the bed profile measurements in the main channel and are therefore a better indication of the bar areas than the bed topography photos only. The bar areas in the main channel area are more accurate than the bar areas outside the main channel in the widened reach, since bed profile measurements were only taken in the main channel.

*Straight channel geometry*

In the straight channel geometry of the experimental flume the flow is forced symmetrically in the channel. The bars that formed in the protected downstream reach are a consequence of the upstream bank protection removal in the experiment, since these bars are forced by the bars in the widened reach. The results showed that the bar height and area of the hybrid bars are smaller as those in the widened reach.

Rivers have bends and other geometrical perturbations that forces asymmetrical flow in the river. Hybrid bars would form in rivers without the need of bank protection removal if the instability conditions for bar formation are met, due to geometrical forcings in rivers. In rivers, the large forced bars in the widened reach would be a direct consequence of the bank protection removal, however, the smaller hybrid bars may also be forced by a river bend.

The bank protection removal is a forcing for formation and stabilization of downstream hybrid bars and can be seen as a secondary benefit for habitat diversity. The formation of the bars in the widened reach is most beneficial for habitat diversity, since these create diversity in the height and area of river bars.

*Gravel-bed river similarity*

The results from the small scale laboratory experiment can be used for natural size rivers. The experiment is a small scale representative for gravel-bed rivers, since the dimensionless parameters characterizing channel bankfull geometry of the laboratory experiment fall in the range of gravel-bed rivers as described in Appendix B. Qualitative results obtained from the laboratory experiment may, however, apply to sand-bed rivers as well (Mosselman, 2017). The main difference between equations that describe the morphodynamic system for gravel- or sand-bed rivers is the threshold of the initiation of motion of sediment particles and this is not relevant for the appearance of bars. Furthermore, bars appear in reality also in sand-bed rivers.

*Limited duration of experimental tests*

The total duration of each experimental test was limited to seven hours, due to practical reasons. Emptying of the sieve and filling of the sediment feeder had to be done at least once every four hours, which made it impossible to let the experiment run overnight. In most experimental tests, the banks were still eroding at the end of the run. The maximum width of the channel in the widened reach at the end of each run may therefore still increase. The erosion rate decreased exponentially in time and thus was significantly reduced at the end of the run. Since bar formation is related to the width of the channel, it might be possible that bars were still developing and no final morphological stage was reached at the end of the run. It is expected that for a longer duration of the experiment, the channel widening will be larger, which results in wider and higher bars in the widened reach. Furthermore, hybrid bars that formed downstream of the widened reach in the experimental tests had smaller wavelengths than the theoretical hybrid bar wavelength of 1.6 metres calculated with equation (4) (Crosato and Mosselman, 2009). It is expected that for a longer duration of the experiment, the final wavelength of the hybrid bars downstream of the widened reach is 1.6 metres.

*Limited length of bank protection removal*

The bars that formed in the widened reach could not develop to its final wavelength even when the maximum length of bank protection was removed. The maximum length of bank protection removal was 10 times the channel width and was apparently too short for bars to develop to its final wavelength. For example, Figure E.12 shows that the bar in the widened reach was widening in longitudinal direction. At the downstream end of the widened reach the bar was interrupted by scour holes at the downstream bank protections. According to the theory, the bar wavelength should be 1.6 metres for a channel width of 0.2 metres (Crosato and Mosselman, 2009). The reach where the bank protection is removed, however, is widened and therefore the bar wavelength is increased as well. For example, lateral erosion of the banks of 10 cm results in a channel width of 30 cm and a bar wavelength of 2.5 metres. In most experiments the final lateral erosion was larger than 10 cm and therefore the theoretical final bar wavelength was in most experiments larger than the length of the widened section. At the end of the widened reach the strong conversion of the channel banks resulted in an interruption of the bar development and bar could not develop to its final wavelength.

*Bank cohesion*

The channel banks were in most tests non-cohesive, since they were composed of the same material as the channel bed. In rivers, however, the banks are usually more cohesive than the river bed. Experimental test R11 was performed with cohesive banks and from this test was concluded that bank cohesiveness did not significantly influence the shape of bank erosion and the formation of bars. The bank erosion rate was reduced with cohesive banks and this resulted in smaller widened reach compared to non-cohesive banks at the end of the test. For a longer duration of experimental tests with cohesive banks is expected that the final bank erosion shape is similar to the final bank erosion shape in tests with non-cohesive banks and thus would not significantly change the results.

## 5.3 Example design of bank protection removal

An example of a bank protection removal design in a general river is given to put the results into perspective. River restoration practisers can change the design of bank protection removal according to their own situation. This example considers the following:

- The solution should have bar formation as a measure to enhance habitat diversity.
- Infrastructure along the riverbanks should not be affected.
- Investment and maintenance costs should be minimised.

- The location is a gravel-bed river reach of 5.5 kilometres length.
- Assume a river width of B=50 m, bankfull water depth of $h_{bf}$=2.5 m, bar mode = 1 (scaling according to Table A.1)

### 5.3.1 Objectives

The first objective of the bank protection removal design is to have formation of bars, which can be quantified by the total bar area in the channel. Penning (2016) stated that diversity in bar wavelength, bar height, bar area, bar location and number of bars in a cross-section is most important when it comes to the ecological river condition. The second aim of the bank protection removal design is therefore to have diversity in bar wavelength, bar height, bar area, bar location and number of bars in a cross-section as a measure to enhance habitat diversity. Bar area is a better indicator for the size of the bar than bar wavelength thus this section focusses on bar area. To obtain diversity in bar location, bar area and maximum bar height in the river, the aim of the design is formation of mid-channel bars with large bar areas and high maximum bar heights in the widened reach, since usually smaller, lower side bars are formed downstream of the widened reach.

### 5.3.2 Considerations

A bank protection removal of ten times the channel width on both sides of the channel with perpendicular bank protections at the downstream end of the widened reach and a groyne upstream resulted in the largest total bar area. The costs for the construction and maintenance of this perpendicular bank protection are high and unpredictable, since it is unknown what the final channel width is. Therefore this design is not selected to use in the example bank protection removal.

Bank protection removal designs of nine times the channel width on one or two sides of the channel width with or without an upstream groyne had the second largest total bar areas. A bank protection removal length of nine times the channel width on both sides of the channel resulted in two high bars in the widened reach on the sides of the river. Addition of a groyne upstream of this design resulted in one mid-channel bar in the widened reach with the same maximum height, but a larger bar area. Construction of a groyne increases the investment and maintenance costs, so it depends on a cost-benefit analysis of the restoration project whether to construct the groyne. These two bank protection removal designs are selected in reaches where no infrastructure is located, since the laterally eroding banks may affect infrastructure. These designs leads to the formation of high, large, side or mid-channel bars in the widened reaches with lower, smaller bars downstream of the widened reach.

When infrastructure is located on one side of the river, it is advised to remove bank protection only on the opposite side of the river to prevent destruction of infrastructure. A bank protection removal design with a length of nine times the channel width on one side of the channel resulted in a high, side bar in the widened reach. Addition of a groyne to this design resulted in a bar with a larger area, but a similar maximum bar height. Again, construction of a groyne increases the investment and maintenance costs, so it depends on a cost-benefit analysis of the restoration project whether to construct the groyne.

A curved bank protection at the downstream end of the widened reach prevents erosion at the back of the remaining bank protection downstream of the widened reach and reduces the size of the scour hole at the same location. This is an effective measure to prevent destruction of the remaining bank protection that is needed to protect infrastructure along the riverbanks.

Construction of a curved bank protection will increase the investment costs, but can reduce maintenance costs of the remaining bank protections.

### 5.3.3 Choice of design

It is chosen to remove the bank protection with a length of at least nine times the river width on either one or both sides of the river with optionally a groyne upstream. Table 5.1 shows the length and bar area of each section and the length, channel width, bar area and bar height of the widened reach within each section. The length of the channel section in which bar formation was measured in the laboratory experiment of this research was 27.5 times the channel width. In this example design, each section with a bank protection removal design will therefore have a length of 27.5 x 50 = 1375 m. Four sections with a specific bank protection removal design have a total length of 5.5 km. The bar areas and bar heights can be calculated with the assumed river width of 50 metres and bankfull water depth of 2.5 metres, based on the relative bar areas and bar heights from the laboratory experiment given in Section 4.5. The hybrid bars that formed downstream of each widened reach have smaller bar areas and lower bar heights than the bars in the widened reaches.
A combination of the four bank protection removal designs given in Table 5.1 leads to formation of bars with diversity in bar area, height and location.

Figure 5.2 shows a schematisation of the example bank protection removal design for the river reach of 5.5 km with infrastructure along the banks. This bank protection removal design can be repeated when a longer river reach has to be restored for a river restoration project.

*Table 5.1 – Quantification of example design of bank protection removal. *The channel width was determined for a non-cohesive, non-vegetated bank at the location where the widening was largest when the bank erosion rate was significantly reduced.*

| Design | Total section | | Widened reach in each section | | | |
|---|---|---|---|---|---|---|
| Bank protection removal length | Length [m] | Bar area [m²] | Length [m] | Channel width* [m] | Bar area [m²] | Bar height [m] |
| 9*B, one side | 1375 | 19000 | 450 | 90 | 11400 | 2 |
| 9*B, one side + groyne | 1375 | 22563 | 450 | 160 | 13775 | 2 |
| 9*B, two sides | 1375 | 23750 | 450 | 120 | 8313 \| 9144 | 2.25 |
| 9*B , two sides + groyne | 1375 | 24937 | 450 | 160 | 14963 | 2.25 |

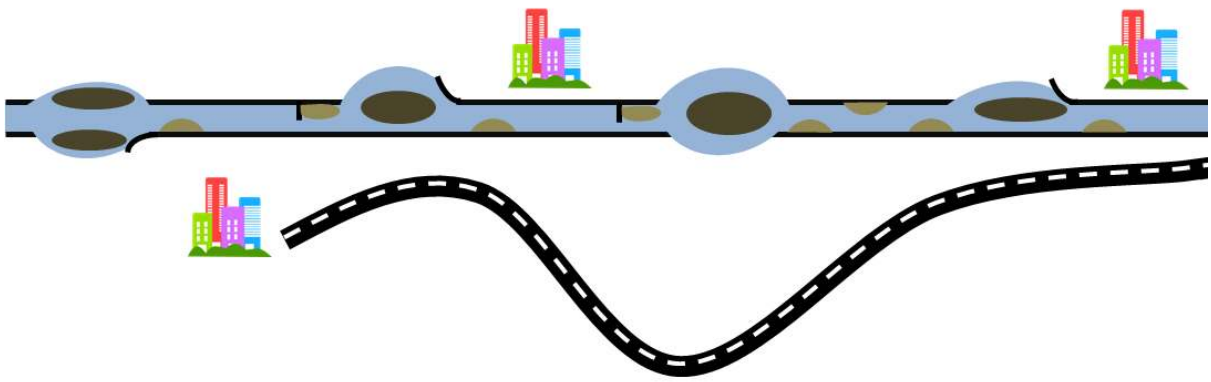

*Figure 5.2 – Example design of bank protection removal for a schematised river with infrastructure along the banks. The remaining riverbank protections (black), deep channel (blue), high bars (dark brown) and low bars (light brown) are shown in the figure. Figure is not to scale.*

# 6 Conclusions and recommendations

## 6.1 Conclusions

Removing riverbank protection has an appreciable effect on bar formation as a measure to enhance habitat diversity. Habitat diversity in rivers is enhanced through the formation of river bars with preferably diversity in height, size and location.

Removing riverbank protections results in lateral erosion of the banks and thus widening of the channel. When the width of the channel increased, the flow decelerated, since $u = Q/Bh$. Sediment transport decreased, since the transport capacity and flow velocity were related by $S \sim u^b$. Sediment was therefore deposited in the widened reach with lower flow velocities. Channel widening therefore caused bed aggradation, which in turn may contribute to the formation of bars as the width-to-depth ratio increased.

When the riverbanks were fixed, relatively low, small, side bars were formed in the channel. In general, the total bar area and bar height increased for an increase in channel widening, due to the removal of bank protection. In most tests, the forced bar(s) in the widened reach had higher maximum heights and larger areas than the hybrid bars downstream of the widened reach. The bars downstream of the widened reach were always located on the side of the channel, whereas the bar(s) in the widened reach could also be located in the middle of the channel.

Three variables of bank protection removal were studied in this work, which are length, location and flow asymmetry, and these resulted in different bar areas shown in Table 6.1. An increased bank protection removal length up to nine times the channel width or an upstream asymmetrical flow forcing, i.e. groyne, increased the total bar area, whereas a bank protection removal at three different locations with a total length of nine times the channel width did not significantly increased the total bar area.

| Bank protection removal design | | Symmetrical flow forcing | | | Asymmetrical flow forcing | | |
|---|---|---|---|---|---|---|---|
| One or two side removal | Removed length | Total bar area [%] | Low bar area [%] | High bar area [%] | Total bar area [%] | Low bar area [%] | High bar area [%] |
| Fixed banks | - | 7 | 7 | 0 | 12 | 12 | 0 |
| One | 3*B | 10 | 10 | 0 | | | |
| One | 6*B | 12 | 5 | 7 | | | |
| One | 9*B | 16 | 6 | 10 | 19 | 4 | 15 |
| One[1] | 9*B | - | - | - | 20 | 13 | 7 |
| Two[2] | 9*B | 10 | 3 | 7 | | | |
| Two | 3*B | 8 | 6 | 2 | | | |
| Two | 6*B | 14 | 7 | 7 | | | |
| Two | 9*B | 20 | 4 | 16 | 21 | 4 | 17 |
| Two[3] | 10*B | 14 | 3 | 11 | 24 | 4 | 20 |

*Table 6.1 - Relative bar areas in the flume at the end of the experimental tests. The total bar area is the sum of the low and high bar area. B is the width of the fixed channel. [1]The bank protection is removed on the opposite side of the groyne, whereas in the other tests the bank protection is*

*removed on same side as the groyne.* [2]*The bank protection is removed at three different locations with a total length of 9*B, whereas in the other tests the bank protection is removed in one section.* [3]*The bank protections at the downstream end of the widened reach were perpendicular to the main channel, whereas in the other tests the bank protection at the downstream end of the widened reach was parallel to the main channel.*

## 6.2 Recommendations

### 6.2.1 Recommendations to river restoration practice

It is recommended to remove riverbank protections over a length of at least nine times the river width on both sides of the river with optionally a groyne upstream as a measure to enhance habitat diversity. It is also valuable to remove the bank protection on one side of the river only. It is advised to construct a groyne upstream of the bank protection removal to increase habitat diversity. The length of the groyne may be in the order of half the channel width and placed at a distance of five times the channel width upstream of the bank protection removal. The groyne should be located on the same side as the bank protection removal if the riverbank protection is removed on one side only. It is recommended to construct a curved bank protection with a radius in the order of the width of the channel at the downstream end of the widened reach to prevent destruction of the remaining bank protection.

### 6.2.2 Recommendations for further research

*Large scale experiment*

The laboratory experiment in this research has been carried out in a flume channel of 0.2 m wide and 6.2 metres long. The small scale experiment in this research represents gravel-bed rivers. It would be useful to conduct larger scale experiments and to move eventually to the field. For larger scale experiments it becomes possible to represent sand-bed rivers, since the larger scales allow dominant suspended-load sediment transport. Furthermore, increasing the scale reduces the sensibility of the experiment to small adjustments in for example the sediment feeder.

When having a constant width-to-depth ratio in the experiment that is representative for rivers, the water depth can only be increased when the channel flume becomes wider. Flow and transport processes in the vertical direction, such as secondary flow, in the experiment represent rivers more accurately when the water depth in the experiment is closer to the water depth in a river. The average water depth in the experiment in this research was 1 cm, whereas water depths in rivers are in the order of metres. Another advantage of a larger water depth is that morphological features such as bars are easier to observe, since their size will increase.

*Hydrograph*

In this study experiments have been carried out with a steady, bankfull discharge. It is recommended to perform experiments with a hydrograph, which means a variable discharge in time. The water level will therefore vary in time and this might affect the final river morphology.

*Vegetation on banks and floodplains*

The laboratory experiment was conducted without vegetation, since this would add too much complexity to the morphological processes. Vegetation is, however, important in river morphodynamics and it therefore recommended to include this in the experimental setup. Vegetation growth on riverbanks and floodplains changes the river bed topography, reduces the bank erosion rates and enhances the development of new floodplains through riverbank accretion (Vargas Luna et al., 2016). Vegetation colonization increases the amplitude and length

of the bars in the main channel, affecting the final river planform. Furthermore, vegetation can grow on mid-channel bars, such that stable islands develop.

*Location and length of groyne*
Several experimental tests had been conducted with an upstream asymmetrical flow forcing, i.e. groyne. The length of the groyne was half of the channel width and the groyne was located five times the channel width upstream of the bank protection removal. It is recommended to do more research into the location and length of the groyne to get insight into the effects on the formation of bars

*Longer bank protection removal length*
In the flume channel a maximum bank protection length of ten times the channel width could be removed. The bar(s) that formed in the widened reach could usually not extend to their maximum length, due to the limited length of the bank protection removal as described in Section 5.2. It is therefore recommended to increase the maximum bank protection removal length. Bank protections might be removed with lengths in the order of 200 times the channel width in river restoration projects, thus this length could be an indicator for the bank protection removal length in an experiment.

*Longer duration of experimental tests*
As described in Section 5.2, the banks were still eroding at the end of the experimental tests and therefore the morphodynamics did not reach a final stage. Furthermore, the final wavelengths of hybrid bars were smaller than in theory (Crosato and Mosselman, 2009). It is therefore recommended to design an experiment setup that allows for a longer duration than seven hours of the experimental tests.

*River bend*
It is recommended to perform more experimental setups with the removal of bank protections to find an optimal geometrical variation as a measure to enhance habitat diversity. Furthermore, the initial experimental setup should aim at representing rivers as close as possible. For example, a curved channel geometry could be included in the experimental setup to represent a river bend.

*Bed topography measurement*
Bed profiles have been measured with lasers and photos of the bed topography have been made to quantify the formation of bars in the experiment. The final bar characteristics had to be estimated based on these measurements. It is recommended to use cameras that can measure the bed topography in three dimensions, such that bar characteristics can be quantified more accurately. Furthermore, it is recommended to find a method to measure bar characteristics during the experimental test when water is present in the flume channel.

*River restoration method*
Finally, further research is necessary to investigate practical issues for bank protection removal in rivers. The river restoration measure discussed in this research, namely the removal of bank protection, may affect other riverine functions than the ecological system, such as navigation, flood management, recreation, agriculture, landscape development, hydropower, water supply, etc. The effects of riverbank protection removal on these riverine functions should be investigated to make this a feasible river restoration method. Uncertainties of bank protection removal designs, investment and maintenance costs of the specific bank protection removal designs and effects on biodiversity should be studied as well.

# References


Blondeaux, P. and Seminara, G. (1985), A unified bar bend theory of river meanders, J. of Fluid Mech., 157, 449-470, doi:10.1017/S0022112085002440

Canestrelli, A., A., Spruyt, B. Jagers, R. Slingerland, M. Borsboom (2015), A mass-conservative staggered immersed boundary model forsolving the shallow water equations on complex geometries, Int. J. Numer. Meth. Fluids, doi: 10.1002/fld.4180

Canestrelli, A. (2016), Personal communication, 12 December, 2016

Colombini, M., G. Seminara, and M. Tubino (1987), Finite-amplitude alternate bars, J. of Fluid Mech., 181, 213-232, doi:10.1017/S0022112087002064

Crosato, A., and E. Mosselman (2009), Simple physics-based predictor for the number of river bars and the transition between meandering and braiding, Water Resour. Res., 45, W03424, doi:10.1029/2008WR007242.

De Vries, M. (1975), A morphological time scale for rivers, In: Proceedings of 16th Congress IAHR, São Paulo, 2, Paper B3, 17-23

Deltares (2016a), Open source software - About Delft3D, [Online] Available from: https://oss.deltares.nl/web/delft3d/about, [Accessed 21 December, 2016]

Deltares (2016b), Delft3D-FLOW User Manual (2016), Simulation of multi-dimensional hydrodynamic flows and transport phenomena, including sediments, Hydro-Morphodynamics, Version: 3.15, Revision: 45038

Duró, G., A. Crosato, P. Tassi (2015), Numerical study on river bar response to spatial variations of channel width, Advances in Water Resources, doi: 10.1016/j.advwatres.2015.10.003

ECRR, European Centre for Restoring Rivers (2016), What is river restoration?, Retrieved 24 May 2016, from http://www.ecrr.org/RiverRestoration/Whatisriverrestoration/tabid/2614/Default.aspx

Eekhout, J. P. C., A. J. F. Hoitink, and E. Mosselman (2013), Field experiment on alternate bar development in a straight sand-bed stream, Water Resour. Res., 49, 8357–8369, doi:10.1002/2013WR014259.

Eke, E.C., G. Parker, Y. Shimizu (2014), Numerical modeling of erosional and depositional bank processes in migrating river bends with self-formed width: Morphodynamics of bar push and bank pull, J. Geophys. Res. Earth Surf., 119, 1455-1483, doi:10.1002/2013JF003020

Exner, F. M. (1920), Zur Physik der Dünen, Akad. Wiss. Wien Math. Naturwiss. Klasse, 129 (2a), 929–952

Exner, F. M. (1925), Über die Wechselwirkung zwischen Wasser und Geschiebe in Flüssen, Akad. Wiss. Wien Math. Naturwiss. Klasse, 134 (2a), 165–204

Frascati, A., S. Lanzoni (2013), A mathematical model for meandering rivers with varying width, J. Geophys. Res. Earth Surf., 118, 1641-1657, doi:10.1002/jgrf.20084

Fredsøe, J. (1978), Meandering and braiding of rivers. J. Fluid Mech., 84(4), 609-624, doi: 10.1017/s0022112078000373,

Friedkin, J. F. (1945), A laboratory study of meandering alluvial rivers, Waterways Experiment Station, U. S. Corps of Engineers

Friend, P.F., and R. Sinha (1993), Braiding and meandering parameters, Geological Society, London, Special Publications, 75(1), 105–111, doi: 10.1144/GSL.SP.1993.075.01.05

Frostick, L. E., S. J. M., T. G. Mercer (2011), User Guide to Physical Modelling and Experimentation: Experience of the HYDRALAB Network, Leiden, The Netherlands, CRC Press/Balkema

Google Earth 7.1.5.1557 (2015), viewed 27 July 2016, http://www.google.com/earth/index.html

Hooke, J. M. (1986), The significance of mid-channel bars in an active meandering river, Sedimentology, 33 (6), 839–850, doi: 10.1111/j.1365-3091

Hunzinger, L. M. (1998), Flussaufweitungen - Morphologie, Geschiebehaushalt und Gtestdsätze zur Bemessung, Miteilungen der Versuchsanstalt für Wasserbau, Hydrologie und Glaziologie der ETH, 159, Zürich

Jansen, P. P., L. Van Bendegom, J. Van den Berg, M. De Vries, Ph. A. Zanen (1979), Principles of river engineering, the non-tidal alluvial river, Delftse Uitgevers Maatschappij BV, Delft 1994 ISBN 978-90-407-1280-7

Janusche, K., S. Btestzel, P. Haase, D. Hering (2011), Effects of stream restorations on riparian mesohabitats, vegetation and carabid beetles, Biodivers. Conserv., 20, 3147–3164, doi:10.1007/s10531-011-0119-8

Julian, J. P. and R. Torres (2006), Hydraulic erosion of cohesive riverbanks, Geomorphology 76, 193 - 206

Kail, J., A. Lorenz, D. Hering (2014), Effects of large- and small-scale river restoration on hydromorphology and ecology, D4.3 Results of the hydromorphological and ecological survey, REFORM

Klaassen, G. J., E. Mosselman, and H. Bruhl (1993), On the prediction of planform changes in braided sand-bed rivers, In: Advances in Hydro-Science and Engineering (Ed. S.S.Y. Wang), 134-146, Publ. University of Mississippi, University, Mississippi

Kleinhans, M. G., W.M. van Dijk, W.I. van de Lageweg, D.C.J.D Hoyal, H. Markies, M. van Maarseveen, C. Roosendaal, W. van Weesep, D. van Breemen, R. Hoendervoogt and N. Cheshier (2014), Quantifiable effectiveness of experimental scaling of river- and delta morphodynamics and stratigraphy, Earth-science reviews., 133 . pp. 43-61, doi: 10.1016/j.earscirev.2014.03.001

Knighton, A. D. (1972), Changes in a braided reach, Geol. Soc. Am. Bull, 83 (12), 3813–3822, doi: 10.1130/0016-7606

Kurth, A., M. Schirmer (2014), Thirty years of river restoration in Switzerland: implemented measures and lessons learned, Environ. Earth Sci., 72, 2065–2079, doi: 10.1007/s12665-014-3115-y

Lawler, D. M., Thorne, C. R., and Hooke, J. M. (1997), Bank erosion and instability, Applied fluvial geomorphology for river engineering and management, C. R. Thorne, et al., eds., Wiley, Chichester, UK, 137–172

Luchi, R., G. Zolezzi, and M. Tubino (2010), Modelling mid-channel bars in meandering channels, Earth Surf. Process. Landf. (Special Issue on River Meander Dynamics, ed. J. M. Hooke, E. Gautier & G. Zolezzi) 35, 902–917, doi:10.1002/esp.1947

Luchi, R., G. Zolezzi, M. Tubino (2011), Bend theory of river meanders with spatial width variations, J. Fluid Mech. (2011), vol. 681, pp. 311–339, doi:10.1017/jfm.2011.200

Luchi, R., J. Hooke, G. Zolezzi, and W. Bertoldi (2010a), Width variations and mid-channel bar inception in meanders: River Bollin (UK), Geomorphology 119, 1–8, doi:10.1016/j.geomorph.2010.01.010

Meyer-Peter, E., and R. Müller (1948), Formulas for bed load transport, paper presented at 2nd Meeting, Int. Assoc. for Hydroaul. Environ. Eng. and Res., Madrid

Mosselman, E. (1989), Theoretical investigation on discharge-induced river-bank erosion, Communications on Hydraulic and Geotechnocal Engineering, 89 (3), Delft University of Technology

Mosselman, E. (1992), Mathematical modelling of morphological processes in river with erodible cohesive banks, Communications on Hydraulic and Geotechnical Engineering, 92 (3), Delft University of Technology

Mosselman, E. (1998), Morphological modelling of rivers with erodible banks, Hydrol. Process., 12, 1357-1370

Mosselman, E. (2017), Personal communication, 17 January, 2017

Odgaard, A. J. (1987), Stream bank erosion along two rivers in Iowa, Water Resources Research 23-7, 1225–1236

Olesen, K. W. (1983), Alternate bars in and meandering of alluvial rivers. C.M. Elliott (Ed.), River meandering, proc. of the conf. rivers ’83, ASCE, New York (1984), pp. 873–884 ISBN 0-87262-393-9

Paillex, A., I. Logar, M. Schirmer, N. Schuwirth, R. Siber, H. Yang, P Reichert (2014), Rewidening and rewilding the Thur river (Switzerland), retrieved from http://reformrivers.eu/news/297

Parker, G. (2004), 1D Sediment Transport Morphodynamics with applications to Rivers and Turbidity Currents, Ch. 3 Bankfull Characteristics of Rivers, retrieved from http://hydrolab.illinois.edu/people/parkerg/powerpoint_lectures.htm

Parker, G. (1976), On the cause and characteristic scales of meandering and braiding in rivers, J. Fluid Mech., 76(3), 457-479, doi:10.1017/s0022112076000748

Penning, E. (2016), Personal communication, December 19, 2016

Piégay. H., S. E. Darby, E. Mosselman, N. Surian (2005), A review of techniques available for delimiting the erodible river corridor: a sustainable approach to managing bank erosion, River Res. Applic. 21. 773 – 789, doi: 10.1002/rra.881

REFORM (2015), Introduction to characterisation: Multi-scale Hierarchal Framework, Retrieved 20 January 2017, Retrieved from http://wiki.reformrivers.eu/index.php/Introduction_to_characterisation:_Multi-scale_Hierarchical_Framework

Repetto, R., M. Tubino, C. Paola (2002), Planimetric instability of channels with variable width, Journal of Fluid Mechanics, 457, 79-109, doi:10.1017/S0022112001007595

Requena, P., R. B. Weichert and H. E. Minor (2006), Self-widening by lateral erosion in gravel bed rivers, In: River flow 2006, Proceedings of the International Conference on Fluvial Hydraulics, Lisbon, eds. R. M. I. Ferreira, E. C. T. I. Alves, J. G. A. B. Leal and A. H. Cardoso, ISBN 0-415-40815-6, doi:10.1201/9781439833865.ch196

Rinaldi, M. and Nardi, L. (2013). Modeling Interactions between Riverbank Hydrology and Mass Failures, J. Hydrol. Eng., 1231-1240, doi: 10.1061/(ASCE)HE.1943-5584.0000716

Schirmer, M., J. Luster, N. Linde, P. Perona, E.A.D. Mitchell, D.A. Barry, J. Hollender, O.A. Cirpka, P. Schneider, T. Vogt, D. Radny, and E. Durisch-Kaiser (2014), Morphological, hydrological, biogeochemical and ecological changes and challenges in river restoration – the Thur River case study, Hydrol. Earth Syst. Sci., 18, 2449–2462, doi:10.5194/hess-18-2449-2014

Seminara, G. (1988), Stability and Morphodynamics, Meccanica 33: 59–99, doi: 10.1023/A:1004225516566

Seminara, G., and M. Tubino (1989), Alternate bar and meandering: Free, forced and mixed interactions, in River Meandering, Water Res. Monogr., vol. 12, edited by S. Ikeda and G. Parker, pp. 267– 320, AGU, Washington, D. C.

Shields, A. F. (1936), Application of similarity principles and turbulence research to bed-load movement, vol 26, Mitteilungen der Preussischen Versuchsanstalt fur Wasserbau und Schiffbau, Berlin, Germany, 5–24

Siviglia, A., R. Repetto, G. Zolezzi, M. Tubino (2008), River bed evolution to channel expansion: general behaviour and application to a case study (Kugart River, Kyrgyz Republic), River Res. Applic, 24, 1271-1280, doi: 10.1002/rra.1095

Struiksma, N., K.W. Olesen, C. Flokstra, and H. J. De Vriend (1985), Bed deformation in curved alluvial channels, J. Hydr. Res., 23(1), 57-79, doi: 10.1080/00221688509499377

Tewolde, M. S. (2015), Effects of suspended sediments on river bars, MSc thesis, UNESCO-IHE Institute for Water Education, Delft

Thorne, C. R., and A. M. Osman (1988), The influence of bank stability on regime geometry of natural channels, Int. Conf. on River Regime, Wallingford, UK, 135-147

Thorne, C.R., S.E. Darby, C.V. Alonso, D.K. Borah, P. Diplas, P. Julien, D.K. Knight, L. Li, J.E. Pizzuto, M. Quick, A. Simon, M. Stevens, C. Watson & S.S.Y. Wang (1998), River width adjustment. I: Processes and mechanisms. Final Report of the ASCE Task Committee on Hydraulics, Bank Mechanics and Modelling of River Width Adjustment, J. Hydr. Engrg., ASCE, Vol.124, pp.881-902.

Toffolon, M. and A. Crosato (2007), Developing macroscale indicators for estuarine morphology: The case of the Scheldt estuary. Journal of Coastal Research, 23 (1), 195–212, West Palm Beach (Florida), ISSN 0749-0208, doi: 10.2112/03-0133.1

Tubino, M., R. Repetto and G. Zolezzi (1999), Free bars in rivers, J. Hydr. Res., 37(6), 759-775, doi:10.1080/00221689909498510

Van den Berghe, J., J. J. W. de Moor, G. Spanjaard (2012), Natural change and human impact in a present-day fluvial catchment: The Geul River, Southern Netherlands, Geomorphology, 159-160, 1-14, doi: 10.1016/j.geomorph.2011.12.034

Van der Mark, E. Mosselman, H. J. Verheij, C.F., R.A.M. van der Sligte, A. Becker (2012), A method for systematic assessment of the morphodynamic response to removal of bank protection, Deltares & Delft Technical University, Delft, The Netherlands

Vargas Luna, A., W. S. J. Uijttewaal, A. Crosato (2016), Role of vegetation on river bank accretion, Environmental Fluid Mechanics, Delft Technical University

Veldt, T. (2015), The length of river bank removal and the formation of bars, BSc Thesis, Delft University of Technology, Delft

Wang, S. S. Y., and W. Wu (2004) River sediment and morphology modelling – The state of the art and future development, In: Proc. 9th Int. Symposium on River Sedimentation, Yichnag, China

Weaver, J. E. (1976), Effects of roots of vegetation in erosion control, In: Symposium, Aspects of Veget. Erosion Control, Am. Soc. Agronomy

Whipple, K. (2004), Surface Processes and Landscape Evolution, Lecture Notes, MIT Open Course Ware, Ch. 1 Flow Mechanics, retrieved from: https://ocw.mit.edu/courses/earth-atmospheric-and-planetary-sciences/12-163-surface-processes-and-landscape-evolution-fall-2004/lecture-notes/

Wright, N., and A. Crosato (2011), The Hydrodynamics and Morphodynamics of Rivers, Peter Wilderer (ed.) Treatise on Water Science, vol. 2, 135–156, Oxford: Academic Press, doi: 10.1016/B978-0-444-53199-5.00033-6

Wu, F.-C., and T.-H. Yeh (2005), Forced bars induced by variations of channel width: Implications for incipient bifurcation, J. Geophys. Res., 110, F02009, doi:10.1029/2004JF000160

Wu, W. and Vieira, D.A. (2002), One-dimensional channel network model CCHE1D 3.0 -- Technical manual, Technical Report No. NCCHE-TR-2002-1, National Center for Computational Hydroscience and Engineering, The University of Mississippi

Zolezzi, G., R. Luchi, M. Tubino (2012), Modeling morphodynamic processes in meandering rivers with spatial width variations, Rev. Geophys., 50, RG4005, doi:10.1029/2012RG000392

# List of figures

Figure 1.1 - Degraded section of the Thur river (left) and restored section (right) after removal of bank protection in 2002 (Paillex et al., 2014) ..... 1
Figure 1.2 – Cross-section of river bar. The high zone, shallow zone, deep zone and intermediate zone indicate different habitats of a bar. ..... 2
Figure 1.3 - Restored section 'Schaffauli' of Thur river in 2009 (left) and 2012 (right) (Google Earth, 2015). ..... 3
Figure 2.1 – River planform stages (from left to right): meandering Cauto River in Cuba, transitional Fraser River in Canada and braiding Waimakariri River in New Zealand (Google Earth, 2015) ..... 7
Figure 2.2 – Bars located in straight channel: (left) first bar mode (alternate bars) and (right) second bar mode (central bars) (Crosato and Mosselman, 2009). ..... 9
Figure 2.3 – Morphological response on the short and long term due to widening of the main channel due to bank erosion (Van der Mark et al., 2012) ..... 11
Figure 2.4- Geomorphology of channel widening: (a) channel enlargement by bank erosion without incision; (b) erosion of outer bank in sinuous channel at faster rate than accretion on bar opposite; (c) deflection of flows by growing braid bar; (d) bank failure and retreat due to mass instability following channel incision; (e) bank erosion due to flow acceleration and deflection in coarse-bedded, aggrading river (Thorne et al., 1998) ..... 14
Figure 2.5 – Conceptual framework of the effects of removing riverbank protection ..... 16
Figure 3.1 - Discharge pump calibration ..... 21
Figure 3.2 – Sieve curve of well-sorted sediment ..... 21
Figure 3.3 – Longitudinal profile of experimental setup: top view (left) and side view (right). Not to scale. ..... 22
Figure 4.1 – Bed profile of test R04: A) Before test when bed profile is smoothened with a chip and B) after one hour testing without removal of bank protections. Vertical lines in the graphs are distortions in the laser measurements caused by a small layer of water that reflect the laser in different directions. ..... 31
Figure 4.2 – Evolution of bank erosion of test R03 with time T in hours. Red arrow indicates channel widening in downstream direction. ..... 32
Figure 4.3 – Erosion rate of test R04 in the middle of the widened reach ..... 36
Figure 4.4 – Eroded area per hour of tests R02 and R11. ..... 37
Figure 4.5 – Scour hole in final bed topography of test R01 at the downstream end of the widened section. Red dye indicates deep bed profile. ..... 38
Figure 4.6 – Scour holes in test R13 after 1.5 hours. The flow is from bottom to top of the figure. ..... 39
Figure 4.7 –Scour hole in test R01 (left) at the straight bank protection with a diameter of 12 cm and a depth of 3,5 cm (flow from left to right). Scour hole in test R14 (right) at the curved bank protection with a width of 4 cm and a depth of 3 cm (flow from right to left). ..... 39
Figure 4.8 - Comparison of measured hybrid bar wavelength in test P02 (Table E.1) and predicted hybrid bar wavelength (equation (4)) related to the degree of non-linearity b. ..... 42

Figure 4.9 – One side removal of bank protection: dimensionless area of the floodplain, deep channel, low bars and high bars in tests P01, R01, R02 and R03 related to the dimensionless length of bank protection removal. 43
Figure 4.10 – Two sides removal of bank protection: dimensionless area of the floodplain, deep channel, low bars and high bars in tests P01, R04, R05 and R06 related to the dimensionless length of bank protection removal. 45
Figure 4.11 – One side bank protection removal with length L/B=9: dimensionless area of the floodplain, deep channel, low bars and high bars in tests R03, R07, R08 and R09. 46
Figure 4.12 –Bank protection removal with asymmetrical flow forcing: dimensionless area of the floodplain, deep channel, low bars and high bars in tests P02, R08, R09 and R10. 48
Figure 4.13 - Dimensionless area of the floodplain, deep channel, low bars and high bars in tests R02 and R11 with respectively a non-cohesive and cohesive bank. 49
Figure 4.14 - Dimensionless area of the floodplain, deep channel, low bars and high bars in tests R12, R13 and R14 with a different bank protection shape at the downstream end of the widened reach. 50
Figure 4.15 - Scatter plot of bar area in widened reach and eroded bank area, i.e. area of channel widening, based on all experimental tests. No distinction is made between a low bar and a high bar. 51
Figure 4.16 - Scatter plot of maximum bar height in widened reach and eroded bank area, i.e. area of channel widening, based on all experimental tests. 51
Figure 4.17 –Scatter plot of bar area and eroded bank area, i.e. area of channel widening, based on all experimental tests. The bar area is divided in low bar area and high bar area and the sum is the total bar area. 52
Figure 5.1 – Hierarchy of spatial scales of rivers, including indicative spatial dimensions and timescales over which these units are likely to persist (REFORM, 2015). 55
Figure 5.2 – Example design of bank protection removal for a schematised river with infrastructure along the banks. The remaining riverbank protections (black), deep channel (blue), high bars (dark brown) and low bars (light brown) are shown in the figure. Figure is not to scale. 59
Figure A.1 – Two-dimensional grid of the numerical models. The main channel is highlighted green, the erodible sections (floodplains) are indicated in blue and the non-erodible sections are indicated in red. 79
Figure A.2 – Froude number in numerical model [1] (top), numerical model [2a] (middle) and numerical model [2b] (bottom) at the end of the simulations. 82
Figure A.3 – Depth average velocity in numerical model [1] (top), numerical model [2a] (middle) and numerical model [2b] (bottom) at the end of the simulations. 82
Figure A.4 – Fraction high ground in numerical model [1] (top), numerical model [2a] (middle) and numerical model [2b] (bottom) at the end of the simulations. The fraction high ground is the area within the input polygon that can still be eroded. 83
Figure A.5 – Cumulative erosion and sedimentation in numerical model [1] (top), numerical model [2a] (middle) and numerical model [2b] (bottom) at the end of the simulations. Sedimentation is indicated with dark red and erosion is indicated with blue. 83

Figure A.6 – Longitudinal profiles in the main channel at y = 162 of numerical model [1] (red line), numerical model [2a] (blue line) and numerical model [2b] (green line) at the end of the simulations. 84
Figure B.1 – Dimensionless width versus dimensionless discharge (Parker, 2004). Red point indicates experiment in plot. 86
Figure B.2 – Dimensionless water depth versus dimensionless discharge (Parker, 2004). Red point indicates experiment in plot. 87
Figure B.3 – Bed slope versus dimensionless discharge (Parker, 2004). Red point indicates experiment in plot. 87
Figure B.4 – Froude number versus bed slope (Parker, 2004). Red point indicates experiment in plot. 88
Figure B.5 – Chézy coefficient versus bed slope (Parker, 2004). Red point indicates experiment in plot. 88
Figure B.6 – Chézy coefficient versus dimensionless water depth (Parker, 2004). Red point indicates experiment in plot. 88
Figure B.7 – Estimate of bankfull Shields number versus dimensionless discharge (Parker, 2004). Red point indicates experiment in plot. 89
Figure B.8 – Estimate of bankfull Shields number versus particle Reynolds number (Parker, 2004). Red point indicates experiment in plot. 89
Figure C.1 – Sieve curve of widely graded sediment of test Pr04 90
Figure D.1 – Setup of experimental tests P01, P02 and R01 to R06. 92
Figure D.2 – Setup of experimental tests R07 to R14. 93
Figure E.1 –Final bed topography photo with bars (top) and detrended bed profile (bottom) of test P01. 97
Figure E.2 - Final bed topography photo with bars (top) and detrended bed profile (bottom) of test P02. 97
Figure E.3 - Final bed topography photo with bars (top) and detrended bed profile (bottom) of test R01. 98
Figure E.4 - Final bed topography photo with bars (top) and detrended bed profile (bottom) of test R02. 98
Figure E.5 - Final bed topography photo with bars (top) and detrended bed profile (bottom) of test R03. 99
Figure E.6 - Final bed topography photo with bars (top) and detrended bed profile (bottom) of test R04. 99
Figure E.7 - Final bed topography photo with bars (top) and detrended bed profile (bottom) of test R05. 100
Figure E.8 - Final bed topography photo with bars (top) and detrended bed profile (bottom) of test R06. 100
Figure E.9 - Final bed topography photo with bars (top) and detrended bed profile (bottom) of test R07. 101
Figure E.10 - Final bed topography photo with bars (top) and detrended bed profile (bottom) of test R08. 101
Figure E.11 - Final bed topography photo with bars (top) and detrended bed profile (bottom) of test R09. 102

Figure E.12 - Final bed topography photo with bars (top) and detrended bed profile (bottom) of test R10. 102
Figure E.13 - Final bed topography photo with bars (top) and detrended bed profile (bottom) of test R11. 103
Figure E.14 - Final bed topography photo with bars (top) and detrended bed profile (bottom) of test R12. 103
Figure E.15 - Final bed topography photo with bars (top) and detrended bed profile (bottom) of test R13. 104
Figure E.16 - Final bed topography photo with bars (top) and detrended bed profile (bottom) of test R14. 104
Figure F.1 – Photo of final topography of test R06 with drawn bar areas and floodplain area. 105
Figure F.2 –Dimensionless area of floodplain, deep channel, high bars and low bars for all tests determined from the photos of bed topographies 106
Figure F.3 – Bed profiles of test R06 from laser measurements in main channel at y=53 cm, y=60 cm and y=67 cm. The regression line is computed from these three bed profiles. 107
Figure F.4 - Dimensionless length of detrended bed profile of deep channel, high bars and low bars for all tests determined from the three bed profiles in the main channel 108
Figure F.5 – One side bank protection removal: dimensionless length of detrended bed profile of deep channel, high bars and low bars of tests P01, R01, R02 and R03 related to the dimensionless length of bank protection removal determined from the three bed profiles in the main channel 110
Figure F.6 – Two sides bank protection removal: dimensionless length of detrended bed profile of deep channel, high bars and low bars of tests P01, R04, R05 and R06 related to the dimensionless length of bank protection removal determined from the three bed profiles in the main channel 110
Figure G.1 – Spatial evolution of bank erosion of test R01. Time T is in hours. 112
Figure G.2 – Spatial evolution of bank erosion of test R02. Time T is in hours. 112
Figure G.3 – Spatial evolution of bank erosion of test R03. Time T is in hours. 113
Figure G.4 - Spatial evolution of bank erosion of test R05. Time T is in hours. 113
Figure G.5 - Spatial evolution of bank erosion of test R08. Time T is in hours. 114
Figure G.6 – Spatial evolution of bank erosion of test R09. Time T is in hours. 114
Figure G.7 - Spatial evolution of bank erosion of test R10. Time T is in hours. 115
Figure G.8 - Spatial evolution of bank erosion of test R11. Time T is in hours. 115
Figure G.9 – Spatial evolution of bank erosion of test R13. Time T is in hours. 116
Figure G.10 – Spatial evolution of bank erosion of test R14. Time T is in hours. 116
Figure H.1 –USB data acquisition board for converting data from lasers to computer. 117
Figure H.2 –Sediment feeder 117
Figure H.3 – Light attached to wooden frame above flume 118
Figure H.4 – Removable bank protection of main channel made out of steel (1.5 mm thick) and wood (2 cm thick) with length of 60 cm and height of 23 cm. 118
Figure H.5 – Removable bank protections in position with duct tape over the seams to prevent water and sediment flowing through the gap. 119
Figure H.6 – Tools used for measuring (e.g. small sieve, tapeline, stop watch, dye) and for preparing the bed and bank profile (e.g. chip, bucket, screwdriver). 119

Figure H.7 – Bag of sediment used for the sand-bed in the main channel and filing the sediment feeder....120
Figure H.8 – Ball valve to control water supply to flume....120
Figure H.9 – Sieve at the downstream end of the flume supported by water basin....121
Figure H.10 – Water basin at downstream end of the flume. Green pipe is for water supply from the ball valve. Water that is sucked to the discharge pump flows through the yellow pipe. Water flowing out of the discharge pump goes through the brown pipe and lies in the water basin to keep any leakage of the connection to a longer green pipe (right in figure), that reaches up to the upstream end of the flume, inside the basin. The grey pipe (right in figure) attached to the water basin is used to drain water that exceeds a certain water level to prevent the basin from flooding and to keep the water level in the basin at a constant height. The red pump is not in use, since the minimum capacity is too large....121
Figure H.11 – Discharge pump with a maximum capacity of about 2 L/s....122
Figure H.12 –Frequency controller of the discharge pump....122
Figure H.13 – Laser installed on platform that can be moved in transversal direction....123
Figure H.14 – Four lasers fixed on platform. Laser number 1, 3 and 4 measure the bed profile in longitudinal direction. Laser number 3 is not in use....123
Figure H.15 – Platform to which lasers are attached drives over rails of steel. Large wheel (right in figure) gives 5000 pulses per rotation and is connected to laser, such that with every pulse the lasers measure the bed profile....124
Figure H.16 – Area where the water flows into the flume and fluctuations in the water level are damped....124
Figure H.17 –Three taps at the bottom of the sediment feeder. Only the green tap is used. The other taps function as backup in case the green tap is clogged and cannot be emptied....125
Figure H.18 – Ten steel grids attached to each other with a distance of 0.5 cm in between them to damp fluctuations in the water level from the area where the water flows into the flume....125
Figure H.19 – Example of DASYLab 13.0 for data acquisition, graphics, control and analysis during an experiment. Each line in the graph represents a different laser in which on the vertical axis the bed elevation is shown and on the horizontal axis the distance in longitudinal direction. In the table each row represents a different laser. The left column shows the voltages and the right column the bed elevation in centimetres....126
Figure H.20 - Sediment from feeder falls in small bowl....126
Figure H.21 –Sediment flowing out of the flume collected in a small sieve....127
Figure H.22 – Measuring erosion rate with tapeline....127
Figure H.23 – Dye in flask that is added to the water flowing in the main channel....128

# List of tables

Table 2.1 – Definition of bars according to the new terminology of Duró et al. (2015) ..... 8
Table 3.1 – Conditions of tests Pr01 to Pr05 in the preliminary phase. Figure 3.2 shows the sieve curve of the sediment used in test Pr01 to Pr03 and Figure C.1 in Appendix C shows the sieve curve of the sediment used in test Pr04..... 23
Table 3.2 – Conditions in preliminary test Pr01..... 24
Table 3.3 – Setup of experimental tests. B=width of the main channel. ..... 26
Table 5.1 – Quantification of example design of bank protection removal. *The channel width was determined for a non-cohesive, non-vegetated bank at the location where the widening was largest when the bank erosion rate was significantly reduced..... 59
Table 6.1 - Relative bar areas in the flume at the end of the experimental tests. The total bar area is the sum of the low and high bar area. B is the width of the fixed channel. [1]The bank protection is removed on the opposite side of the groyne, whereas in the other tests the bank protection is removed on same side as the groyne. [2]The bank protection is removed at three different locations with a total length of 9*B, whereas in the other tests the bank protection is removed in one section. [3]The bank protections at the downstream end of the widened reach were perpendicular to the main channel, whereas in the other tests the bank protection at the downstream end of the widened reach was parallel to the main channel. ..... 60
Table A.1 - Similarity scaling between flume experiment and numerical model. ..... 78
Table B.1 – Values of calculated dimensionless parameters characterizing bankfull geometry in the laboratory experiment in preliminary phase..... 86
Table C.1 - Particle size distribution of widely graded sediment of test Pr04 ..... 90
Table E.1 - Bar type, location, wave length and maximum height in final bed topography for each experimental test. The bar is located on the left side of the channel when y=53 cm, in the middle of the channel for y=60 cm and on the right side of the channel for y=67 cm. The relative bar area is a percentage of the area of the whole channel and the floodplains. The relative maximum bar height is the bar maximum height divided by the average water depth of $h_0$ = 1 cm given... 95
Table F.1 – Areas of floodplain, deep channel, low bar and high bar in square centimetres and percentages for all tests that were obtained by drawing the areas in the final bed topography photos..... 105
Table F.2 – Eroded bank area in square centimetres and percentages that were obtained by drawing the areas in the final bed topography photos for all tests. ..... 106
Table G.1 – Maximum channel width in the widened reach at the end of the each experimental test. The location in longitudinal direction of the maximum channel widening may be different for each test. The initial width of the main channel is B = 0.2 metres. ..... 111

# Appendices

## Appendix A. Numerical modelling

In this appendix, a brief description is given of the numerical modelling software Delft3D and in particular of a special version of this software for modelling bank scour. Furthermore, the setup and results of the upscaled laboratory experiment modelled in the Delft3D bank scour version are explained.

### A.1. Numerical modelling in Delft3D

Delft3D is a multi-dimensional (2D or 3D) modelling suite to investigate hydrodynamics, sediment transport and morphology and water quality for fluvial, estuarine and coastal environments (Deltares, 2016a). Delft3D consists of three main modules, which are Delft3D flow (FLOW), morphology (MOR) and waves (WAVE). The FLOW module of Delft3D is used in this research and is a multi-dimensional hydrodynamic and transport simulation programme which calculates non-steady flow and transport phenomena resulting from tidal and meteorological forcing on a curvilinear, boundary fitted grid or spherical coordinates.

### A.2. Bank erosion in Delft3D-FLOW

In Delft3D-FLOW version 4.02.02 the standard scheme will not allow erosion of the adjacent cells, even when a steep scour hole would develop right next to a dry bank (Deltares, 2016b). A user-defined factor ThetSD can change the scheme such that it allows the (partial) redistribution of an erosion flux from a wet cell to the adjacent dry cells. ThetSD determines the fraction of the erosion to assign to the adjacent cells and can be assigned a value between zero and one. ThetSD equals zero means that all erosion occurs at the wet cell and ThetSD equals one means that all erosion that would occur in the wet cell is assigned to the adjacent dry cells. The eroded sediment will be redistributed to adjacent cells. The erosion from the adjacent cells will replenish the eroded cell with different sediment fractions than those that were eroded, depending on the availability of individual sediment fractions at the central 'wet' cell and the surrounding 'dry' cells.

This bank erosion process works to a certain extent, but is very simplistic. The bank erosion rate might be sensitive to grid resolution and can stall in certain situations. Therefore a new approach to include bank erosion in Delft3D-FLOW is being developed.

### A.3. New approach of bank erosion in Delft3D-FLOW

Canestrelli (2016) developed a new approach to reproduce movable banks in Delft3D-FLOW, in a way that the hydraulic geometry of a channel can then be varied both vertically and laterally.

First, the method for solving hydrodynamics in Delft3D was adapted in order to include lateral erosion in the model. A scheme for solving the 3D shallow water equations on complex geometries was proposed in Canestrelli et al. (2015), since a moving bank line will result in embedded boundaries that are not aligned with the underlying horizontal Cartesian grid. In this scheme, ghost cells are used for the momentum equations in order to prescribe the correct boundary condition at the immersed boundary, while cut cells are used in the continuity equation in order to conserve mass.

Second, the erosion mechanism and numeric approach of the morphology for including lateral erosion in Delft3D was adapted. The bank erosion mechanism that is applied in the new

approach of bank erosion in Delft3D is described in Julian and Torres (2006) (Canestrelli, 2016). Lateral erosion of the banks was computed by the commonly used formula for the erosion of cohesive soils (e.g. Osman and Thorne, 1988):

$$E = k(\tau - \tau_c)$$

where E is the lateral erosion rate, k is an erodibility coefficient, $\tau$ is applied shear stress by flow and $\tau_c$ is critical shear stress for entrainment. The erodibility coefficient depends on e.g. vegetation, soil cohesion, etc. For example, an increase in the erodibility coefficient k results in a higher erosion rate, thus less cohesive banks are attained higher values of k. The lateral erosion formula assumes that the amount of hydraulic erosion is a function of the magnitude of excess shear stress (Julian and Torres, 2006). In Delft3D, the values of the erodibility coefficient and critical shear stress are defined by the user and the shear stress along the bank is computed according to:

$$\tau = \frac{u_b^2 \rho_w g}{C^2}$$

where $u_b$ is the flow velocity along the bank line, $\rho_w$ the density of water, g the gravitational acceleration and C the Chézy coefficient.

Using the cut-cell, immersed boundary method by Canestrelli et al. (2015) as described above, the banks in Delft3D are described as piecewise linear reconstructions. Based on the computed erosion rates E, banks are moved perpendicular to their local direction for each cell, after which the banks are newly reconstructed (Canestrelli, 2016). From the bank, all available material above the free-surface level of the adjacent wet cell is eroded.

The erosion rate is independent of the bank height above the water level in the model. When a higher bank height is eroded, however, more sediment will be available in channel dependent on the parameters that define how much of the eroded material is added to the bed load. Sediment that comes available from the retreating bank cells is distributed both or either in the water columns among the non-bank cells in the 3 x 3 cell stencil centred in the cell itself (Canestrelli, 2016). Two keywords, fracBANKdepos and fracBANKsuspWASH, control how this occurs by attaining a value between zero and one to the keywords. The keyword fracBANKdepos controls the percentage of eroded material which is deposited in adjacent cells. The remaining part is bank material which goes in suspension. They keyword fracBANKsuspWASH controls the percentage of suspended bank material which is lost as wash load (or maybe it is oxidized because it is organic). Therefore, if VOLeros is the volume eroded from the banks, the volume deposited in the adjacent cells bed is VOLUMEonTHEbed = fracBANKdepos*VOLeros. The volume of material entering the water column at each time step is given by SOURCEtermINwaterCOLUMN = (1-fracBANKsuspWASH) (1 -fracBANKdepos)*VOLeros.

## A.4. Scaling of flume experiment

An upscaled version of the flume experiment was modelled in Delft3D-FLOW with the new approach of bank erosion. In the flume experiment, bank protection was removed which allowed lateral erosion of the banks. The flume experiment was upscaled to a natural river size, since Delft3D-FLOW is not suited to model water depths in the order of 1 cm.

The classical approach to scale a laboratory experiment follows dimensional analysis procedures of the governing equations of both flow and sediment motion (Kleinhans et al., 2014). The resulting scaling should represent the most important hydromorphodynamic processes.

The similarity scaling of the first numerical model was based on geometrical similarity and hydraulic similarity. Geometrical similarity was obtained by multiplying the width, length and water depth by a scaling factor of 250. Hydraulic similarity of free surface flow required Froude number similarity. Table A.1 shows the scaled parameters such that the Froude number was equal in the experiment and model. The Froude number is close to critical and this resulted in numerical problems in the model. Therefore in the second model, hydraulic similarity was not obtained.

The similarity scaling of the second numerical is based on the procedure of Tewolde (2015), except from having hydraulic similarity. The Shields parameter and bar mode are similar in the model and experiment to produce similarity between the model and experiment. Sediment transport similarity of the bed load requires Shields parameter similarity. Morphological similarity, however, cannot be guaranteed by hydrodynamic and sediment mobility similarity (Kleinhans et al., 2014). In the experiment, the main morphological features were bars. Therefore, the bar mode of the linear theory by Crosato and Mosselman (2009) is used in order to achieve morphological similarity. Table A.1 shows the upscaled parameters that were determined with an iterative procedure for the numerical models.

*Table A.1 - Similarity scaling between flume experiment and numerical model.*

| Parameter | Unit | Experiment | Numerical model [1] | Numerical model [2a] | Numerical model [2b] |
|---|---|---|---|---|---|
| Width B | m | 0.2 | 50 | 50 | 50 |
| Discharge Q | $m^3/s$ | 0.0006 | 593 | 265 | 265 |
| Bed slope i | - | 0.008 | 0.008 | 0.0017 | 0.0017 |
| Median sediment diameter $D_{50}$ | m | 0.00052 | 0.04 | 0.03 | 0.03 |
| Reach-average water depth $h_0$ | m | 0.01 | 2.53 | 2.48 | 2.48 |
| Reach-average flow velocity $u_0$ | m/s | 0.30 | 4.74 | 2.14 | 2.14 |
| Chézy coefficient C | $m^{1/2}/s$ | 33 | 33 | 33 | 33 |
| Width-to-depth ratio B/h | - | 20 | 20 | 20 | 20 |
| **Froude number Fr** | **-** | **0.94** | **0.94** | 0.43 | 0.43 |
| **Shields parameter θ** | **-** | **0.09** | 0.3 | **0.09** | **0.09** |
| **Bar mode m** | **-** | **1.14** | 1.52 | **1.14** | **1.14** |
| Erodibility coefficient k | m/s | - | 0.00005 | 0.00005 | 0.0005 |

## A.5. Setup numerical model

Table A.1 shows the parameters in the setup of the numerical models. The numerical models are two-dimensional, since this reduces the computational time. The grid of the numerical model has 350 cells in longitudinal direction and 50 cells in transversal direction. The numerical model is geometrically upscaled from the experiment. In the numerical model, the length of the main channel is 1540 metres, the width of the main channel is 50 metres and the width of the floodplains is 125 metres. Figure A.1 shows the main channel and floodplains that functioned as erodible sections. The erodible sections were indicated with polygons in the model setup, which were the only sections where the banks could erode laterally. The floodplains were five metres elevated above the main channel bed.

The model runs for 24 hours with a time step of 0.025 min to ensure a Courant number lower than ten. The sediment process is turned on in the model, which allows sediment transport. The horizontal eddy viscosity and diffusivity are both 0.001 $m^2/s$. The bathymetry is updated during the FLOW simulation. There is an equilibrium sand concentration profile at the inflow boundary. The morphological scale factor is one, such that the morphodynamics changes with the same speed as the hydrodynamics.

The initial condition is a water depth of 2.5 metres in the main channel. An open inflow boundary is defined upstream of the main channel with a constant discharge specified in Table A.1. The open outflow boundary is defined downstream of the main channel with a constant water level specified in Table A.1.

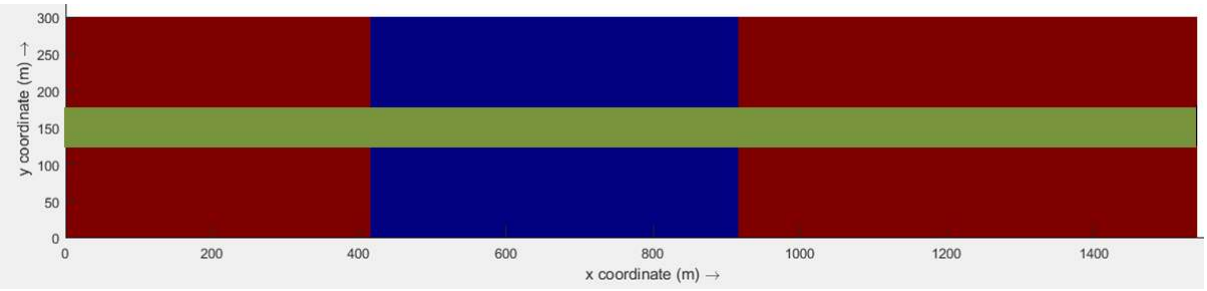


*Figure A.1 – Two-dimensional grid of the numerical models. The main channel is highlighted green, the erodible sections (floodplains) are indicated in blue and the non-erodible sections are indicated in red.*

## A.6. Results

Three numerical models were analysed and their results compared with the flume experiment. Experimental test R06 is most representative for comparison, since on both sides of the flume a bank protection length of nine times the channel width was removed.

In the first numerical model the flow upstream in the main channel changes to supercritical, since the bed slope increases due to an increase in bed load transport. Numerical model [1] was stalled after 17 timesteps, due to the high Froude numbers in the model (Figure A.2). Delft3D-FLOW assumes that the flow at the open boundaries is subcritical, which means that the magnitude of the flow is smaller than the velocity of wave propagation (Deltares, 2016b). The second numerical model is therefore adapted to have Froude numbers lower than one during the simulation. The simulation of the first model at time step 17 time steps is shown in all figures, whereas the second model simulation is shown at time step 289 (after 24 hours).

At the start of each simulation, the bank eroded on the sides of the channel. The widening of the channel decreased the flow velocity and thereby the shear stress at the banks (Figure A.3). The erosion rate decreased in time, but was not zero at the end of the simulations. Numerical model [2b] was aimed at decreasing the erosion rate to zero to show the final bank shape. The erodibility coefficient in numerical model [2b] was therefore a factor 10 larger than in numerical model [2a], since this increases the erosion rate by a factor 10. At the end of simulation [2b] the bank was still eroding, but at a lower rate than at the end of simulation [2a]. The erosion rate differed slightly between the banks in simulation [2b], which may be caused by a small disturbance in the hydrodynamics. Figure A.4 shows the final shapes of the eroded banks. The shape of the eroded bank is determined by the velocity field (figure). After some initial bank erosion at the beginning of the erodible bank part (upstream) the velocity detached from the wall and two areas of lower velocity form next to the wall. The banks erode slower,

while there is still high flow velocity in the centre of the erodible part. Similar as in the experiments, the widening started upstream and moved in downstream direction. The final shape of the erode bank line of simulation [2b] is approximately similar as in the experiment. The angle of the eroded banks with the main channel in simulation [2b] is 9 degrees, which is slightly larger than the angle in the experiment.

Figure A.5 shows the cumulative sedimentation and erosion of the simulations. A sediment hump is developed at the upstream end of the widened reach. This hump is caused by the flow deceleration from the main channel towards the widened reach (Figure A.3). The flow velocity decrease results in less transport capacity of sediment and thus deposition. The sediment hump is slowly moving in downstream direction. This sediment hump is not seen in the experiment. The aggradation of the bed is more gradual in the widened reach in the experiment. Figure A.6 shows the sediment hump at the upstream end and a scour hole at the downstream end of the widening. The scour hole has a depth of approximately 1.7 metres in simulation [1] and 0.6 metres in simulation [2a] and [2b]. The scour hole was also present in the experiment, but was relatively larger than the scour hole in the model.

There were no bars formed in the channel bed of the simulations. This might be due to a simulation time that is too short for bars to form. Another reason might be that for the formation of bars an asymmetrical upstream flow forcing is needed in the model.

## A.7. Discussion

Scaling of the flume experiment has been conducted with two different methods. The first numerical model was not scaled properly, since the bar mode similarity and Shields parameter similarity were not taken into account. The second numerical model was also not scaled properly, since the Froude number was much lower in the model than in the experiment. This was however a condition for the model, since with too high Froude numbers the model stalled. For this research, accurate upscaling of the experiment was not a main goal, since the research into the numerical model is in its initial stages. The model could have been made with parameters for a general river, since it is most important that the hydrological and morphological processes are modelled well in the new approach of bank erosion in Delft3D-FLOW.

The distance and direction of bank retreat are computed using one bank erosion formula. The bank erosion mechanism does not include erosion due to groundwater as well as many other erosion mechanisms. The bank erosion formula can be easily extended to incorporate other bank erosion mechanisms.

The final eroded bank shape might be partially a result of the numeric treatment at the discontinuity between erodible and non-erodible bank (Canestrelli, 2016). To avoid loss of smoothness in the bank at the entrance and at the exit of the widened reach, the entire area at the sides of the main channel should be prescribed as bank in the input polygon. The part which should not erode should have a high critical erosional stress.

The numerical models run in two-dimensional mode (one computational layer), which corresponds to solving the depth-averaged equations. Secondary flow (spiral motion) is automatically taken into account in a 3D simulation, but in 2D simulations the flow equations must be extended to take this effect into account. The flow in a river bend is basically three-dimensional. The spiral flow effect is important in calculations of changes of the river bed in

morphological models, e.g. in a depth-averaged simulation to get point bar formation in river bends (Deltares, 2016b).

Delft3D cannot model local scour, so usually the size of a scour hole is under predicted in a numerical model in Delft3D. This was also observed in this research, where the scour hole in the numerical model was relatively smaller than in the laboratory experiment.

No bars were seen in the model runs which can have several reasons. One reason is that Delft3D has more diffusion that supresses the formation of bars (Mosselman, 2017). Another reason that no bars were formed could be due to the choice of the numerical scheme (Mosselman, 2017).

## A.8. Conclusions and recommendations

The new approach of bank erosion in Delft3D has been used in this research. The results of the simulations show that the banks erode with a rate and shape that seems appropriate. The shape of the eroded bank line in the numerical model was approximately similar to the shape of the eroded bank line in the flume experiment. The main differences between the experiment and model are the size of the scour hole and the sedimentation in the main channel. The scour holes at the downstream end of the widened reach were larger in the experiment. In the model a high sedimentation hump is formed upstream in the widened reach, whereas in the experiment the sedimentation is more spread in the widened reach.

It is recommended to do more simulations with the new approach of bank erosion in Delft3D-FLOW. The simulations can be extended with including the process secondary flow or including more vertical layers for a three-dimensional model. Furthermore, research should be done into extending the bank erosion mechanism in the new approach of bank erosion in Delft3D-FLOW, since groundwater and other bank erosion mechanisms are not included. Finally, the numerical simulations should be compared with bank erosion in natural rivers and adapted according to the outcome of the comparisons. This will improve the new approach of bank erosion in Delft3D-FLOW and extend the applicability of the model.

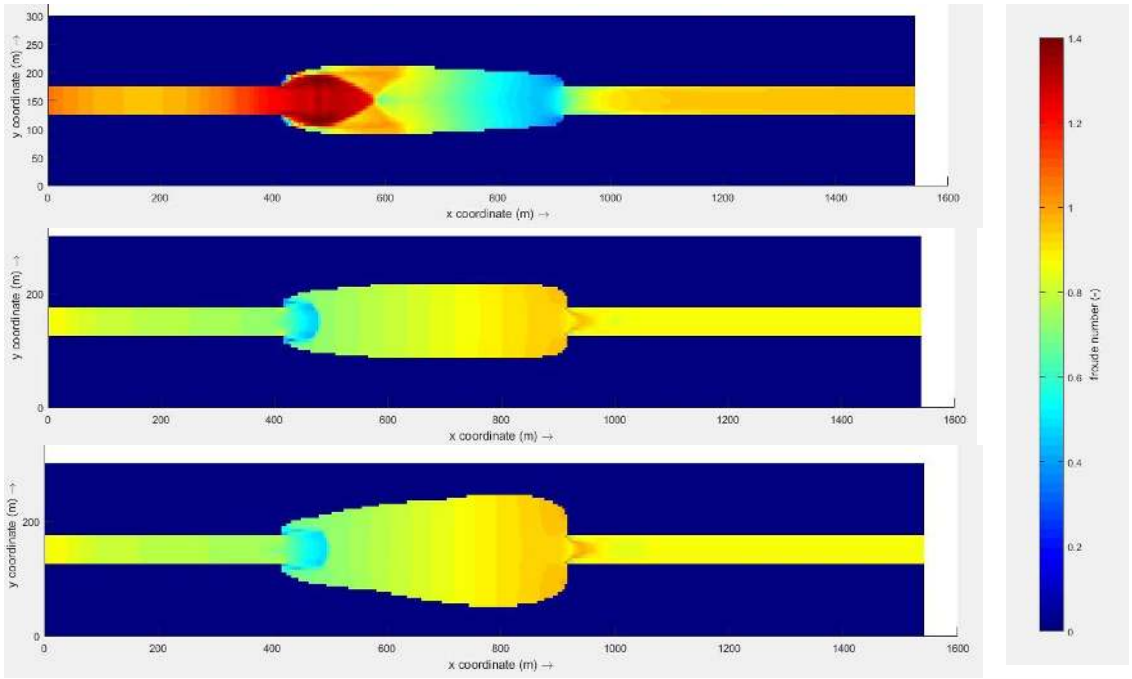


*Figure A.2 – Froude number in numerical model [1] (top), numerical model [2a] (middle) and numerical model [2b] (bottom) at the end of the simulations.*

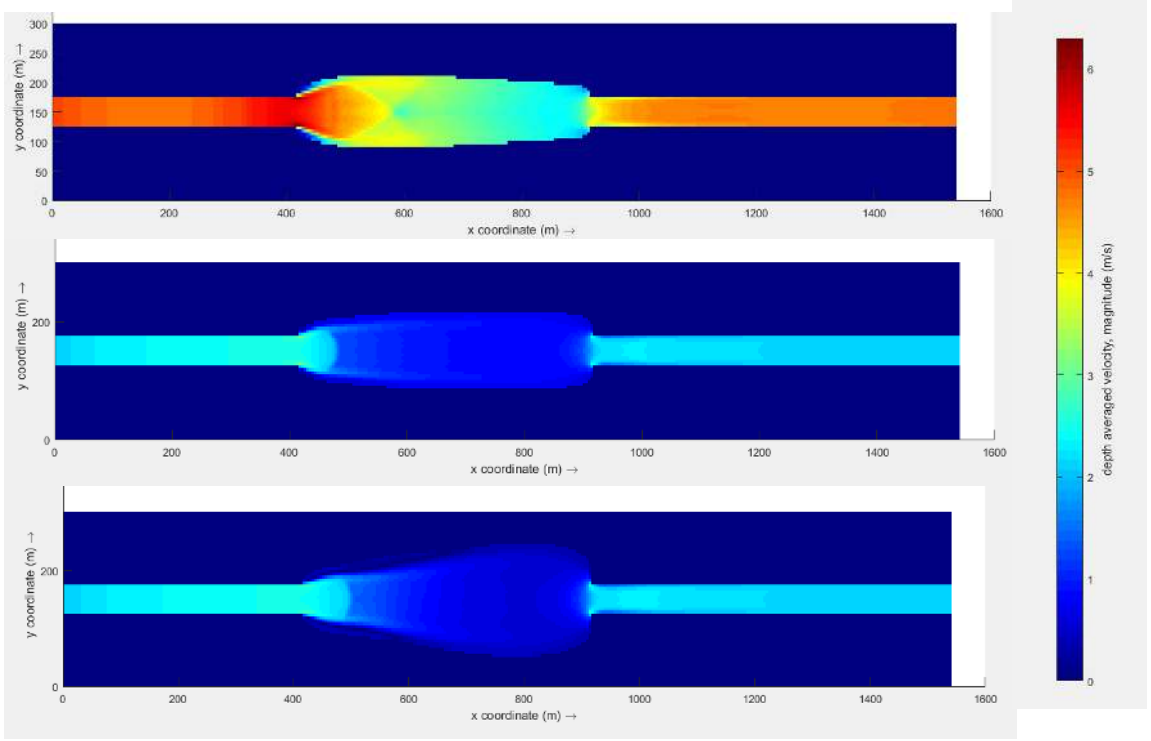


*Figure A.3 – Depth average velocity in numerical model [1] (top), numerical model [2a] (middle) and numerical model [2b] (bottom) at the end of the simulations.*

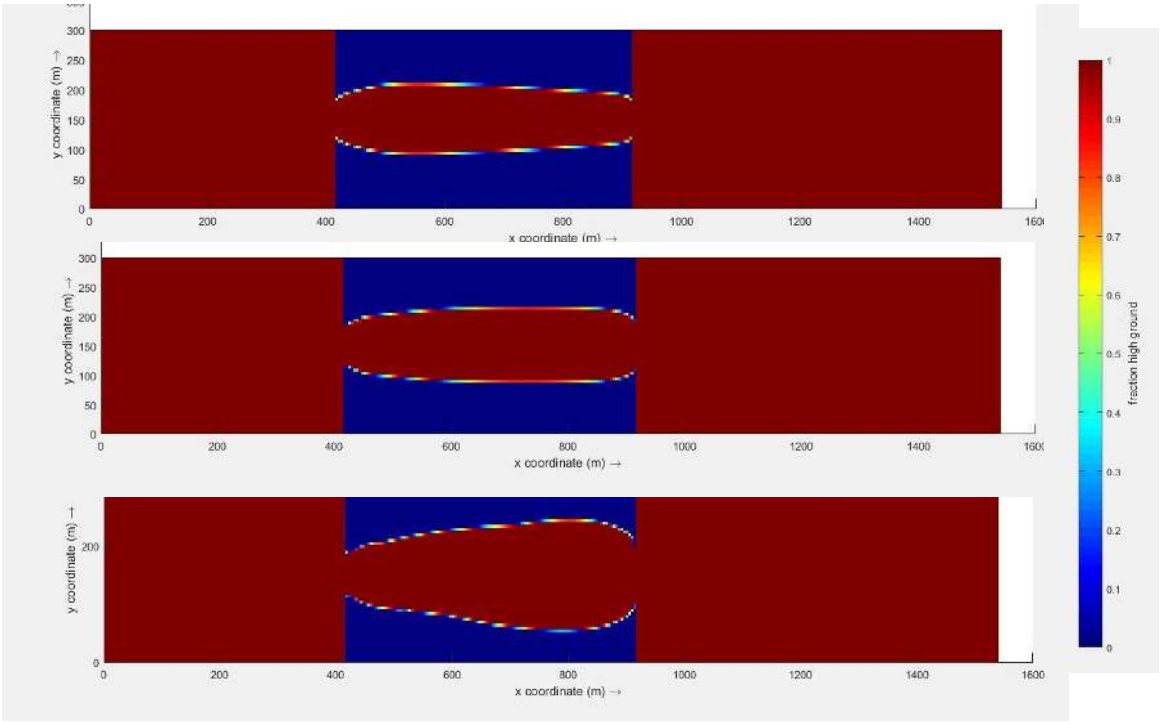


*Figure A.4 – Fraction high ground in numerical model [1] (top), numerical model [2a] (middle) and numerical model [2b] (bottom) at the end of the simulations. The fraction high ground is the area within the input polygon that can still be eroded.*

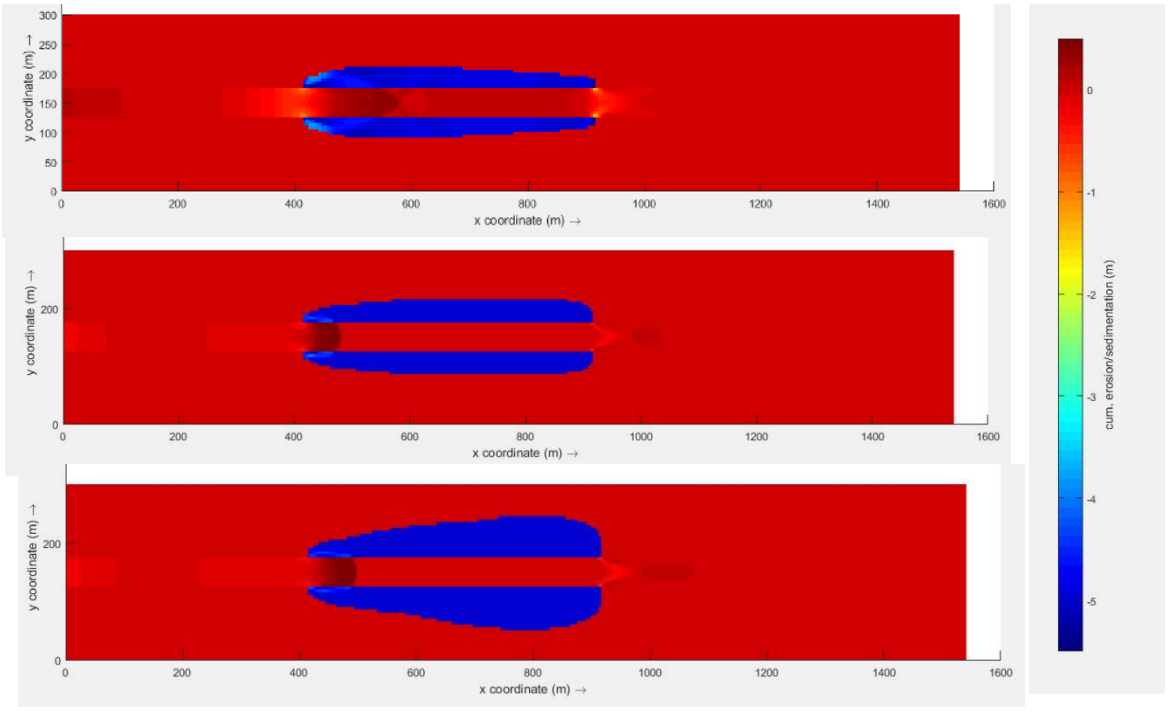


*Figure A.5 – Cumulative erosion and sedimentation in numerical model [1] (top), numerical model [2a] (middle) and numerical model [2b] (bottom) at the end of the simulations. Sedimentation is indicated with dark red and erosion is indicated with blue.*

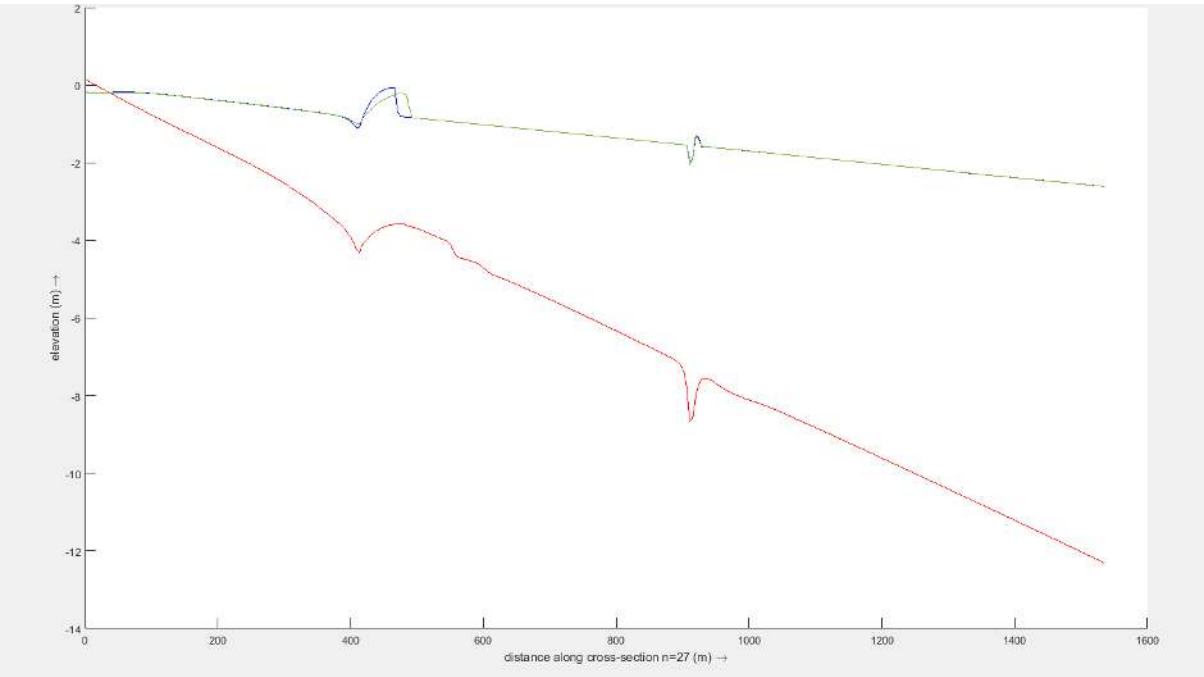


*Figure A.6 – Longitudinal profiles in the main channel at y = 162 of numerical model [1] (red line), numerical model [2a] (blue line) and numerical model [2b] (green line) at the end of the simulations.*

## Appendix B. Gravel-bed river similarity

This appendix describes the scaling of the laboratory experiment to gravel-bed rivers.

The dimensionless parameters characterizing channel bankfull geometry are defined as (Parker, 2004):

$$\hat{Q} = \frac{Q_{bf}}{\sqrt{gD_{50}}D_{50}^2} \tag{12}$$

$$\hat{H} = \frac{h_{bf}}{D_{50}} \tag{13}$$

$$\hat{B} = \frac{B_{bf}}{D_{50}} \tag{14}$$

$$Fr = \frac{Q_{bf}}{B_{bf}h_{bf}\sqrt{gh_{bf}}} \tag{15}$$

$$\tau_{bf}^* = \frac{h_{bf}i}{\Delta D_{50}} \tag{16}$$

$$C_{bf} = \frac{Q_{bf}}{B_{bf}h_{bf}\sqrt{gh_{bf}i}} \tag{17}$$

$$Re^* = \frac{\sqrt{\Delta gD_{50}}D_{50}}{\upsilon} \tag{18}$$

In which the parameters are defined as the dimensionless bankfull discharge $\hat{Q}$, dimensionless bankfull depth $\hat{H}$, dimensionless bankfull width $\hat{B}$, bankfull Froude number $Fr$, estimate of bankfull Shields number $\tau_{bf}^*$, bankfull Chézy coefficient $C_{bf}$, particle Reynolds number $Re^*$, bankfull discharge $Q_{bf}$, bankfull width $B_{bf}$, bankfull water depth $h_{bf}$, bed slope $i$, and kinematic viscosity of water $\upsilon$.

The dimensionless parameters of conditions in the laboratory experiment in preliminary phase can be calculated with parameter values from Table 3.2. Substituting these parameter values in equation (12) to (18) gives values of dimensionless parameters shown in Table B.1.

Dimensionless parameters of the experiment can be compared with dimensionless parameters of natural rivers. Parker (2004) plotted several combinations of dimensionless parameters and indicated multiple gravel- and sand-bed rivers in these plots (Figure B.1 to Figure B.8). Alluvial

rivers show a considerable degree of commonality, however, a distinction can be made between gravel- and sand-bed rivers as shown in Figure B.1 to Figure B.8. In these figures dimensionless parameters of the experiment are indicated with a red point. Figure B.1 to Figure B.7 show that plotted relations between dimensionless parameters of the experiment are in the same range as in gravel-bed rivers. Figure B.8 shows, however, that the particle Reynolds number in the experiment is a factor 1000 smaller than in gravel-bed rivers. The channel bed in the flume is hydraulically smoother than a gravel-bed in a river. The characteristic of gravel-bed rivers that can be obtained from Figure B.8 is that the sediment is not in suspension, but transported as bed-load material. Furthermore, the majority of gravel-bed rivers consist of material that is in motion. Sediment is also not in suspension in the experiment and consists of material that is in motion. The characteristics of gravel-bed rivers therefore equals those in the experiments. Finally, it can be concluded that the experiment is a small scale representative for natural gravel-bed rivers.

*Table B.1 – Values of calculated dimensionless parameters characterizing bankfull geometry in the laboratory experiment in preliminary phase.*

| Dimensionless parameter | $\hat{Q}$ | $\hat{H}$ | $\hat{B}$ | $Fr$ | $\tau^*_{bf}$ | $C_{bf}$ | $Re^*$ |
|---|---|---|---|---|---|---|---|
| Value | $3.4*10^4$ | $2.0*10^1$ | $4.0*10^2$ | $9.5*10^{-1}$ | $9.7*10^{-2}$ | $1.1*10^1$ | $4.5*10^1$ |

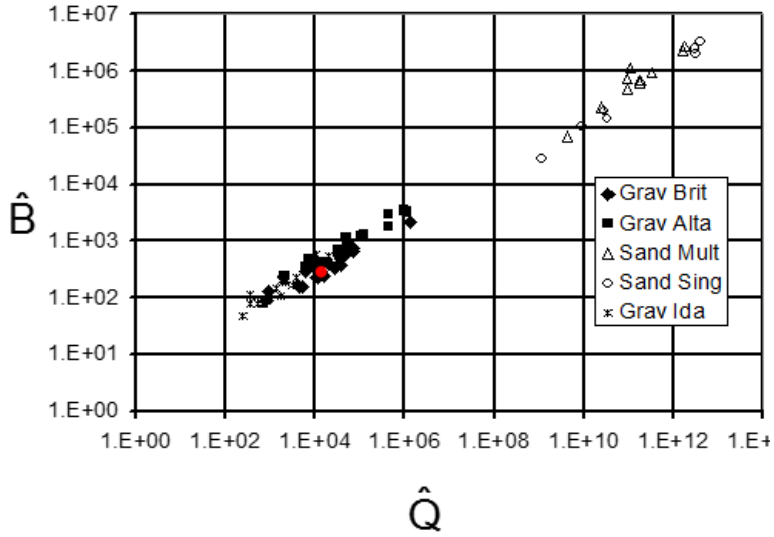


*Figure B.1 – Dimensionless width versus dimensionless discharge (Parker, 2004). Red point indicates experiment in plot.*

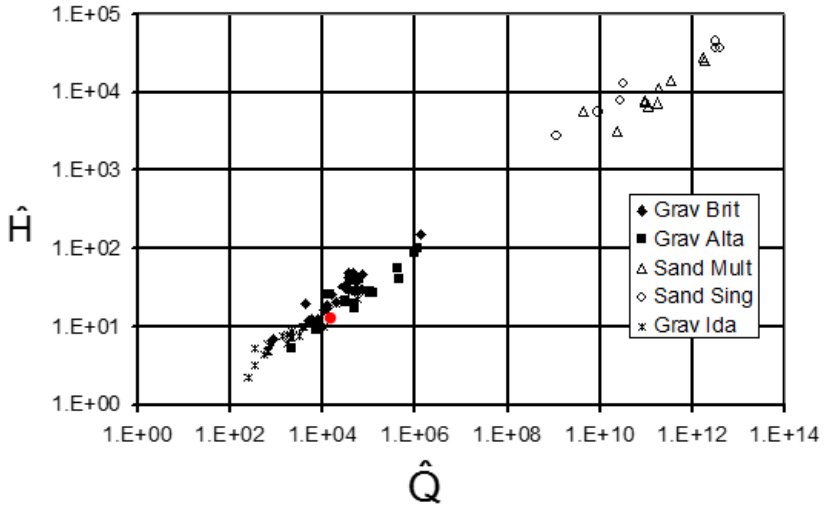


*Figure B.2 – Dimensionless water depth versus dimensionless discharge (Parker, 2004). Red point indicates experiment in plot.*

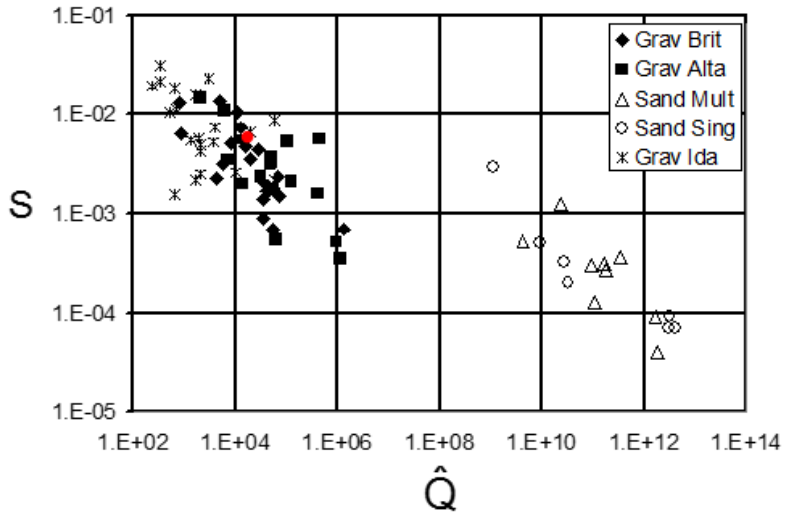


*Figure B.3 – Bed slope versus dimensionless discharge (Parker, 2004). Red point indicates experiment in plot.*

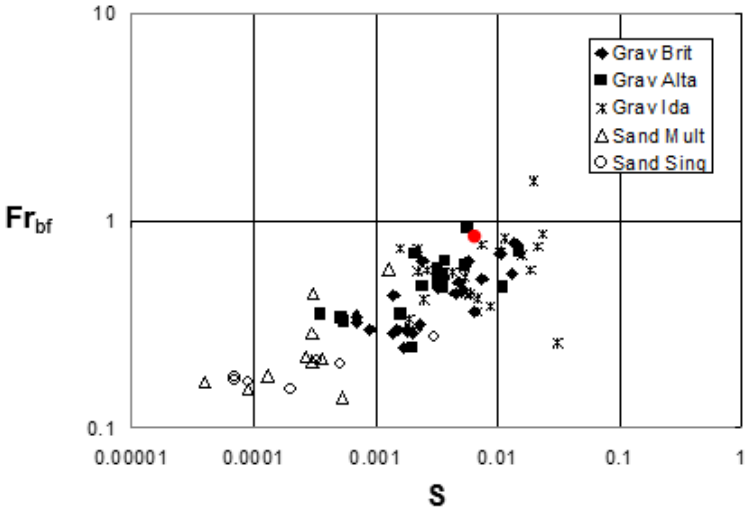


*Figure B.4 – Froude number versus bed slope (Parker, 2004). Red point indicates experiment in plot.*

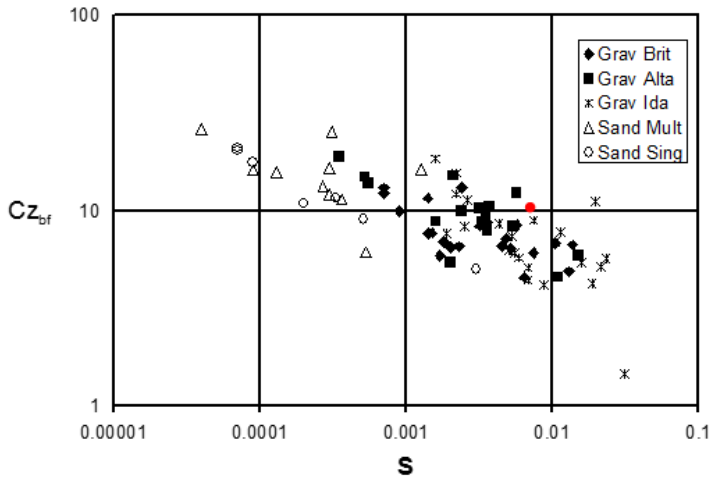


*Figure B.5 – Chézy coefficient versus bed slope (Parker, 2004). Red point indicates experiment in plot.*

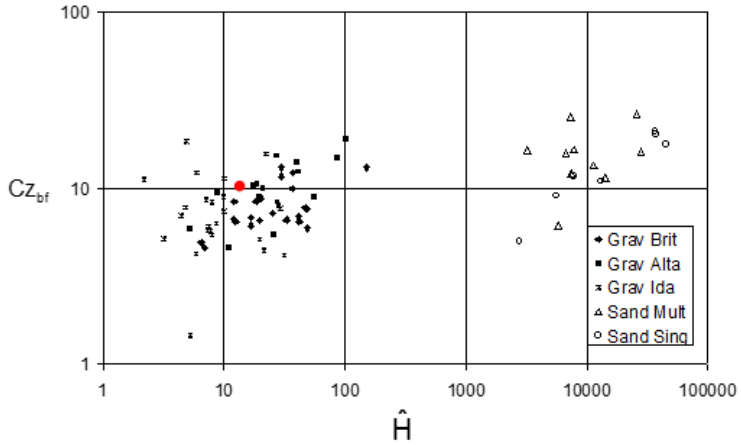


*Figure B.6 – Chézy coefficient versus dimensionless water depth (Parker, 2004). Red point indicates experiment in plot.*

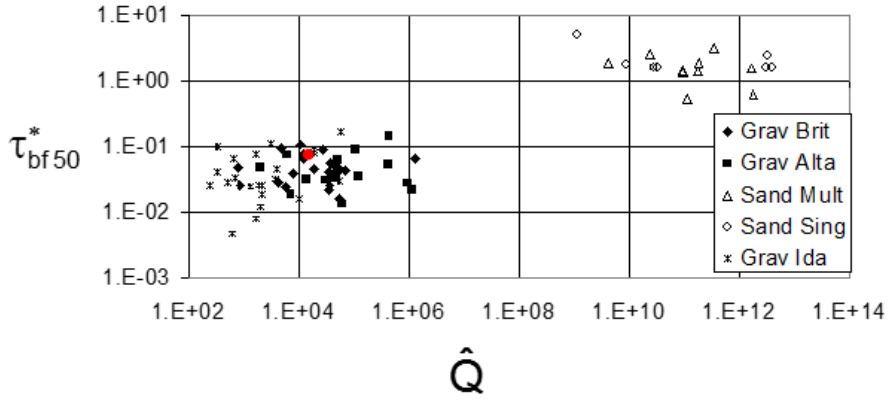


*Figure B.7 – Estimate of bankfull Shields number versus dimensionless discharge (Parker, 2004). Red point indicates experiment in plot.*

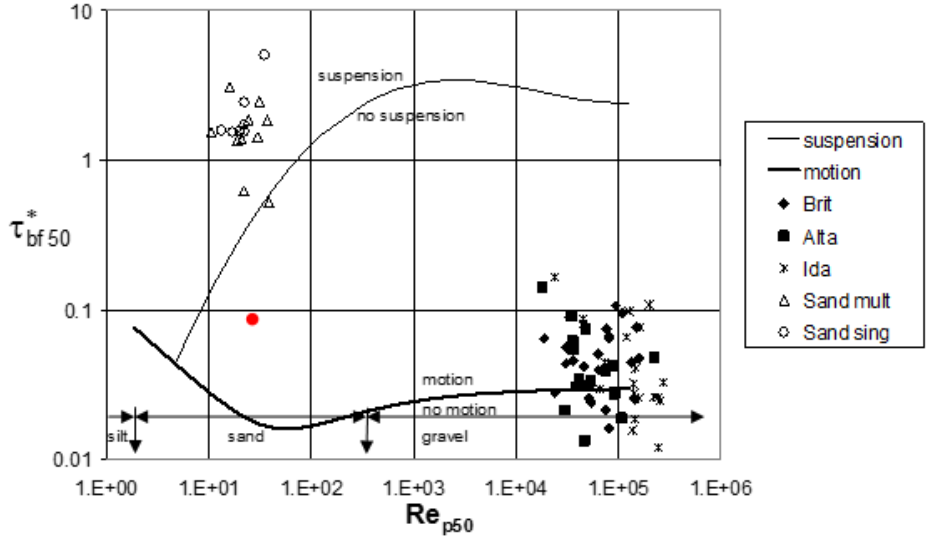


*Figure B.8 – Estimate of bankfull Shields number versus particle Reynolds number (Parker, 2004). Red point indicates experiment in plot.*

## Appendix C. Widely graded sediment

In this appendix, Table C.1 shows the particle size distribution and Figure C.1 shows the sieve curve of the widely graded sediment used in test Pr04 in the preliminary phase in Section 3.2.1.

*Table C.1 - Particle size distribution of widely graded sediment of test Pr04*

| Characteristic parameter of a size distribution | Sediment grain size [mm] |
|---|---|
| D15 | 0.3 |
| D50 | 0.63 |
| D65 | 0.85 |
| D90 | 1.35 |

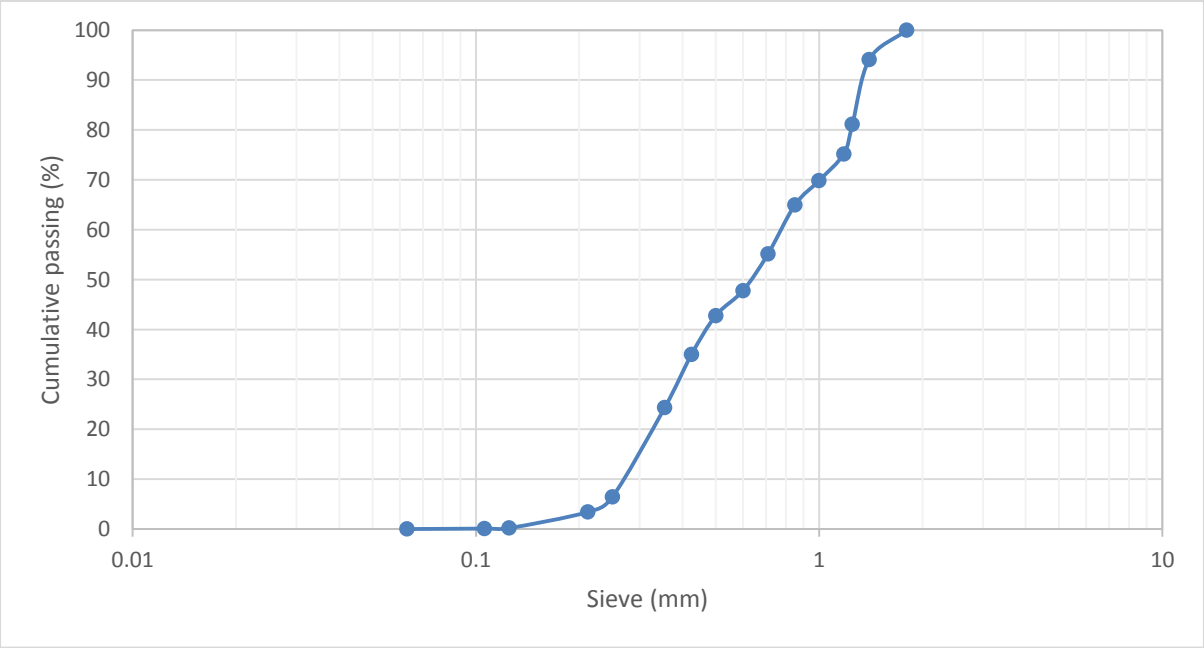


*Figure C.1 – Sieve curve of widely graded sediment of test Pr04*

## Appendix D. Setup experimental tests

In this appendix, Figure D.1 and Figure D.2 show the setup of the experimental tests.

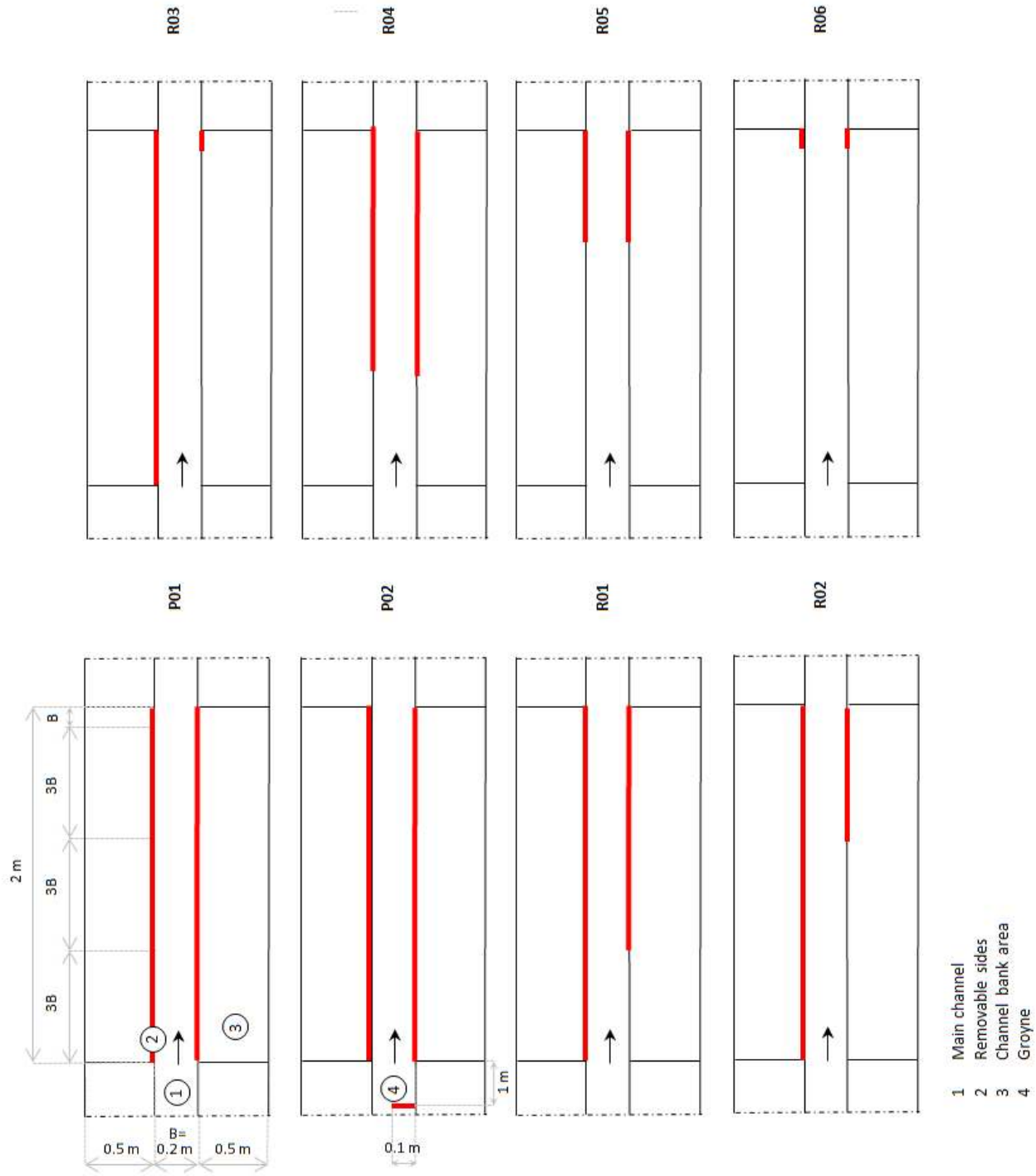


*Figure D.1 – Setup of experimental tests P01, P02 and R01 to R06.*

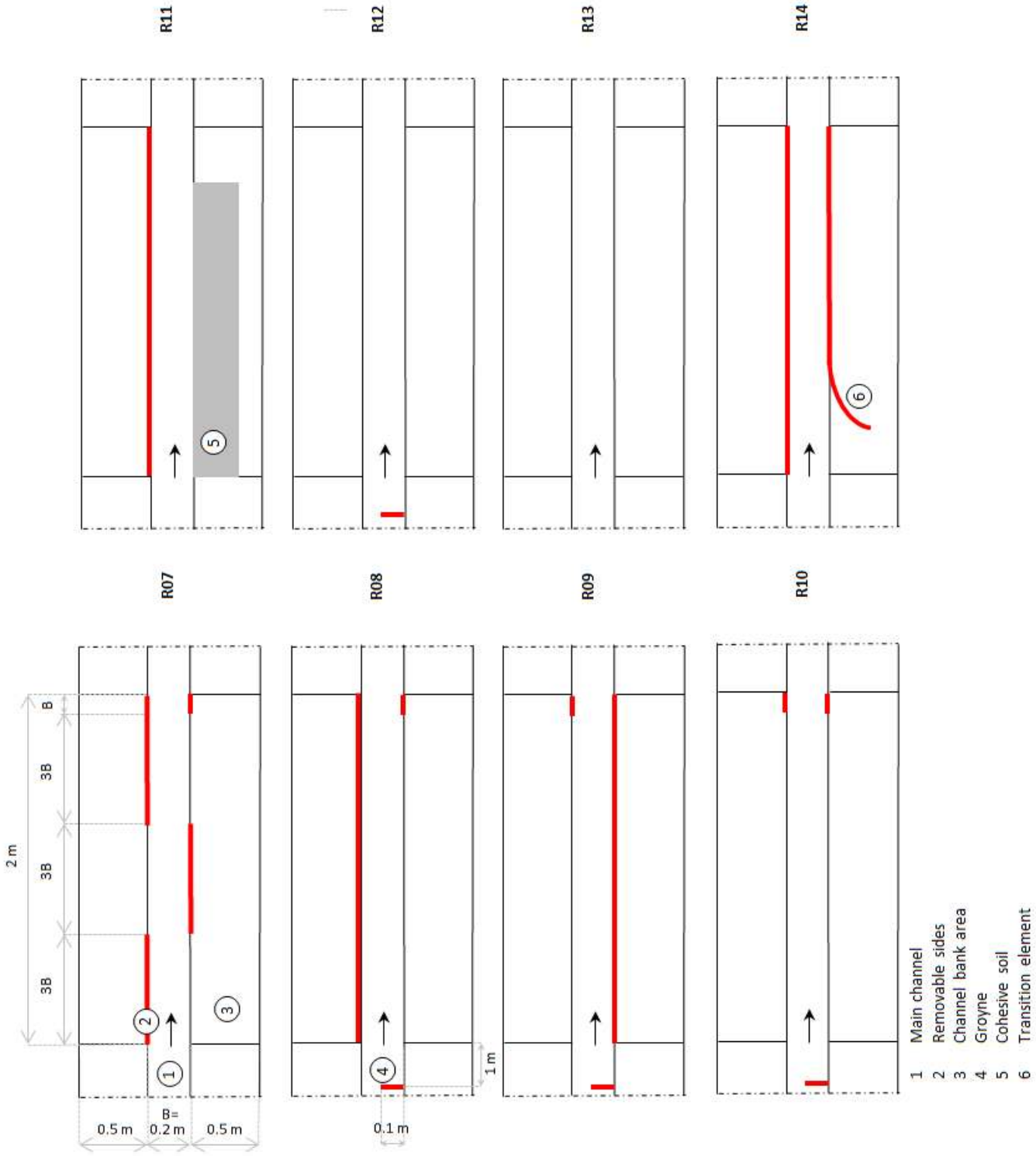


*Figure D.2 – Setup of experimental tests R07 to R14.*

## Appendix E. Bar formation in laboratory experiment

In this appendix photos of the final bed topography and detrended bed profiles of the experimental tests are shown in Figure E.1 to Figure E.16. The photos are taken when dye is added upstream to the flow at low discharges in the flume. Areas with the largest water depths are coloured red. The bar areas are drawn in these figures and are determined with a method described in Appendix F. The bar height is indicated in two classes, based on the average maximum bar height of 0.45 m determined from the bed profiles. Table E.1 shows the height class of each bar and the relative bar area.

The bed profiles were measured at three locations in the main channel. One laser is located in the middle of the main channel and the other lasers are 3 cm located from the main channel sides. The bed profiles are detrended, since bars area more clear in detrended bed profile figures. The large troughs in the graphs are scour holes that formed at the downstream end of the widened reach.

Bar formation is analysed on the basis of the final detrended bed profiles and photos of bed topographies collected during the experiment. The bar types, locations, wave length, maximum heights, height class and relative bar area of each experimental test are summarized in Table E.1. The bar wave length and maximum bar height could be determined from the detrended bed profiles.

*Table E.1 - Bar type, location, wave length and maximum height in final bed topography for each experimental test. The bar is located on the left side of the channel when y=53 cm, in the middle of the channel for y=60 cm and on the right side of the channel for y=67 cm. The relative bar area is a percentage of the area of the whole channel and the floodplains. The relative maximum bar height is the bar maximum height divided by the average water depth of $h_0$ = 1 cm given.*

| Test | Bar type | Location y [cm] | Location x [cm] | Wave length [cm] | Relative maximum bar height [-] | Height class | Relative bar area [%] |
|---|---|---|---|---|---|---|---|
| P01 | Free | 53 | -50 – 100 | 150 | 0.3 | Low | 1.9 |
| | Free | 67 | 60 - 360 | 300 | 0.2 | Low | 3.5 |
| | Free | 53 | 350 – 415 | 65 | 0.3 | Low | 1.3 |
| P02 | Forced | 67 | 0-140 | 140 | - | Low | 3.7 |
| | Hybrid | 53 | 30 - 240 | 210 | 0.25 | Low | 5.2 |
| | Hybrid | 67 | 240 – 370 | 130 | 0.25 | Low | 3.0 |
| R01 | Forced | 53 | -100 – 80 | 180 | 0.35 | Low | 2.9 |
| | Hybrid | 67 | 80 - 320 | 240 | 0.35 | Low | 4.4 |
| | Hybrid | 53 | 280 – 415 | 35 | 0.35 | Low | 2.6 |
| R02 | Forced | 53 | -100 – 60 | 160 | 0.15 | Low | 2.6 |
| | Forced | 67 | 20 – 160 | 140 | 0.65 | High | 5.9 |
| | Hybrid | 53 | 190 – 310 | 120 | 0.25 | Low | 2.6 |
| | Free | 67 | 310 – 400 | 90 | 0.55 | High | 1.3 |
| R03 | Forced | 53 | -100 – 70 | 170 | 0.45 | Low | 2.5 |
| | Forced | 67 | 70 – 300 | 230 | 0.8 | High | 9.6 |
| | Hybrid | 53 | 300 – 430 | 130 | 0.3 | Low | 4.0 |
| R04 | Forced | 67 | 0 – 175 | 175 | 0.15 | Low | 2.9 |
| | Hybrid | 53 | 175 – 310 | 135 | 0.25 | Low | 2.9 |
| | Free | 67 | 310 - 430 | 120 | 0.6 | High | 2.2 |
| R05 | Forced | 53 | -10 – 110 | 120 | 0.6 | High | 6.5 |
| | Hybrid | 67 | 140 - 220 | 80 | 0.35 | Low | 2.3 |
| | Hybrid | 53 | 220 – 310 | 90 | 0.3 | Low | 2.0 |
| | Free | 67 | 320 – 415 | 95 | 0.4 | Low | 2.8 |
| R06 | Forced | 74 | 15 - 180 | 165 | 0.9 | High | 7.0 |
| | Forced | 34 | 15 – 200 | 185 | 0.9 | High | 7.7 |
| | Hybrid | 67 | 210 – 380 | 170 | 0.4 | Low | 3.9 |
| | Hybrid | 53 | 370 – 450 | 80 | 0.55 | High | 1.2 |

| Test | Bar type | Location y [cm] | Location x [cm] | Wave length [cm] | Relative maximum bar height [-] | Height class | Relative bar area [%] |
|---|---|---|---|---|---|---|---|
| R07 | Forced | 53 | 0 – 110 | 110 | 0.5 | High | 3.5 |
| | Forced | 67 | 140 – 205 | 65 | 0.7 | High | 1.6 |
| | Hybrid | 53 | 220 – 370 | 150 | 0.4 | Low | 3.1 |
| | Free | 67 | 385 – 450 | 65 | 0.55 | High | 1.5 |
| R08 | Forced | 67 | -100 – 0 | 100 | - | Low | 3.7 |
| | Forced | 67 | 40 – 270 | 230 | 0.8 | High | 11.6 |
| | Hybrid | 53 | 290 – 430 | 140 | 0.45 | High | 3.8 |
| R09 | Forced | 67 | -100 – 30 | 130 | - | Low | 4.5 |
| | Forced | 53 | 40 – 280 | 240 | 0.75 | High | 6.7 |
| | Hybrid | 67 | 280 – 415 | 135 | 0.2 | Low | 4.3 |
| R10 | Forced | 67 | -100 – 0 | 100 | - | Low | 4.0 |
| | Forced | 60 | 40 - 170 | 130 | 0.9 | High | 12.6 |
| | Hybrid | 67 | 190 – 230 | 40 | 0.6 | High | 0.9 |
| | Hybrid | 53 | 280 - 430 | 150 | 0.55 | High | 3.5 |
| R11 | Forced | 53 | -100-100 | 200 | 0.2 | Low | 4.7 |
| | Forced | 67 | 30 – 250 | 220 | 0.4 | Low | 4.2 |
| | Hybrid | 53 | 250 – 370 | 120 | 0.3 | Low | 2.9 |
| | Free | 67 | 380 – 420 | 40 | 0.2 | Low | 0.7 |
| R12 | Forced | 67 | -100-0 | 100 | - | Low | 3.6 |
| | Forced | 60 | 50 – 200 | 150 | 0.9 | High | 16.1 |
| | Hybrid | 67 | 210 – 270 | 60 | 0.55 | High | 1.3 |
| | Free | 53 | 320 – 420 | 100 | 0.65 | High | 2.4 |
| R13 | Forced | 60 | 70 – 200 | 130 | 0.95 | High | 11.4 |
| | Hybrid | 67 | 210 – 280 | 70 | 0.3 | Low | 1.2 |
| | Free | 53 | 290 – 370 | 80 | 0.3 | Low | 2.1 |
| R14 | Forced | 53 | -80 – 80 | 160 | 0.3 | Low | 1.9 |
| | Hybrid | 67 | 80 – 260 | 180 | 0.35 | Low | 3.4 |
| | Free | 53 | 260 – 395 | 135 | 0.25 | Low | 2.8 |

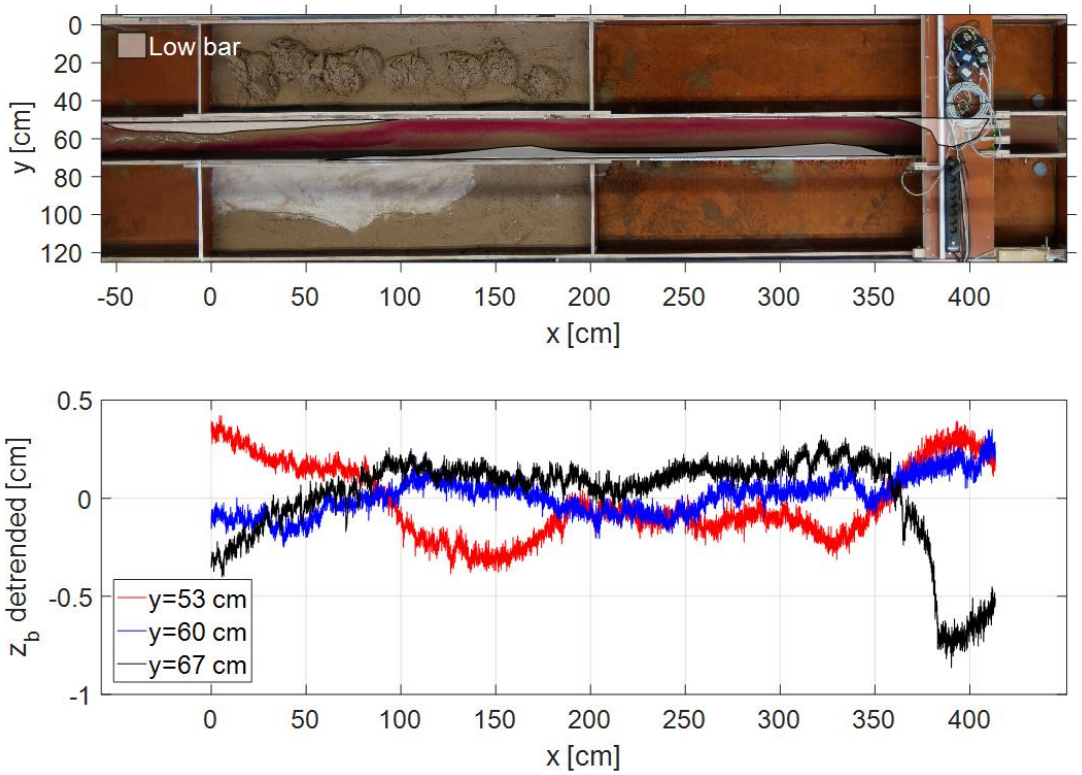


*Figure E.1 –Final bed topography photo with bars (top) and detrended bed profile (bottom) of test P01.*

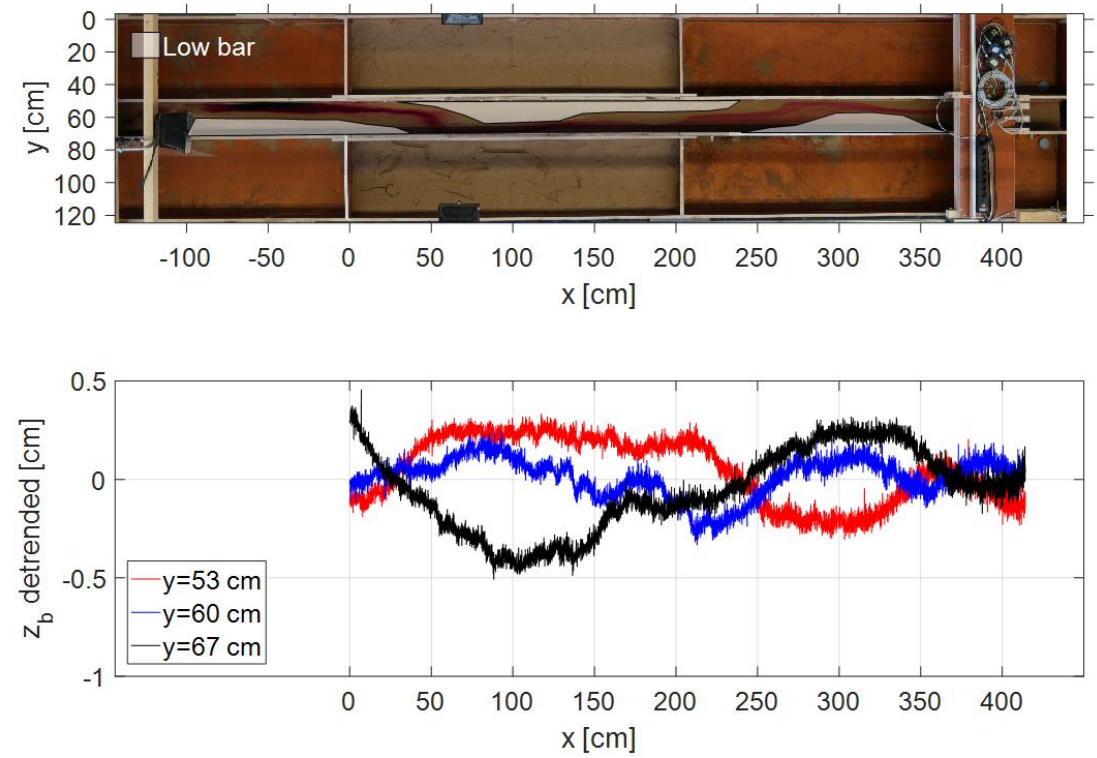


*Figure E.2 - Final bed topography photo with bars (top) and detrended bed profile (bottom) of test P02.*

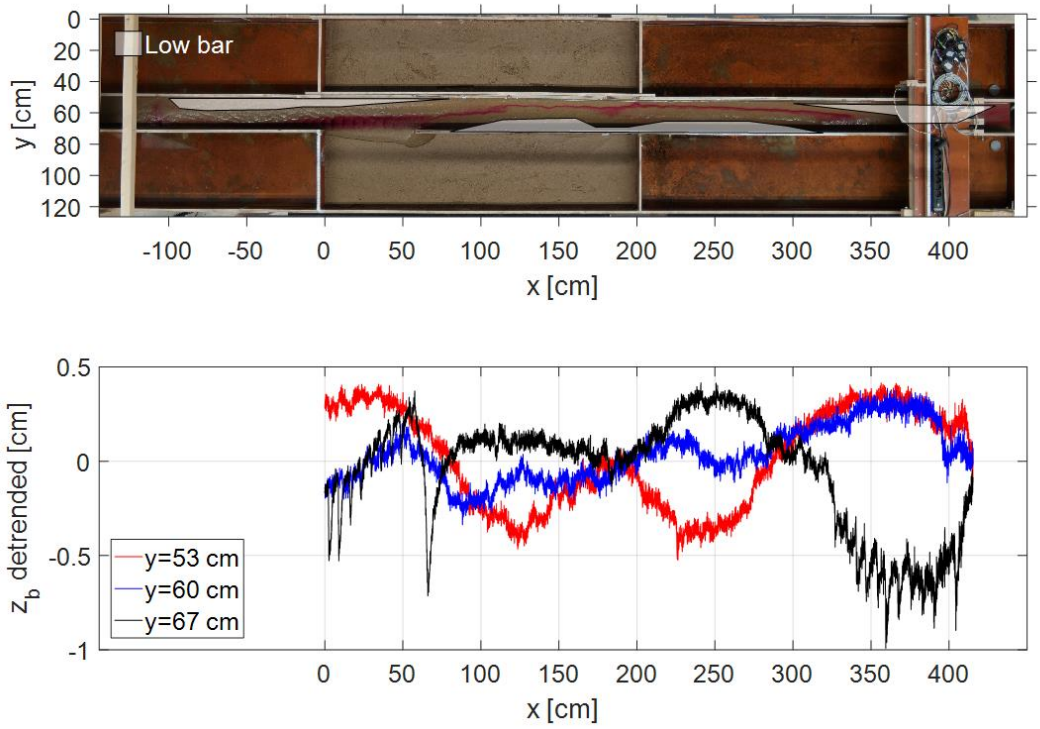


*Figure E.3 - Final bed topography photo with bars (top) and detrended bed profile (bottom) of test R01.*

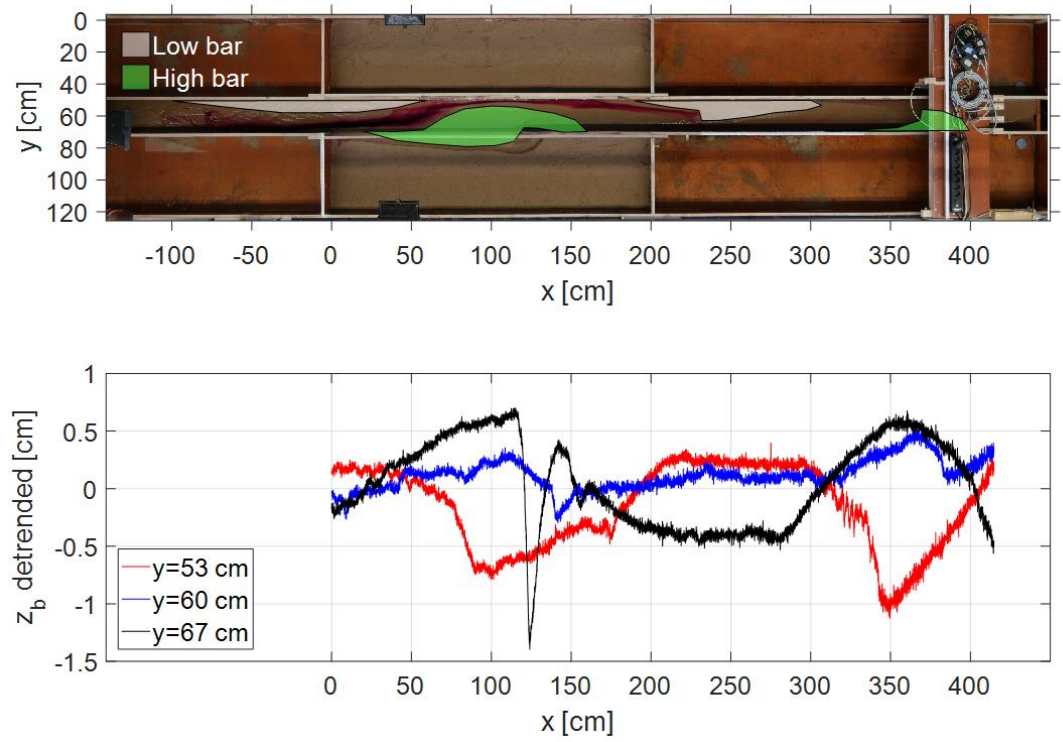


*Figure E.4 - Final bed topography photo with bars (top) and detrended bed profile (bottom) of test R02.*

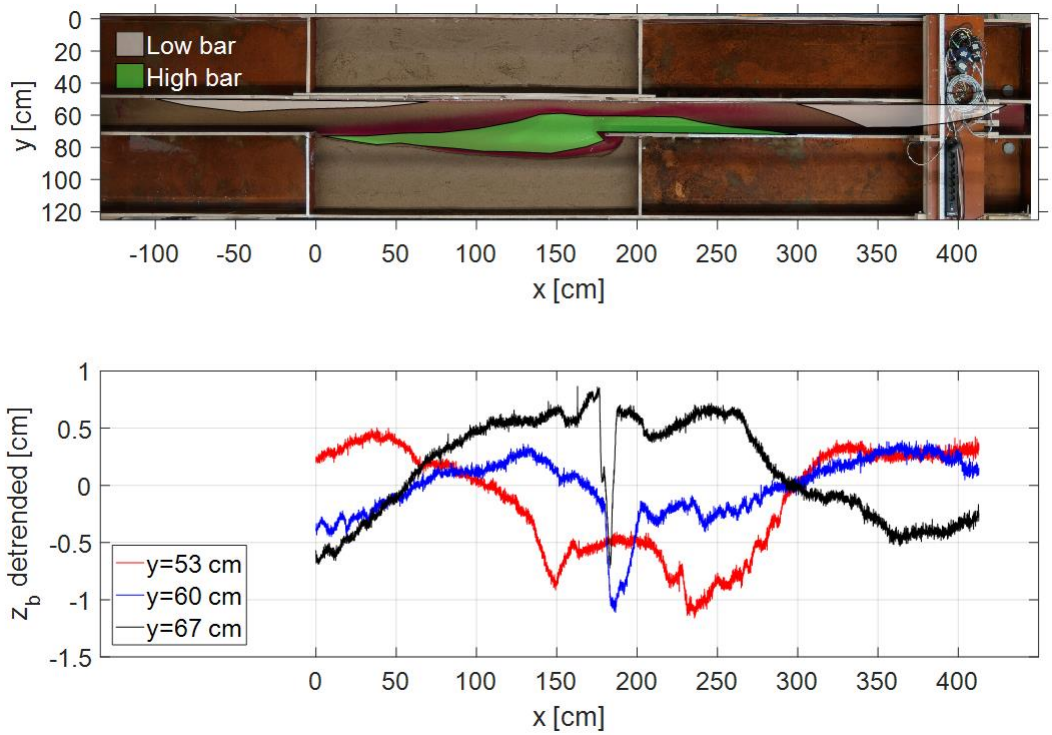


*Figure E.5 - Final bed topography photo with bars (top) and detrended bed profile (bottom) of test R03.*

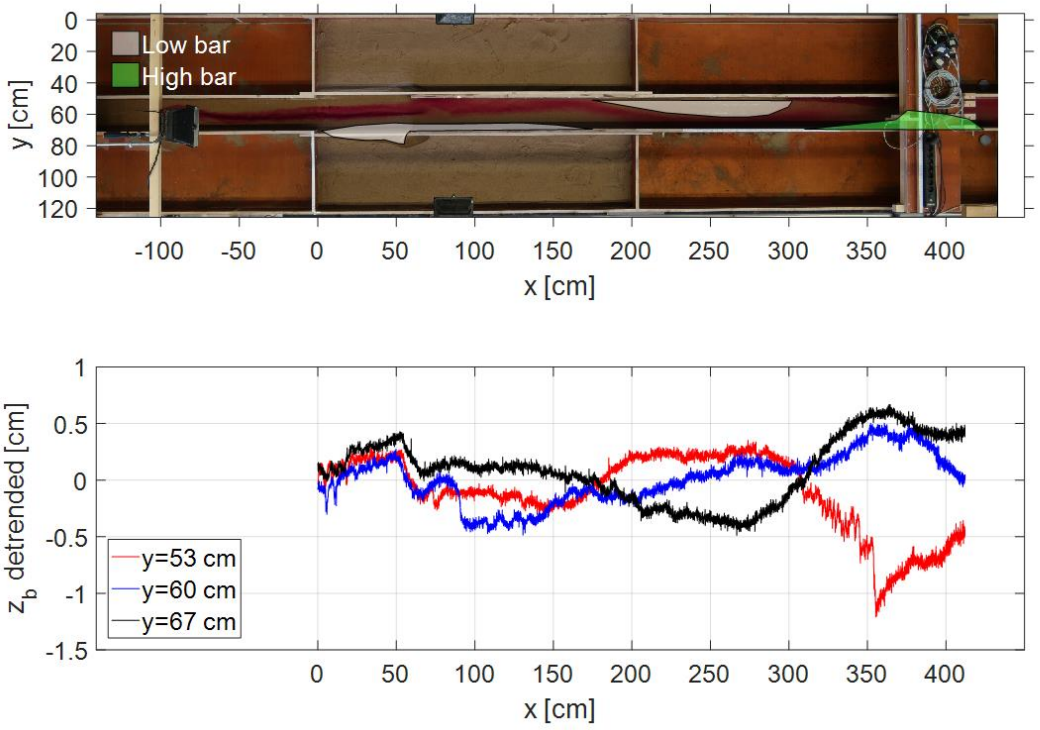


*Figure E.6 - Final bed topography photo with bars (top) and detrended bed profile (bottom) of test R04.*

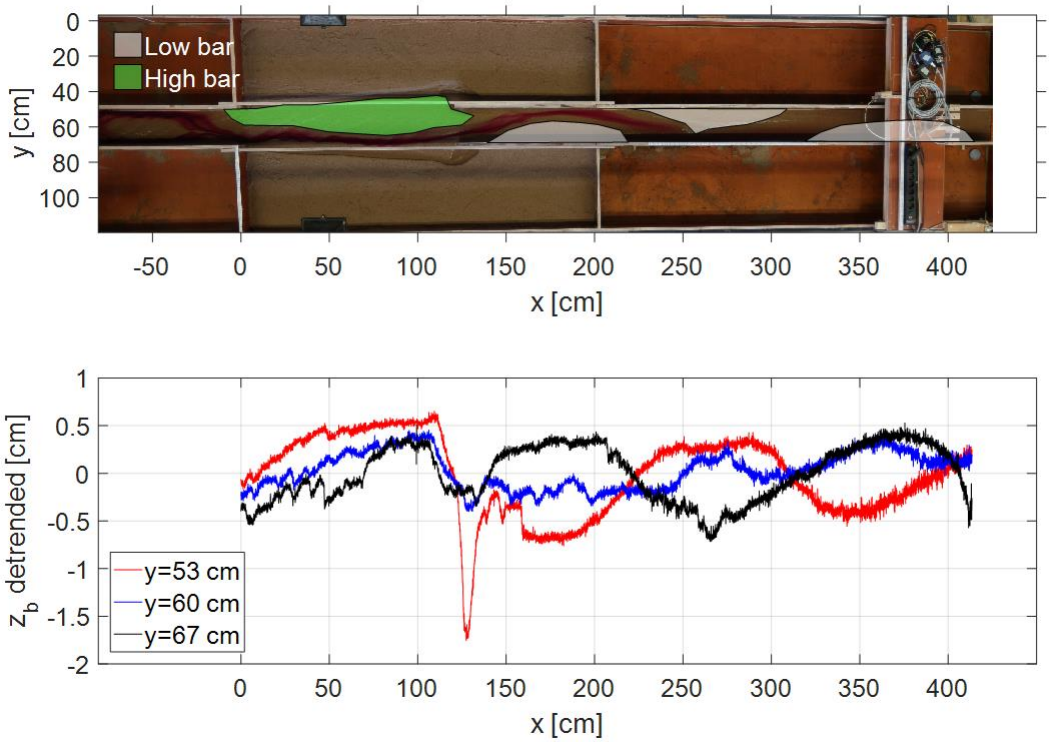


*Figure E.7 - Final bed topography photo with bars (top) and detrended bed profile (bottom) of test R05.*

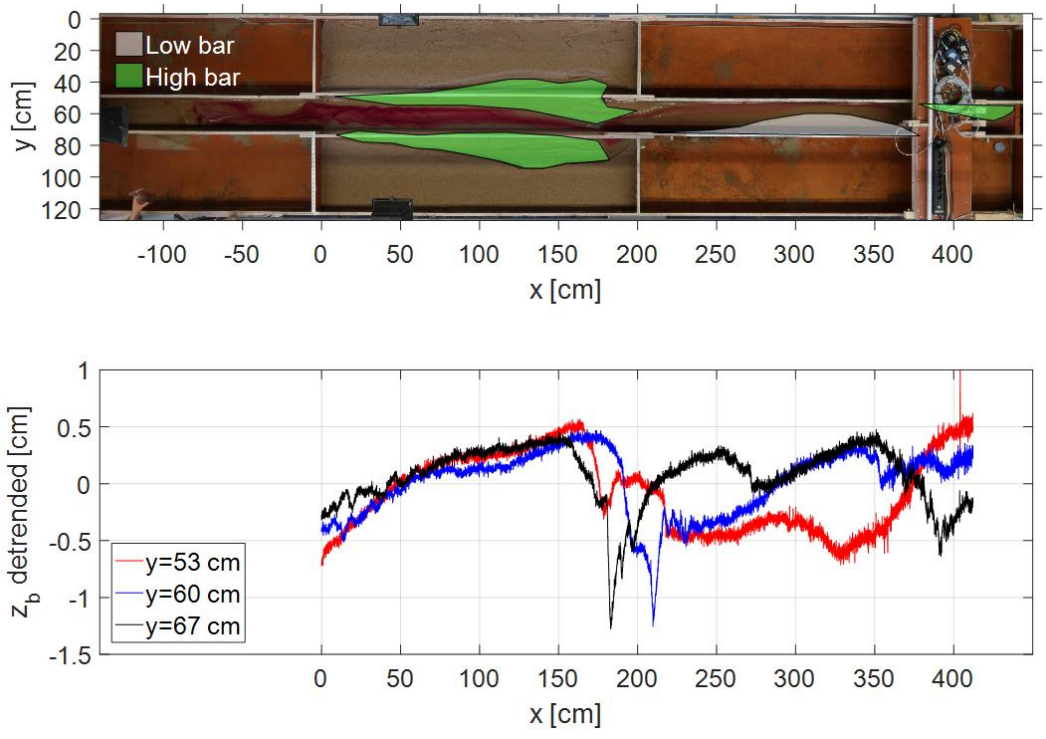


*Figure E.8 - Final bed topography photo with bars (top) and detrended bed profile (bottom) of test R06.*

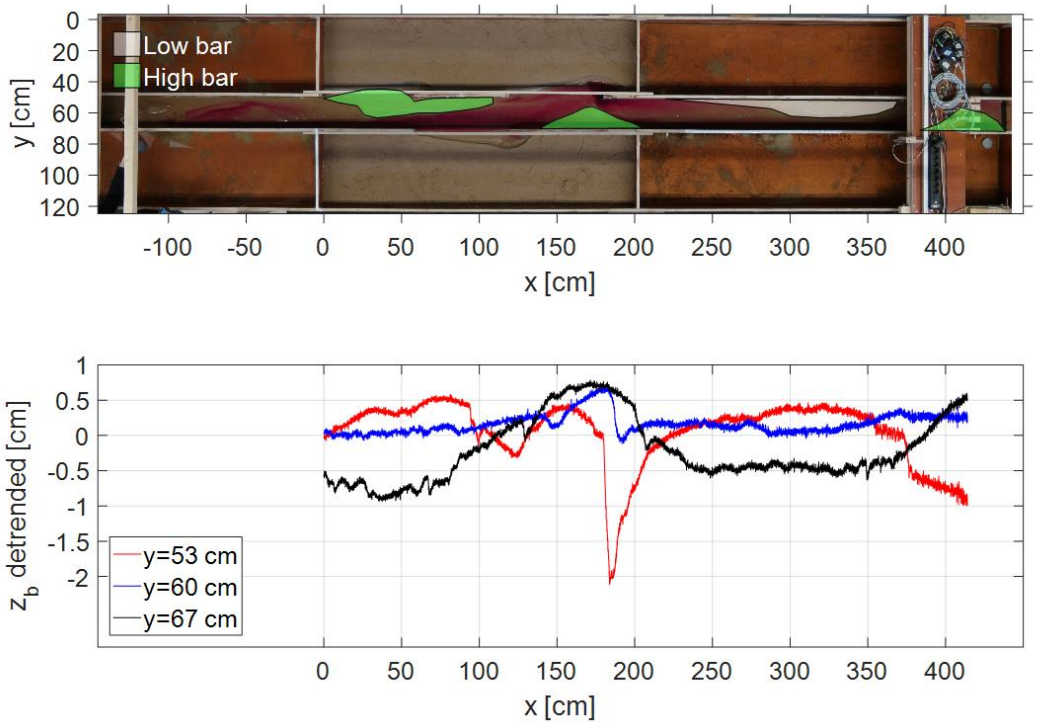


*Figure E.9 - Final bed topography photo with bars (top) and detrended bed profile (bottom) of test R07.*

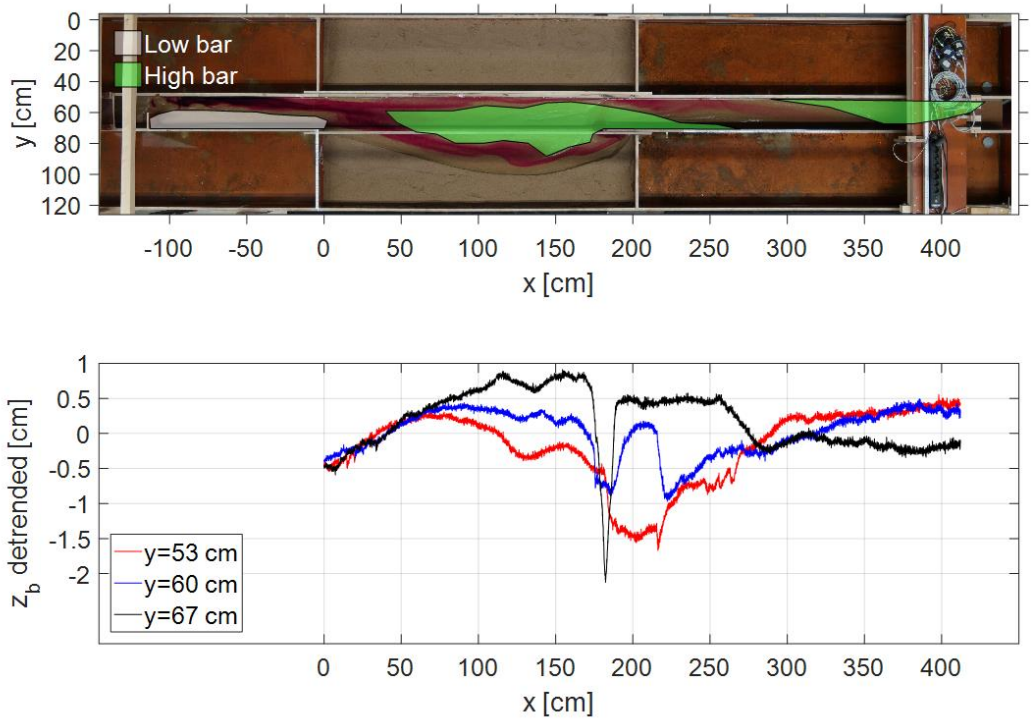


*Figure E.10 - Final bed topography photo with bars (top) and detrended bed profile (bottom) of test R08.*

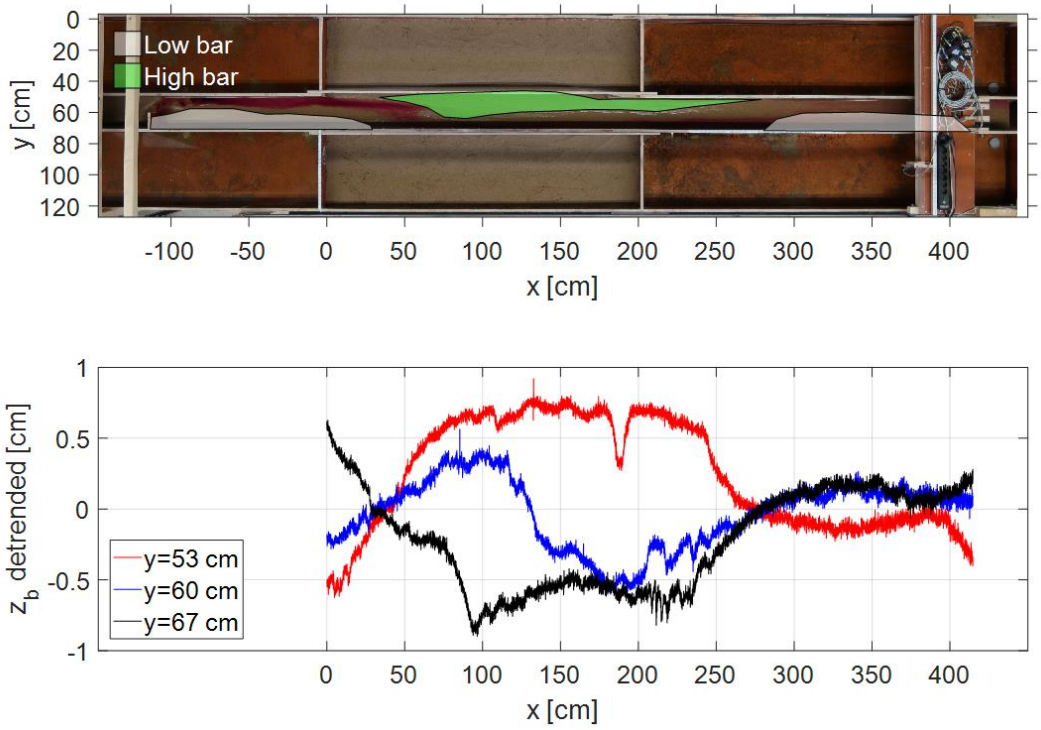


*Figure E.11 - Final bed topography photo with bars (top) and detrended bed profile (bottom) of test R09.*

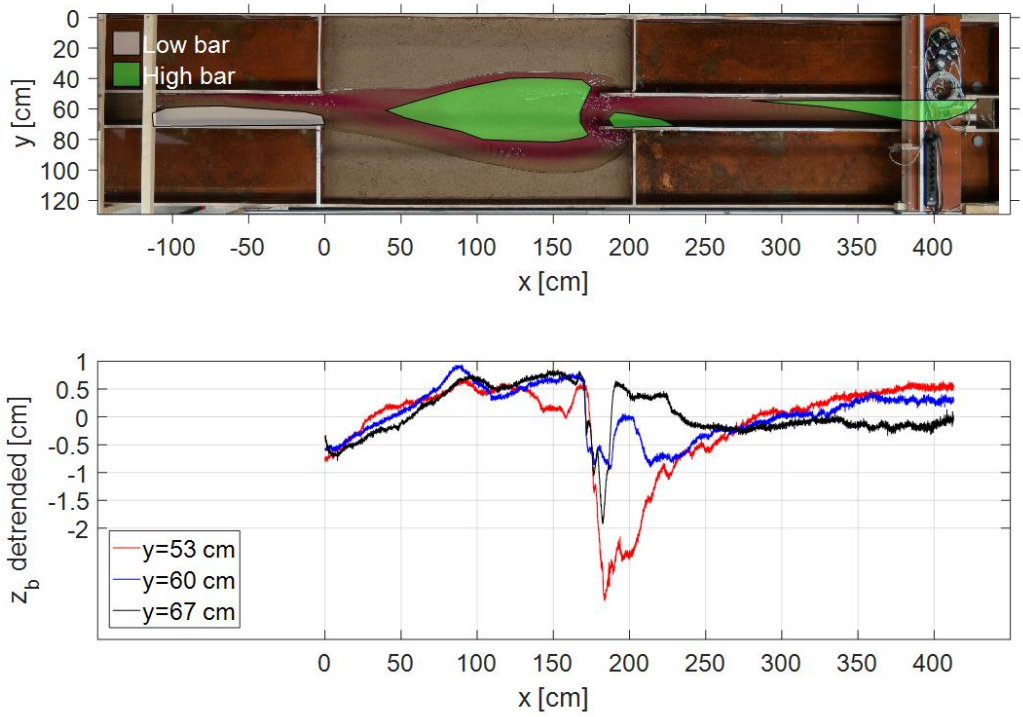


*Figure E.12 - Final bed topography photo with bars (top) and detrended bed profile (bottom) of test R10.*

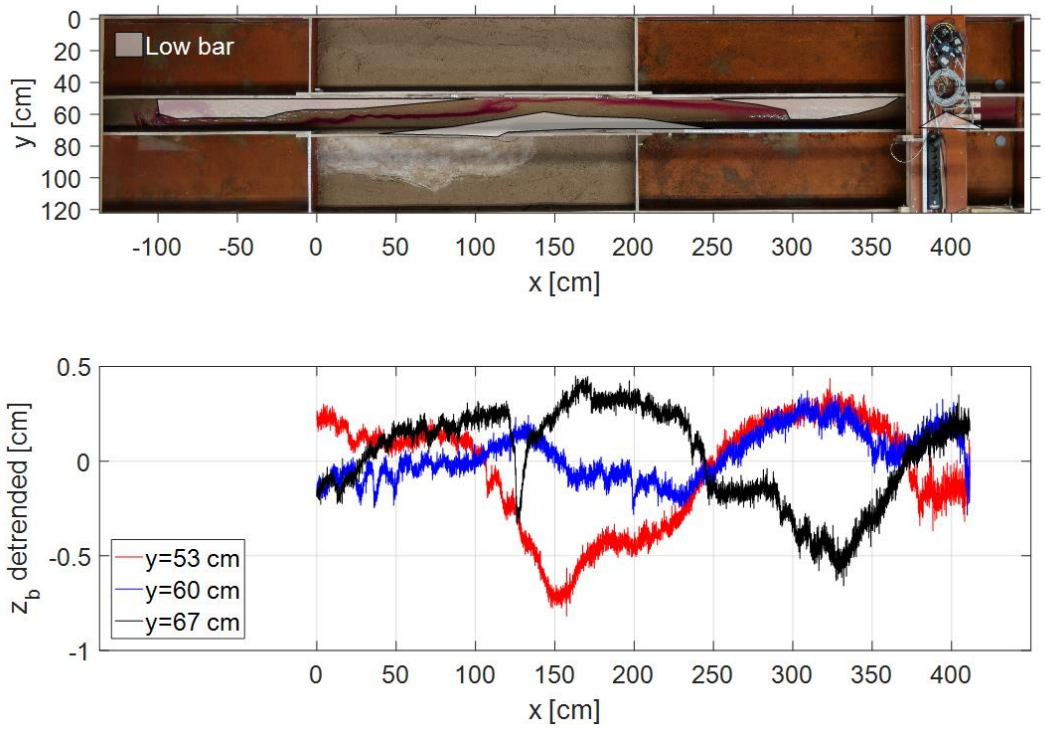


*Figure E.13 - Final bed topography photo with bars (top) and detrended bed profile (bottom) of test R11.*

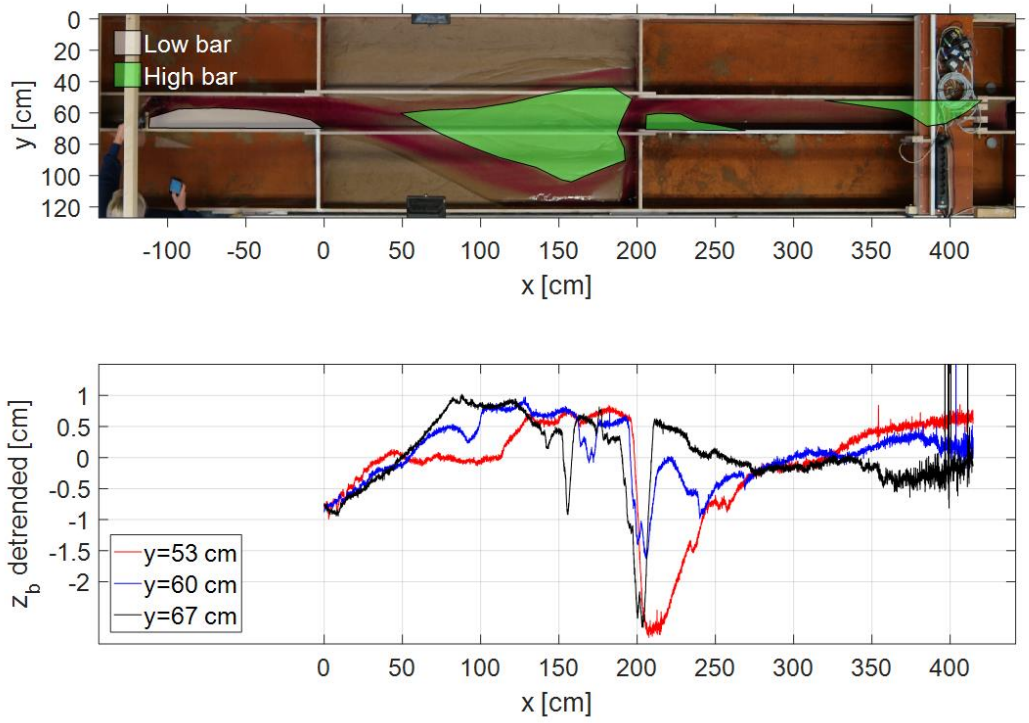


*Figure E.14 - Final bed topography photo with bars (top) and detrended bed profile (bottom) of test R12.*

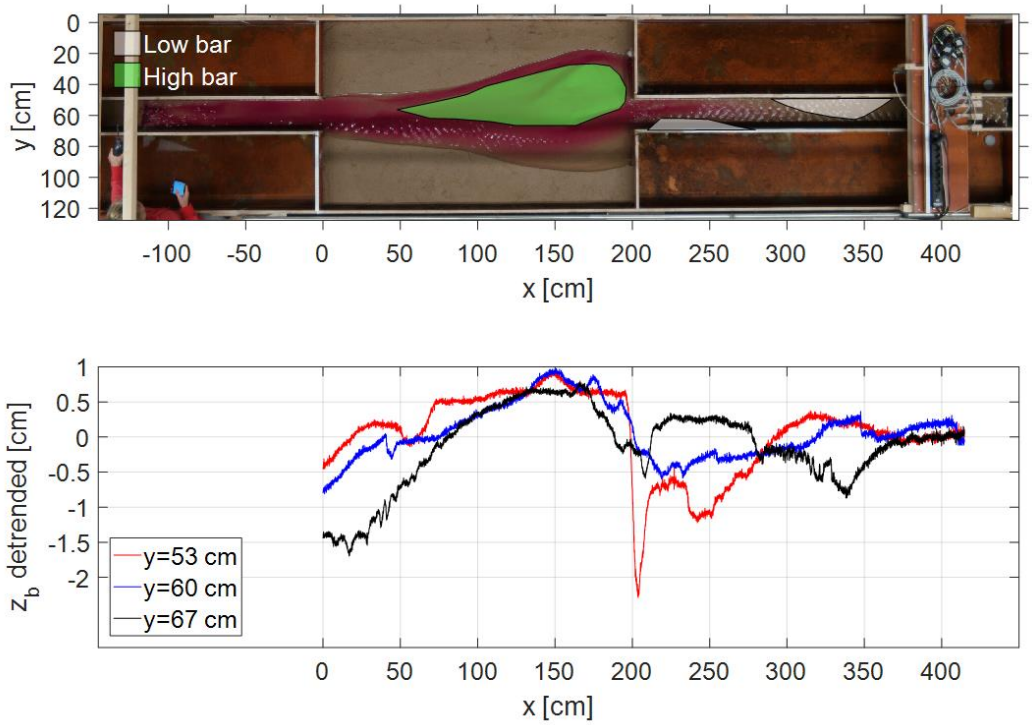


*Figure E.15 - Final bed topography photo with bars (top) and detrended bed profile (bottom) of test R13.*

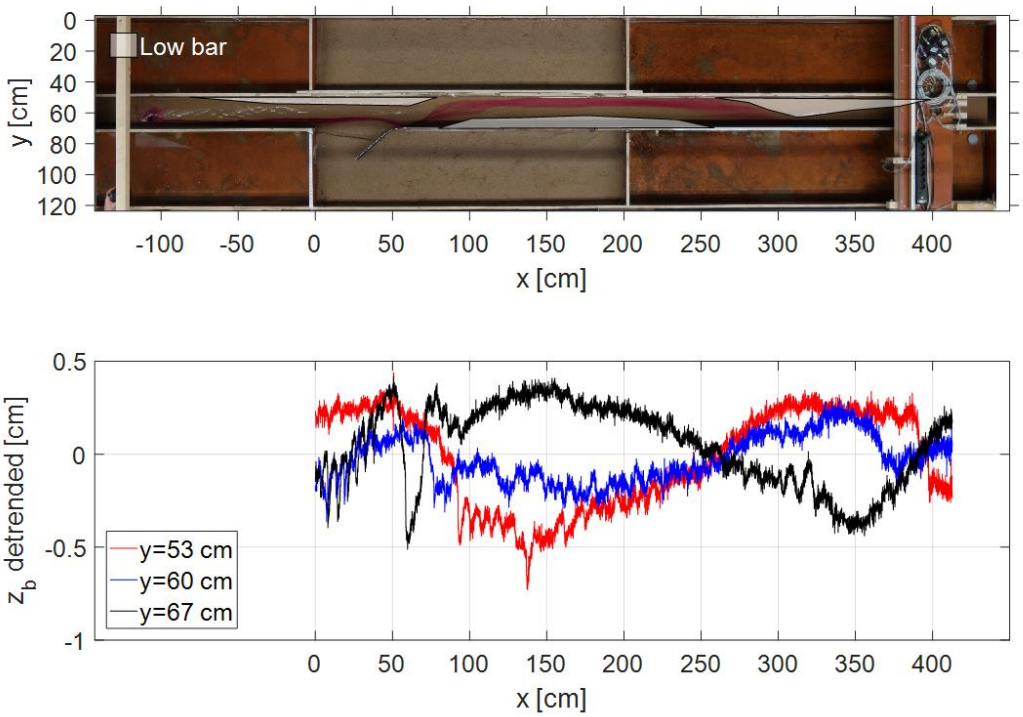


*Figure E.16 - Final bed topography photo with bars (top) and detrended bed profile (bottom) of test R14.*

## Appendix F. Bar area quantification methods

In this appendix two methods to quantify the bar area in the experimental tests are described. The first method used the bed topography photos and the second method used the bed profiles from the lasers. Finally, both methods are compared.

### F.1. Bed topography

The area of the high bars, low bars, floodplain and deep channel are determined from the photos of the bed topography and the detrended bed profiles in Appendix E. In Matlab the bed topography photos are scaled to real world coordinates. First, the bar areas were drawn on the photos and the size of the areas were determined with a Matlab script. Second, the floodplains were drawn in the same photos in Matlab from which the sizes could be determined. Third, the total area was drawn in the same photos. The deep channel area was difficult to draw around the bars and therefore the deep channel area could be determined from subtracting the bar area and floodplain area from the total area. The total area was defined as the main channel plus the floodplains, since the total area had to be constant to compare the tests. The main channel was defined as the area where bars were formed in the tests. This was the distance starting one metre upstream of the widened section until the end of the flume multiplied by the main channel width. The total area was defined as $A_{total} = A_{channel} + A_{floodplains} = 20 * 550 + 100 * 200 = 31000\ cm^2$ .

In Figure F.1 an example of the drawn bar areas and floodplain area on the topography photos is given. Table F.1 shows the sizes of the floodplain area, high bar area, low bar area and deep channel area. The relative areas of the floodplain, high bars, low bars and deep channel were determined by dividing them by the total area and are shown in Table F.1. Figure F.2 shows the relative areas in a column chart.

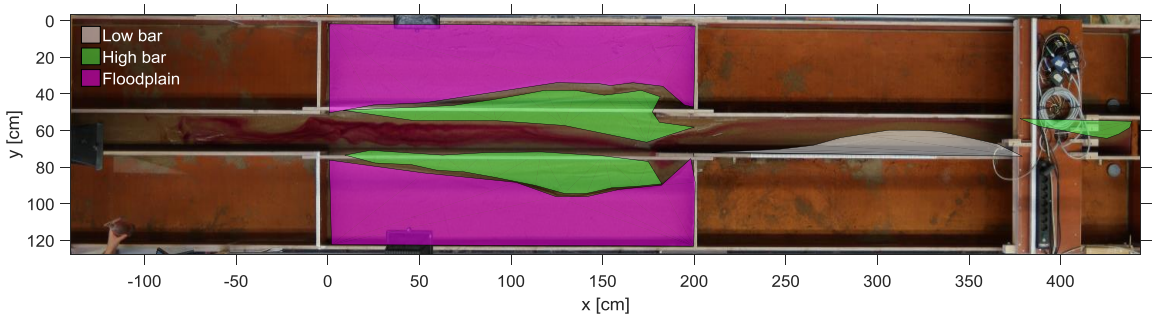


*Figure F.1 – Photo of final topography of test R06 with drawn bar areas and floodplain area.*

*Table F.1 – Areas of floodplain, deep channel, low bar and high bar in square centimetres and percentages for all tests that were obtained by drawing the areas in the final bed topography photos.*

| Test | Total area [$cm^2$] | High bar area [$cm^2$] | Low bar area [$cm^2$] | Deep channel area [$cm^2$] | Floodplain area [$cm^2$] | Total area [%] | High bar area [%] | Low bar area [%] | Deep channel area [%] | Floodplain area [%] |
|---|---|---|---|---|---|---|---|---|---|---|
| P01 | 31000 | 0 | 2109 | 8739 | 20152 | 100 | 0,0 | 6,8 | 28,2 | 65,0 |
| P02 | 31000 | 0 | 3666 | 7232 | 20102 | 100 | 0,0 | 11,8 | 23,3 | 64,8 |
| R01 | 31000 | 0 | 3056 | 8639 | 19305 | 100 | 0,0 | 9,9 | 27,9 | 62,3 |

| | | | | | | | | | | |
|---|---|---|---|---|---|---|---|---|---|---|
| R02 | 31000 | 2229 | 1612 | 8592 | 18567 | 100 | 7,2 | 5,2 | 27,7 | 59,9 |
| R03 | 31000 | 2977 | 1998 | 8020 | 18005 | 100 | 9,6 | 6,4 | 25,9 | 58,1 |
| R04 | 31000 | 674 | 1813 | 9321 | 19192 | 100 | 2,2 | 5,8 | 30,1 | 61,9 |
| R05 | 31000 | 2006 | 2208 | 9092 | 17694 | 100 | 6,5 | 7,1 | 29,3 | 57,1 |
| R06 | 31000 | 4930 | 1215 | 10192 | 14663 | 100 | 15,9 | 3,9 | 32,9 | 47,3 |
| R07 | 31000 | 2042 | 952 | 9942 | 18064 | 100 | 6,6 | 3,1 | 32,1 | 58,3 |
| R08 | 31000 | 4775 | 1159 | 9029 | 16036 | 100 | 15,4 | 3,7 | 29,1 | 51,7 |
| R09 | 31000 | 2076 | 3976 | 7170 | 19012 | 100 | 6,7 | 12,8 | 23,1 | 61,3 |
| R10 | 31000 | 5269 | 1234 | 9838 | 14659 | 100 | 17,0 | 4,0 | 31,7 | 47,3 |
| R11 | 31000 | 0 | 3894 | 7477 | 19629 | 100 | 0,0 | 12,6 | 24,1 | 63,3 |
| R12 | 31000 | 6106 | 1130 | 13481 | 10283 | 100 | 19,7 | 3,6 | 43,5 | 33,2 |
| R13 | 31000 | 3534 | 1008 | 12465 | 13993 | 100 | 11,4 | 3,3 | 40,2 | 45,1 |
| R14 | 31000 | 0 | 2504 | 8918 | 19579 | 100 | 0,0 | 8,1 | 28,8 | 63,2 |

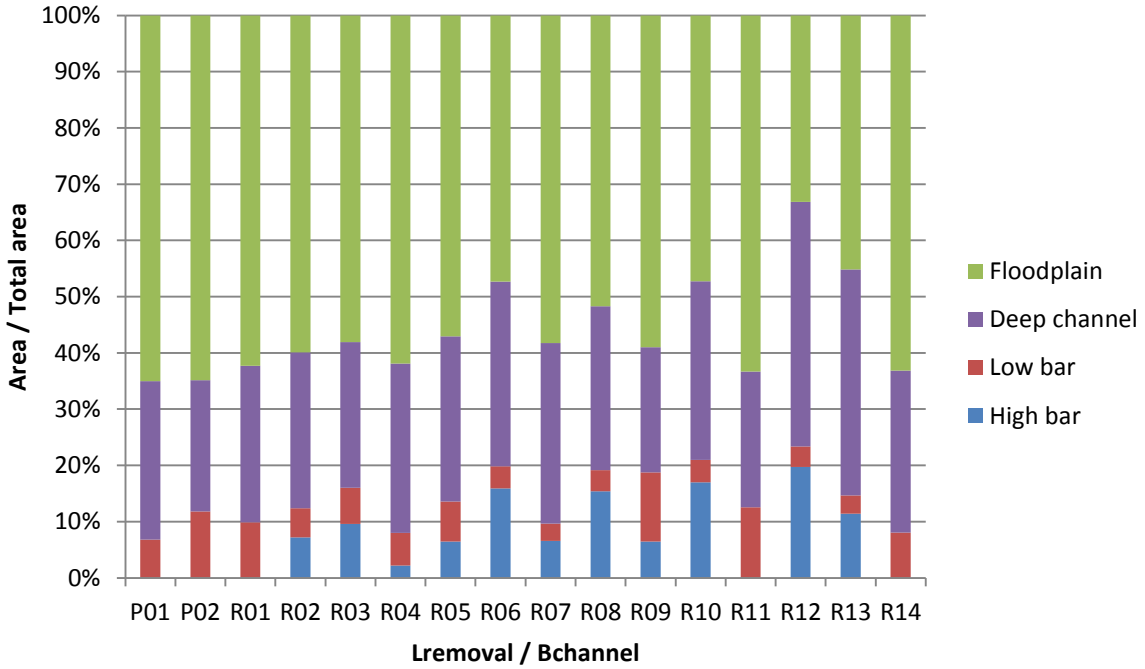


*Figure F.2 –Dimensionless area of floodplain, deep channel, high bars and low bars for all tests determined from the photos of bed topographies*

The eroded bank area for each test could be determined from the drawn floodplain areas. The eroded bank area was calculated by subtracting the floodplain area from Table F.1 of the total floodplain area. The total floodplain area has an area of $A_{total\ floodplain} = 2\ x\ 50\ x\ 200 =$ 20000 cm$^2$. Table F.2 shows the eroded bank areas of all tests.

*Table F.2 – Eroded bank area in square centimetres and percentages that were obtained by drawing the areas in the final bed topography photos for all tests.*

| Test | Eroded bank area [cm$^2$] | Eroded bank area [%] |
|---|---|---|

| | | |
|---|---|---|
| P01 | 0 | 0,0 |
| P02 | 0 | 0,0 |
| R01 | 695 | 2,2 |
| R02 | 1433 | 4,6 |
| R03 | 1995 | 6,4 |
| R04 | 808 | 2,6 |
| R05 | 2306 | 7,4 |
| R06 | 5337 | 17,2 |
| R07 | 1936 | 6,2 |
| R08 | 3964 | 12,8 |
| R09 | 988 | 3,2 |
| R10 | 5341 | 17,2 |
| R11 | 371 | 1,2 |
| R12 | 9717 | 31,3 |
| R13 | 6007 | 19,4 |
| R14 | 421 | 1,4 |

## F.2. Bed profile

The three lasers in the main channel measured the bed profile. A regression line was computed from these three bed profiles. Figure F.3 shows an example of the bed profiles and the regression line of test R06. Detrended bed profiles were obtained by subtracting the regression line from the individual bed profiles. The detrended bed profiles are shown in Appendix E.

The detrended bed profiles were defined as deep channel when $z_{b\ detrended} < 0.2$ cm, low bar when $0.2\ cm < z_{b\ detrended} < 0.45$ cm and high bar when $z_{b\ detrended} > 0.45$ cm. For each category the detrended bed profile included a certain amount of data points. The amount of data points per category were divided by the total amount of data points to determine the relative 'length' of the categories in the main channel. Figure F.4 shows the relative 'length' of the deep channel, high bars and low bars in the main channel.

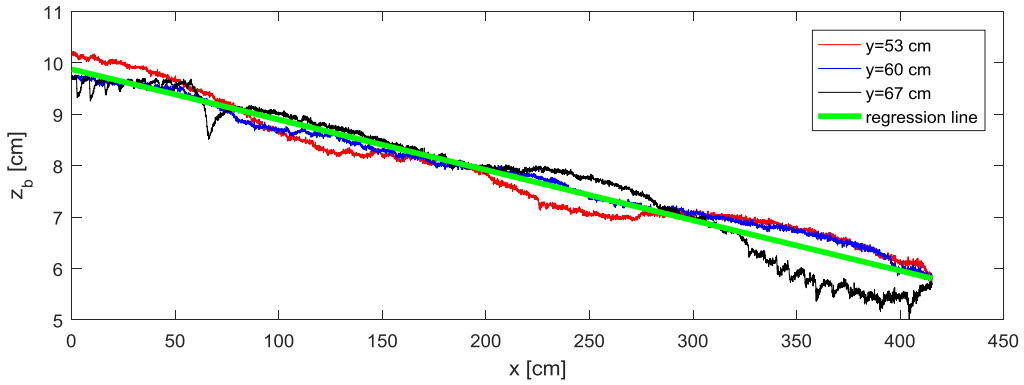


*Figure F.3 – Bed profiles of test R06 from laser measurements in main channel at y=53 cm, y=60 cm and y=67 cm. The regression line is computed from these three bed profiles.*

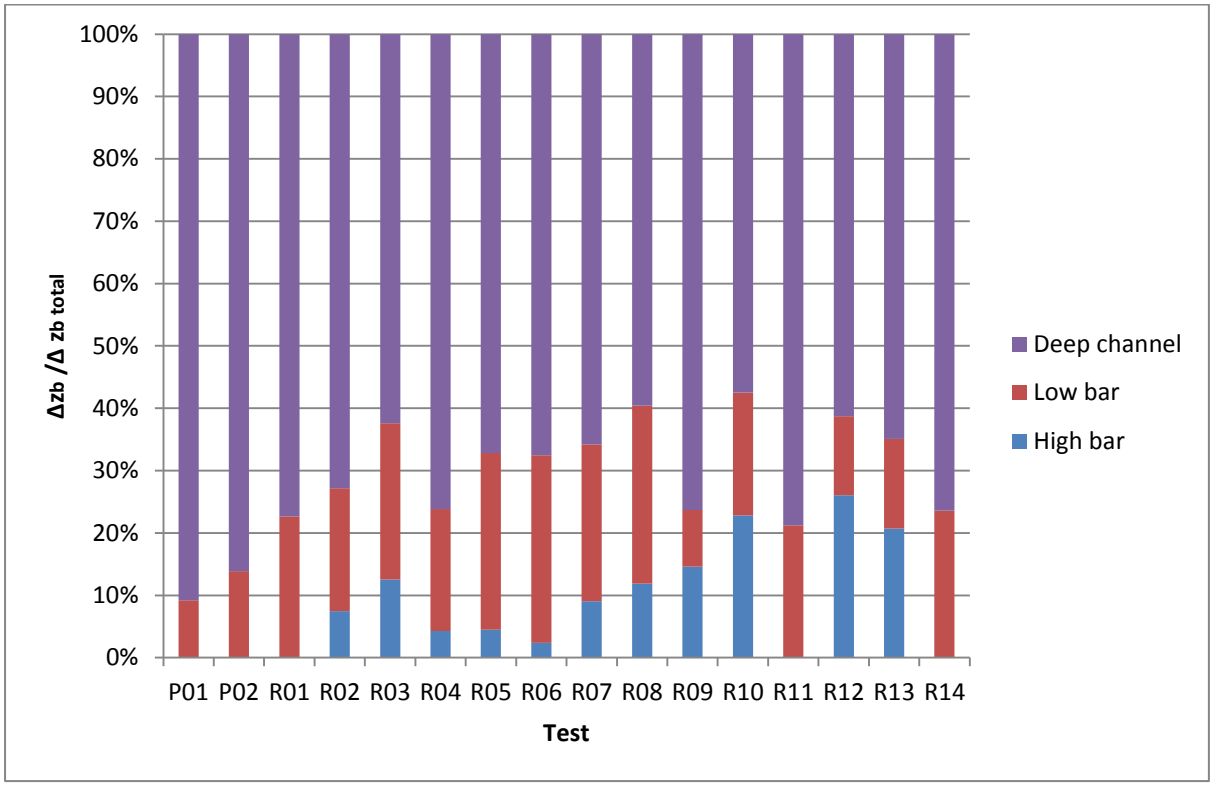


*Figure F.4 - Dimensionless length of detrended bed profile of deep channel, high bars and low bars for all tests determined from the three bed profiles in the main channel*

## F.3. Comparison methods

The first method to quantify the low and high bar size is using the bar areas that are drawn on the bed topography photos. The second method uses the bed profiles measured by the lasers.

An advantage of the first method is that it takes into account the entire surface area of the channel. The main channel plus the eroded section is part of the surface areas. It is important that the eroded section is taken into account for quantifying the bar areas, since bars are also formed outside of the main channel. A disadvantage of the first method is that the drawn areas of the bars and deep channel are not exact values. The areas are estimated based on photos of the bed topography and detrended bed profiles.

An advantage of the second method is that the measured bar heights are accurate, since they are measured with the lasers. A disadvantage of the second method is that the bars outside the main channel are not taken into account. Furthermore, the bar heights were not measured over the full width of the main channel, but at three longitudinal profiles. The bar area in the main channel cannot be determined from these three bed profiles, since interpolation of the longitudinal bed profiles over the channel width would give inaccurate values. The longitudinal bed profiles next to the measured three profiles might have higher bar heights than measured with the three lasers.

Figure 4.9 and Figure F.5 show the relative size of the bars for a bank protection removal on one side of the channel determined with respectively the first and the second method. No high bars are present when no lateral erosion is allowed and for a bank protection removal of three times the channel width in both methods. The high bar size increases in both methods for a bank protection removal of six times the channel width to a bank protection removal of nine times

the channel width. The low bar size is higher for a bank protection removal length of three times the channel width than when no bank protection is removed in both methods. A decrease in low bar size occurs in both methods when the bank protection removal is three times the channel width to six times the channel width. The low bar size increases in both methods for a bank protection removal length of six times the channel width to a bank protection removal length of nine times the channel width. It can thus be concluded that the methods show similar results when quantifying the bar sizes.

Figure 4.10 and Figure F.4 show the relative size of the bars for a bank protection removal on two sides of the channel determined with respectively the first and the second method. No high bars are present when no lateral erosion is allowed in both methods. For a bank protection removal of three times the channel width there are high bars in the channel in both methods. In the first method the high bar area is larger for a bank protection removal length of nine times the channel width than for a bank protection removal of six times the channel width, whereas in the second method the high bar area is smaller for a bank protection removal length of nine times the channel width than for a bank protection removal of six times the channel width. The higher bar area in the first method compared to the second method is due to the large widening of the channel and thus formation of high bars outside of the main channel that were not measured by the lasers from the second method. The second method therefore underestimates the high bar area in tests with a large widening. The tests with a bank protection removal length of nine times the channel width was widened most. In this test a large high bar area was formed outside of the main channel, and thus these are not taken into account in the second method and explains the differences in the bar sizes in Figure 4.10 and Figure F.4. The low bar area in the first method remains approximately constant for a longer length of bank protection removal whereas in the second method the low bar size increases for a longer length of bank protection removal. This increase in low bar size in the second method might be due to high bars that were formed on the sides of the main channel, which cause a small elevation of the bed in the main channel.

Figure F.2 and Figure F.4 show the relative size of the bars for all experimental tests determined with respectively the first and the second method. The relative size of the low and high bar areas show similar results in both methods. The second method, however, underestimates the bar size for tests where bars formed outside the main channel, since this method used the lasers that measured the bed profiles in the main channel only.

It can be concluded that the first method is more suitable to determine the relative bar size in the channel. The bars that formed outside of the main channel are included with this method. Furthermore, the bar areas can be determined with the first method, which are valuable results for ecologists. In the first method the values of the bar areas were estimated and therefore could slightly differ from the ‘true’ values . The second method shows similar results for quantifying the bar areas and therefore gives strength to the reliability of the values for the bar areas from the first method.

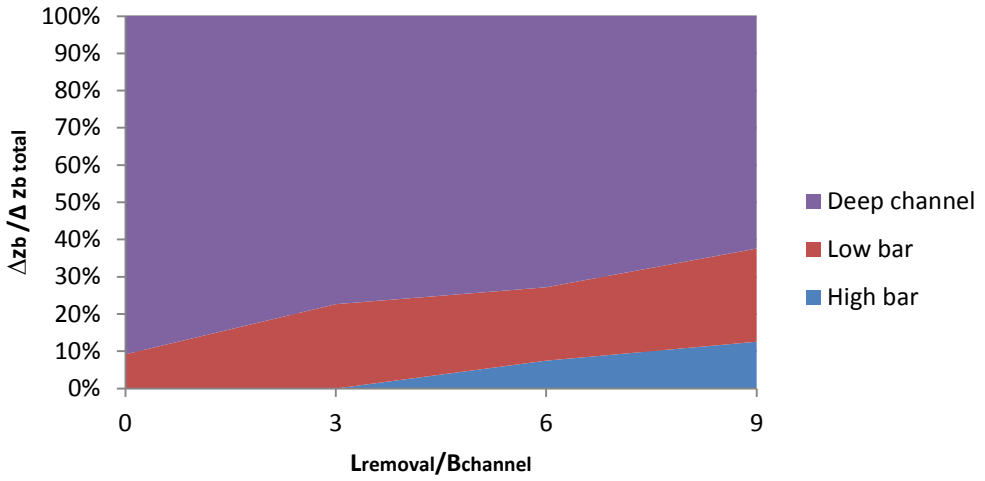


*Figure F.5 – One side bank protection removal: dimensionless length of detrended bed profile of deep channel, high bars and low bars of tests P01, R01, R02 and R03 related to the dimensionless length of bank protection removal determined from the three bed profiles in the main channel*

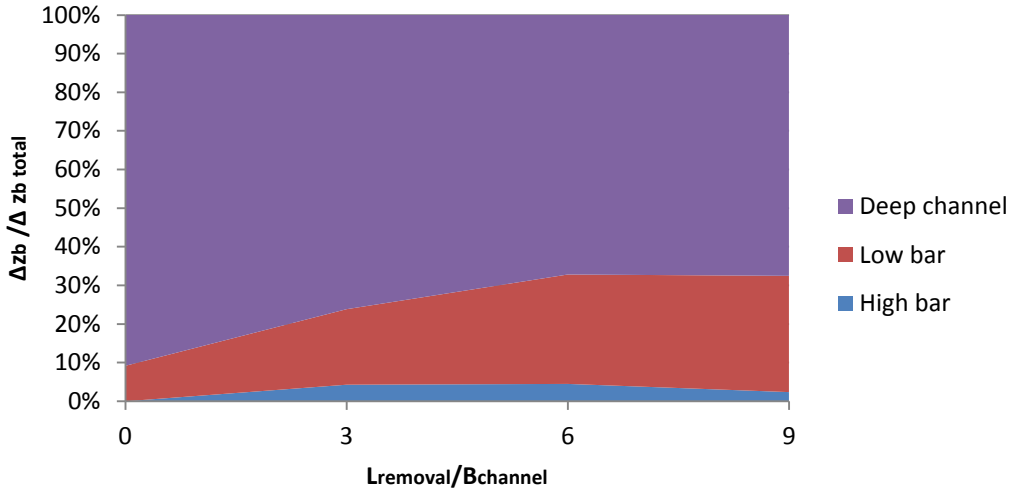


*Figure F.6 – Two sides bank protection removal: dimensionless length of detrended bed profile of deep channel, high bars and low bars of tests P01, R04, R05 and R06 related to the dimensionless length of bank protection removal determined from the three bed profiles in the main channel*

## Appendix G. Bank erosion in laboratory experiment

In this appendix, the evolution of the bank line of tests R01, R03, R08, R09, R10, R13 and R14 is shown in Figure G.1 to Figure G.10 at a time interval of one hour. Table G.1 shows the maximum width of the channel in the widened reach at the end of each test. The location in longitudinal direction of the maximum channel widening may be different for each test. It should be noted that the banks were still (slowly) eroding at the end of the tests.

*Table G.1 – Maximum channel width in the widened reach at the end of the each experimental test. The location in longitudinal direction of the maximum channel widening may be different for each test. The initial width of the main channel is B = 0.2 metres.*

| Test | Maximum channel width [cm] | Relative maximum channel width [-] |
|---|---|---|
| R01 | 31 | 1.55*B |
| R02 | 34 | 1.70*B |
| R03 | 36.5 | 1.83*B |
| R04 | 41 | 2.05*B |
| R05 | 45 | 2.25*B |
| R06 | 63.5 | 3.18*B |
| R07 | 30 | 1.50*B |
| R08 | 48 | 2.40*B |
| R09 | 29.5 | 1.48*B |
| R10 | 66.5 | 3.33*B |
| R11 | 27.5 | 1.38*B |
| R12 | 98 | 4.90*B |
| R13 | 80 | 4.00*B |
| R14 | 31 | 1.55*B |

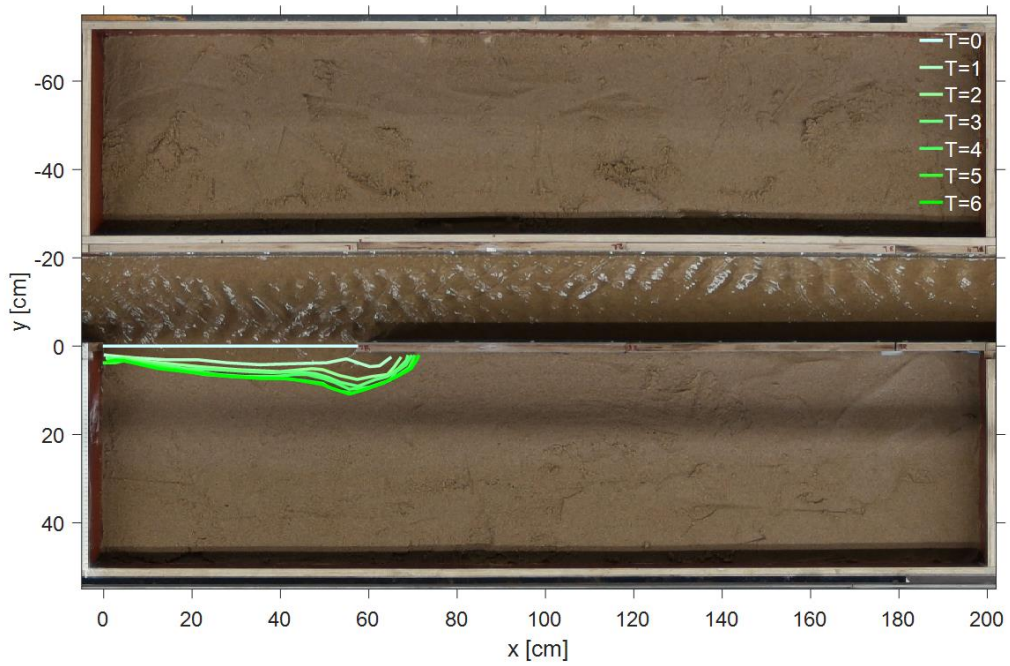


*Figure G.1 – Spatial evolution of bank erosion of test R01. Time T is in hours.*

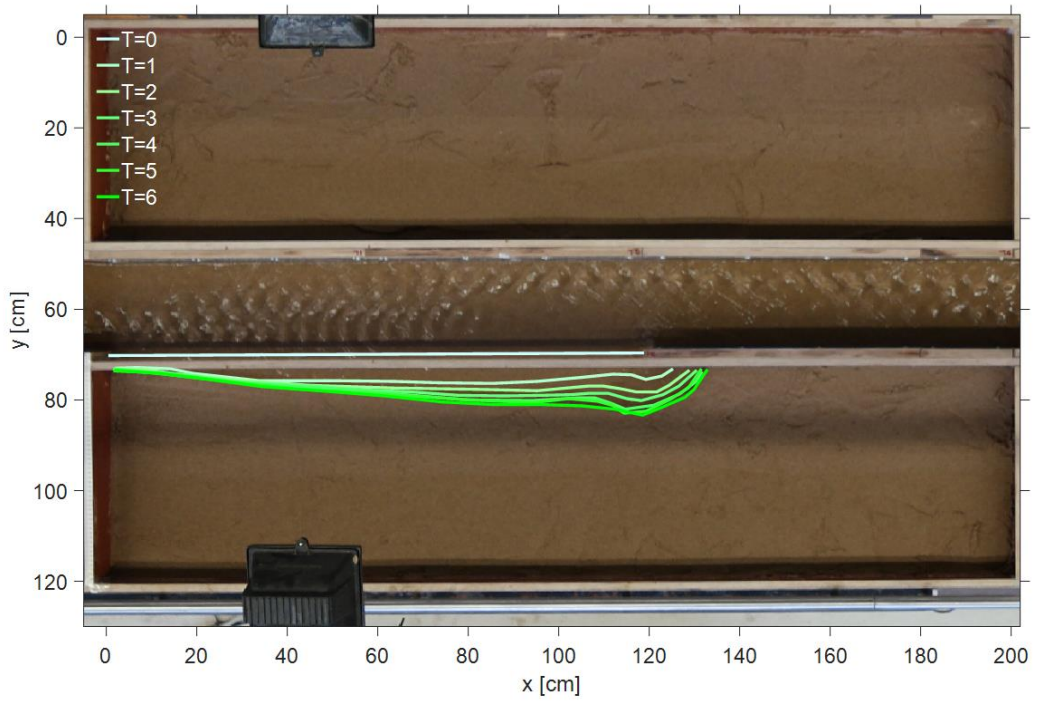


*Figure G.2 – Spatial evolution of bank erosion of test R02. Time T is in hours.*

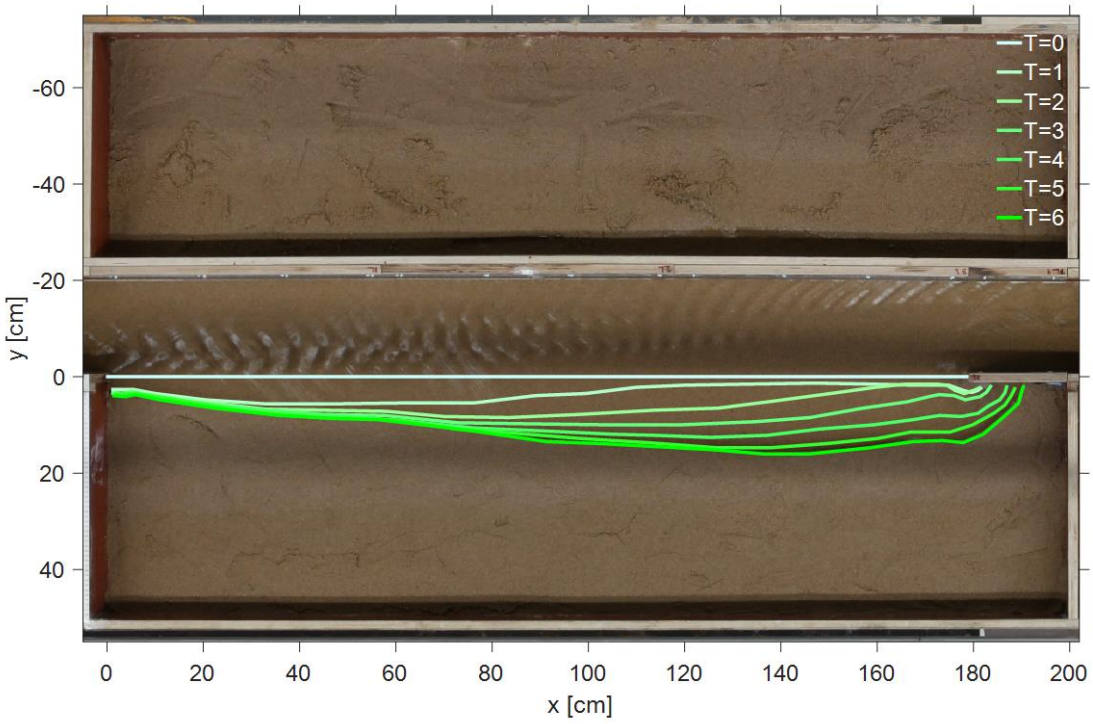


*Figure G.3 – Spatial evolution of bank erosion of test R03. Time T is in hours.*

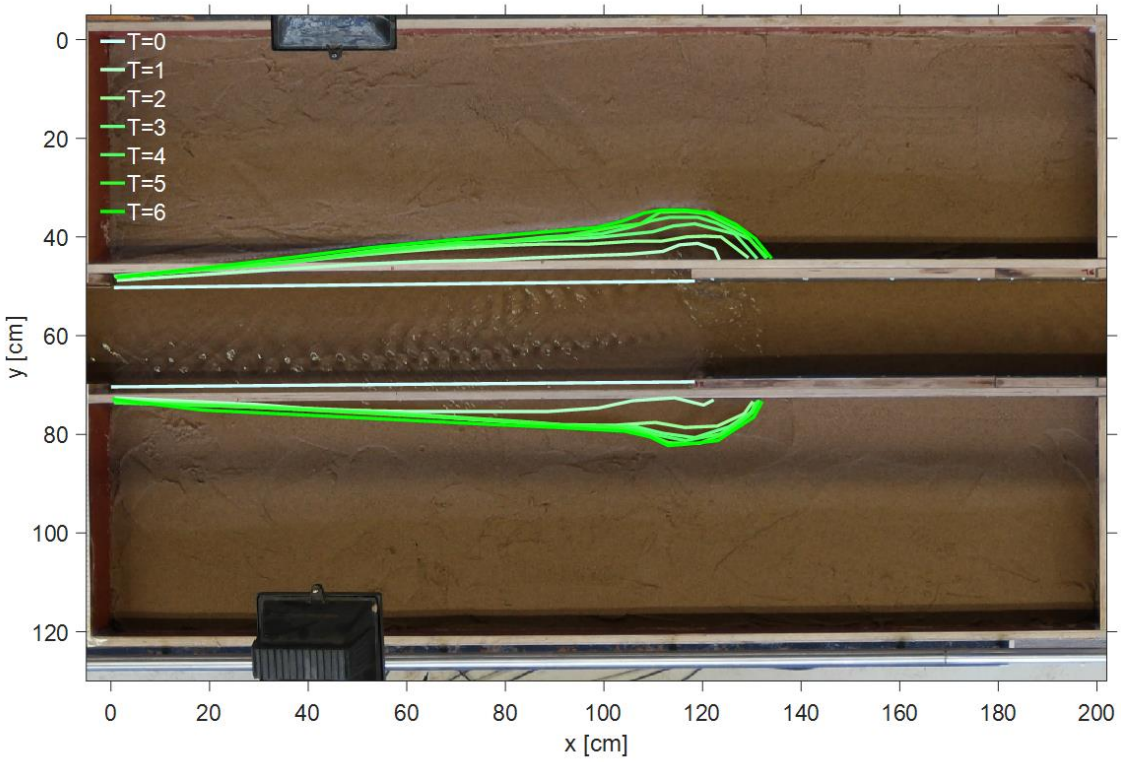


*Figure G.4 - Spatial evolution of bank erosion of test R05. Time T is in hours.*

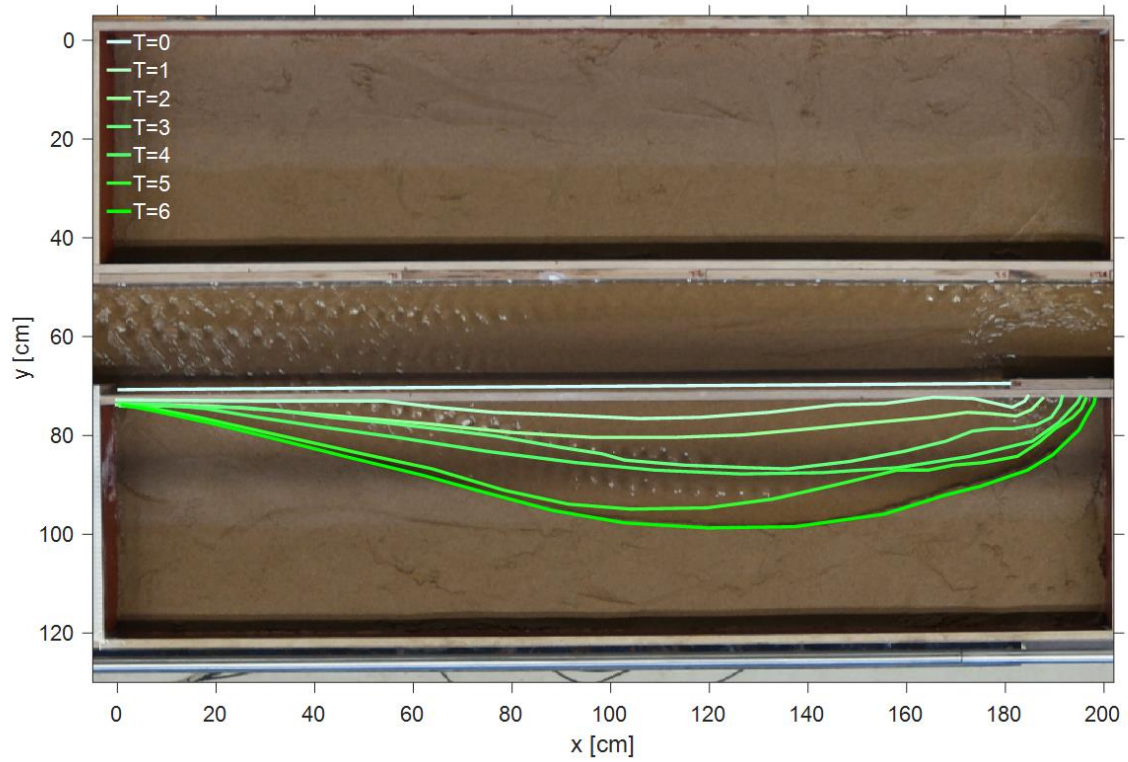


*Figure G.5 - Spatial evolution of bank erosion of test R08. Time T is in hours.*

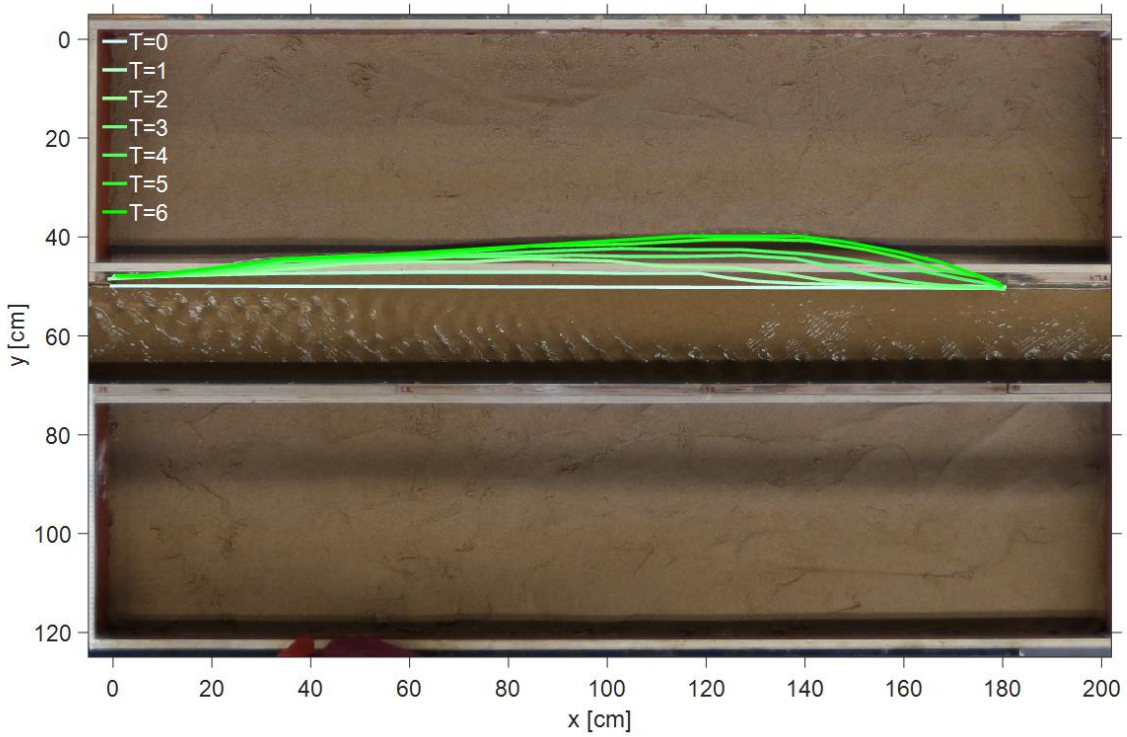


*Figure G.6 – Spatial evolution of bank erosion of test R09. Time T is in hours.*

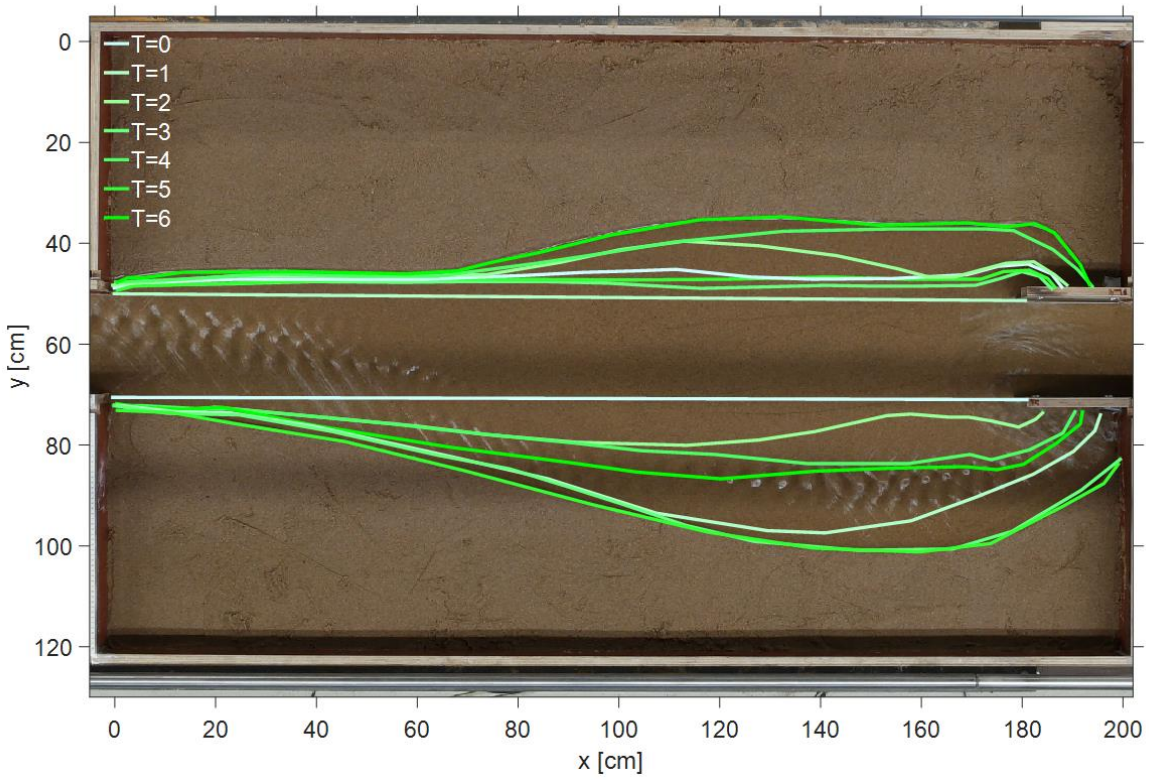


*Figure G.7 - Spatial evolution of bank erosion of test R10. Time T is in hours.*

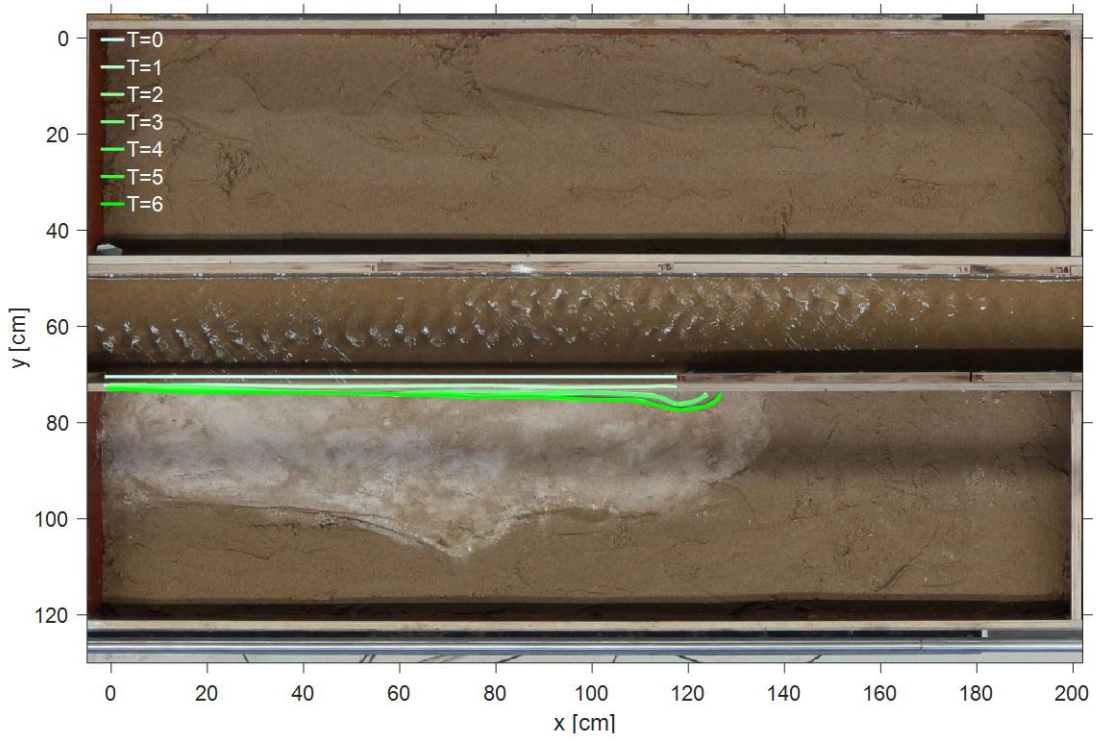


*Figure G.8 - Spatial evolution of bank erosion of test R11. Time T is in hours.*

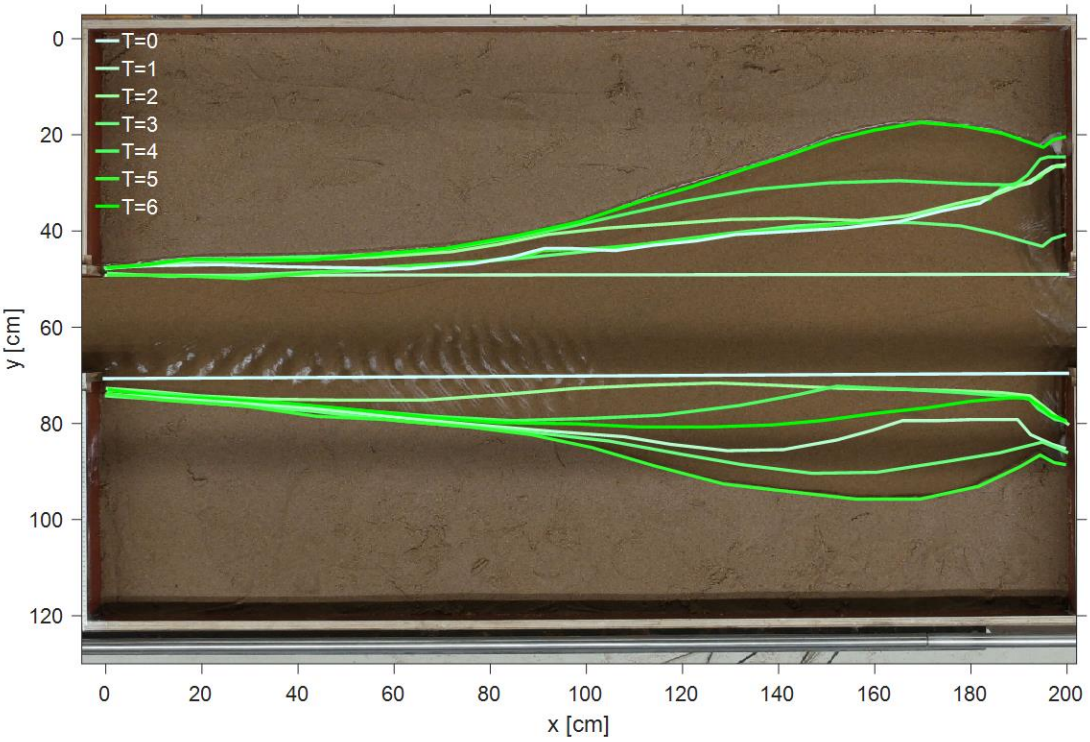


*Figure G.9 – Spatial evolution of bank erosion of test R13. Time T is in hours.*

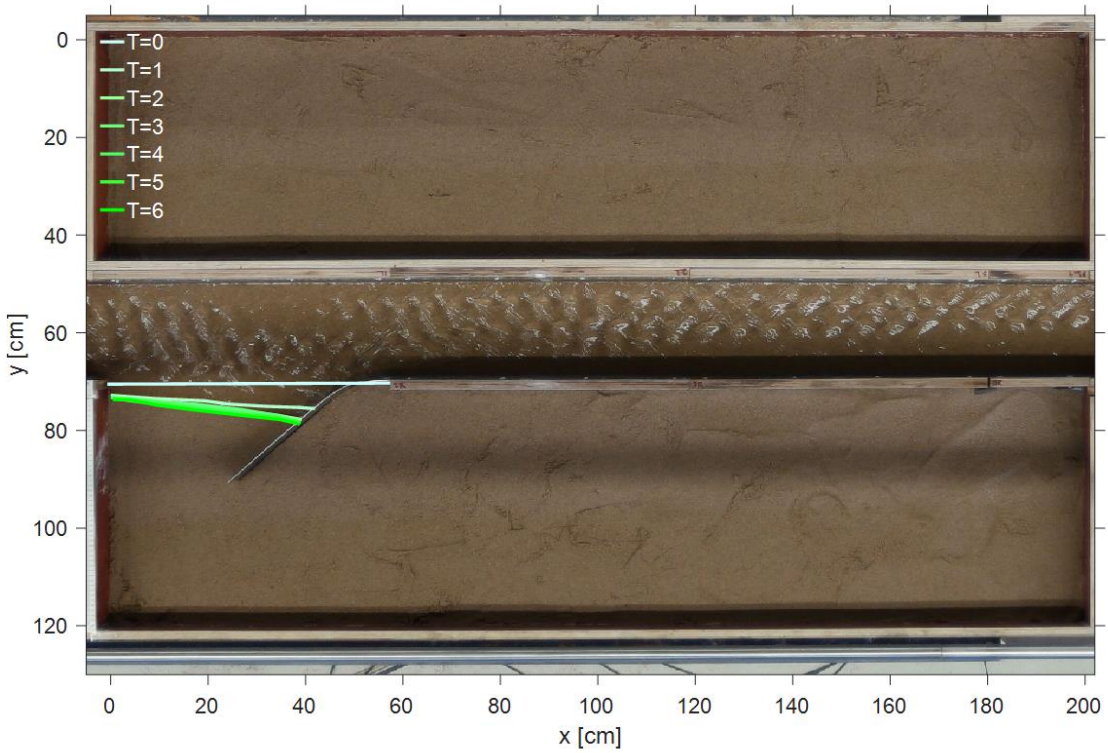


*Figure G.10 – Spatial evolution of bank erosion of test R14. Time T is in hours.*

## Appendix H. Photos of experimental setup

This appendix shows photos of elements of the experimental setup and photos of collecting data during the experiment.

### H.1. Photos of experimental setup

The photos of elements of the experimental setup are shown in this section.

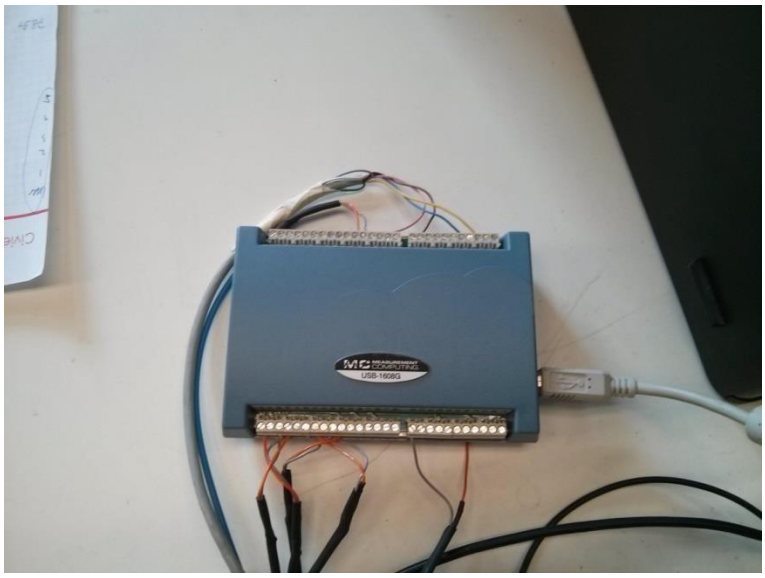

*Figure H.1 –USB data acquisition board for converting data from lasers to computer.*

*Figure H.2 –Sediment feeder*

*Figure H.3 – Light attached to wooden frame above flume*

*Figure H.4 – Removable bank protection of main channel made out of steel (1.5 mm thick) and wood (2 cm thick) with length of 60 cm and height of 23 cm.*

*Figure H.5 – Removable bank protections in position with duct tape over the seams to prevent water and sediment flowing through the gap.*

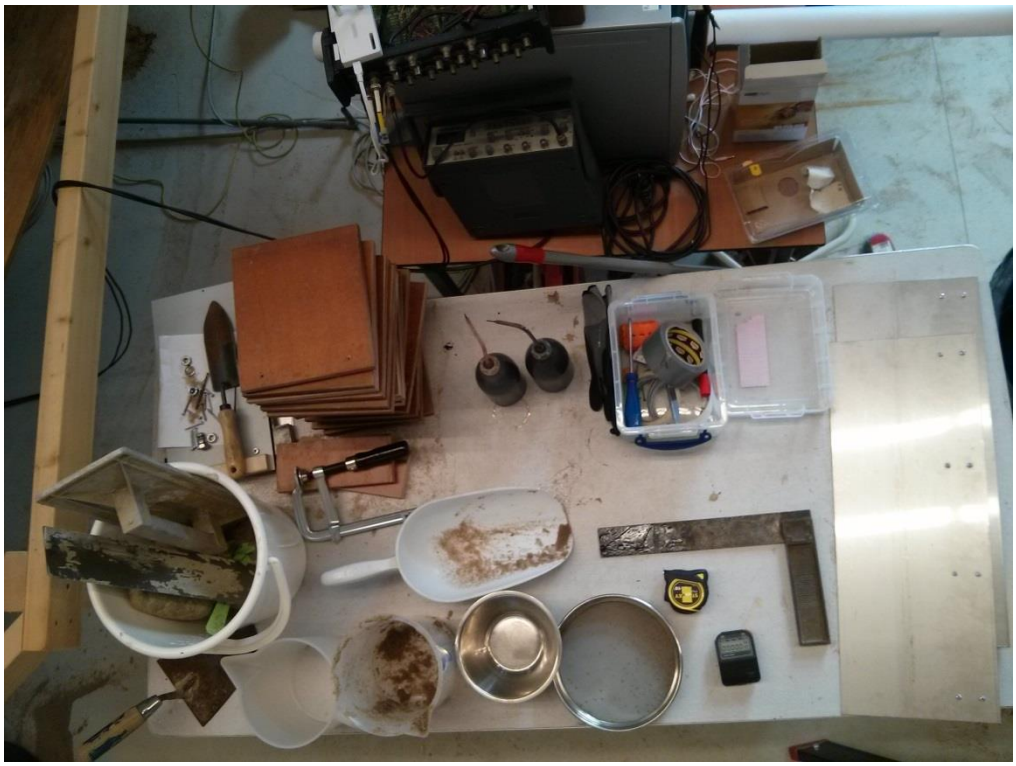

*Figure H.6 – Tools used for measuring (e.g. small sieve, tapeline, stop watch, dye) and for preparing the bed and bank profile (e.g. chip, bucket, screwdriver).*

*Figure H.7 – Bag of sediment used for the sand-bed in the main channel and filing the sediment feeder*


*Figure H.8 – Ball valve to control water supply to flume*

*Figure H.9 – Sieve at the downstream end of the flume supported by water basin*


*Figure H.10 – Water basin at downstream end of the flume. Green pipe is for water supply from the ball valve. Water that is sucked to the discharge pump flows through the yellow pipe. Water flowing out of the discharge pump goes through the brown pipe and lies in the water basin to keep any leakage of the connection to a longer green pipe (right in figure), that reaches up to the upstream end of the flume, inside the basin. The grey pipe (right in figure) attached to the water basin is used to drain water that exceeds a certain water level to prevent the basin from flooding and to keep the*

*water level in the basin at a constant height. The red pump is not in use, since the minimum capacity is too large.*

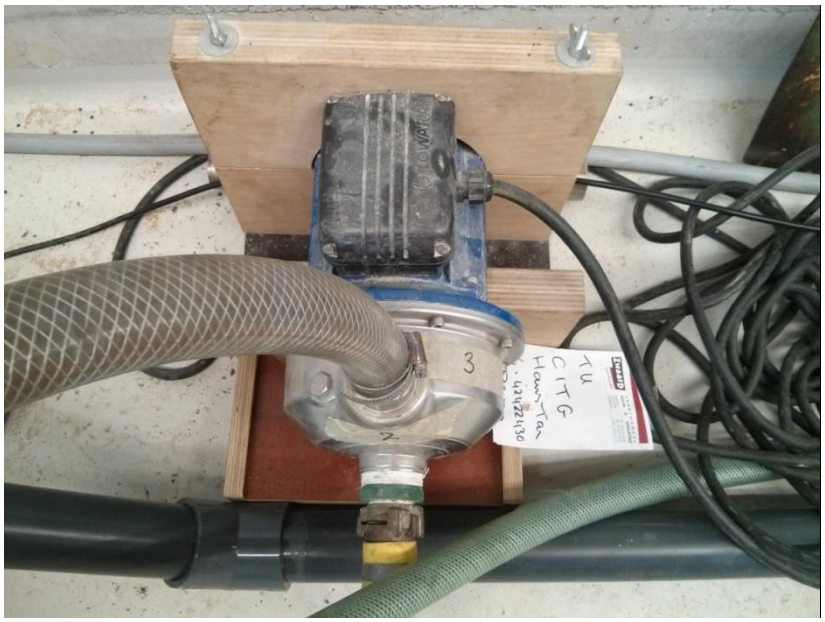

*Figure H.11 – Discharge pump with a maximum capacity of about 2 L/s*


*Figure H.12 –Frequency controller of the discharge pump.*

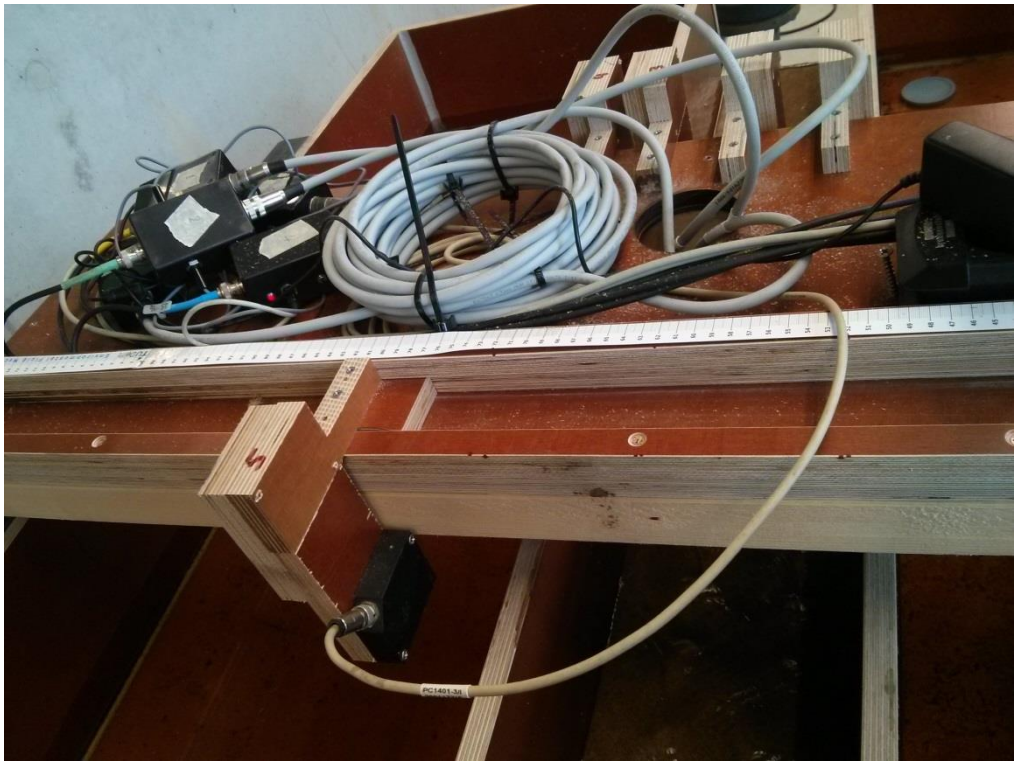

*Figure H.13 – Laser installed on platform that can be moved in transversal direction.*

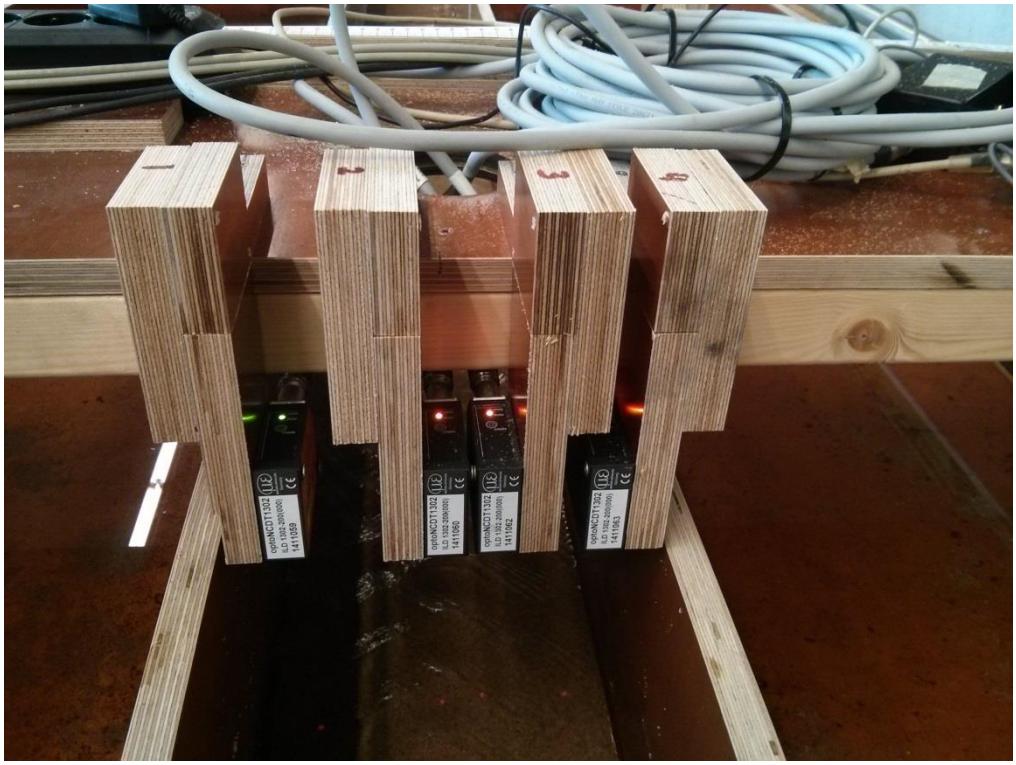

*Figure H.14 – Four lasers fixed on platform. Laser number 1, 3 and 4 measure the bed profile in longitudinal direction. Laser number 3 is not in use.*

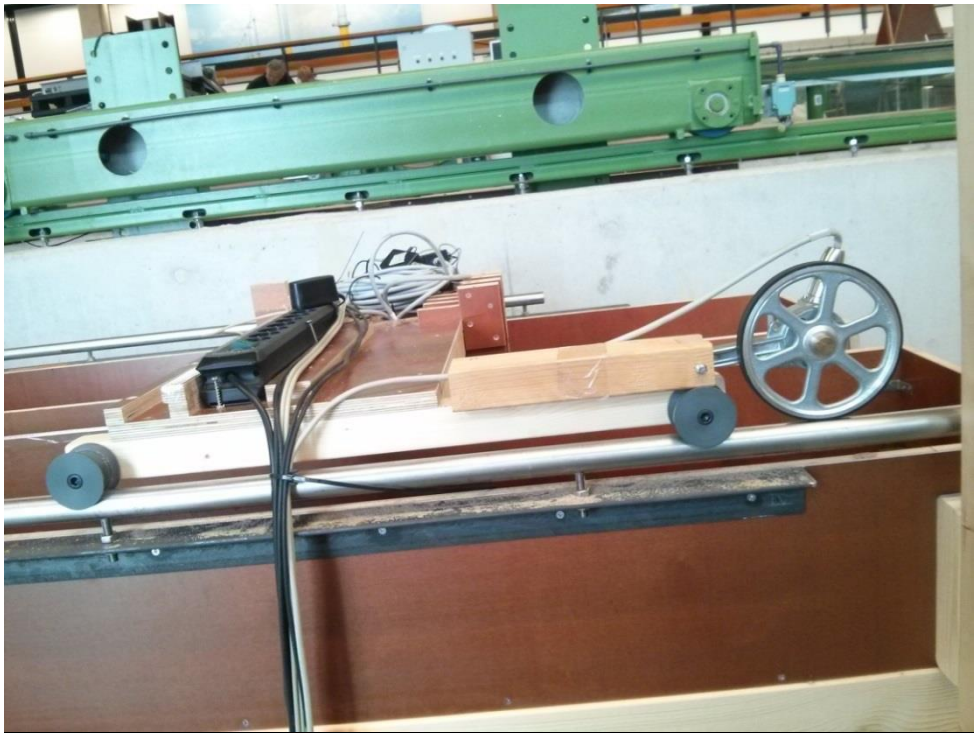

*Figure H.15 – Platform to which lasers are attached drives over rails of steel. Large wheel (right in figure) gives 5000 pulses per rotation and is connected to laser, such that with every pulse the lasers measure the bed profile.*

*Figure H.16 – Area where the water flows into the flume and fluctuations in the water level are damped.*

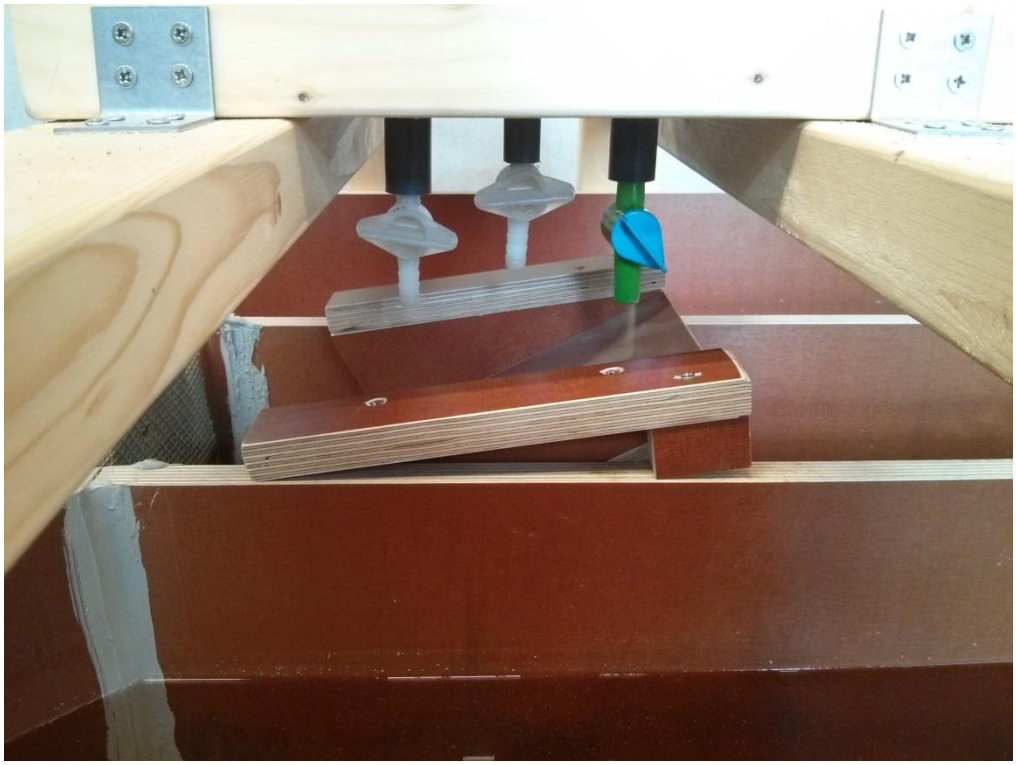

*Figure H.17 –Three taps at the bottom of the sediment feeder. Only the green tap is used. The other taps function as backup in case the green tap is clogged and cannot be emptied.*

*Figure H.18 – Ten steel grids attached to each other with a distance of 0.5 cm in between them to damp fluctuations in the water level from the area where the water flows into the flume.*

## H.2. Photos of data collection in experiment

In this appendix, photos are shown of the data collections during the experiments.

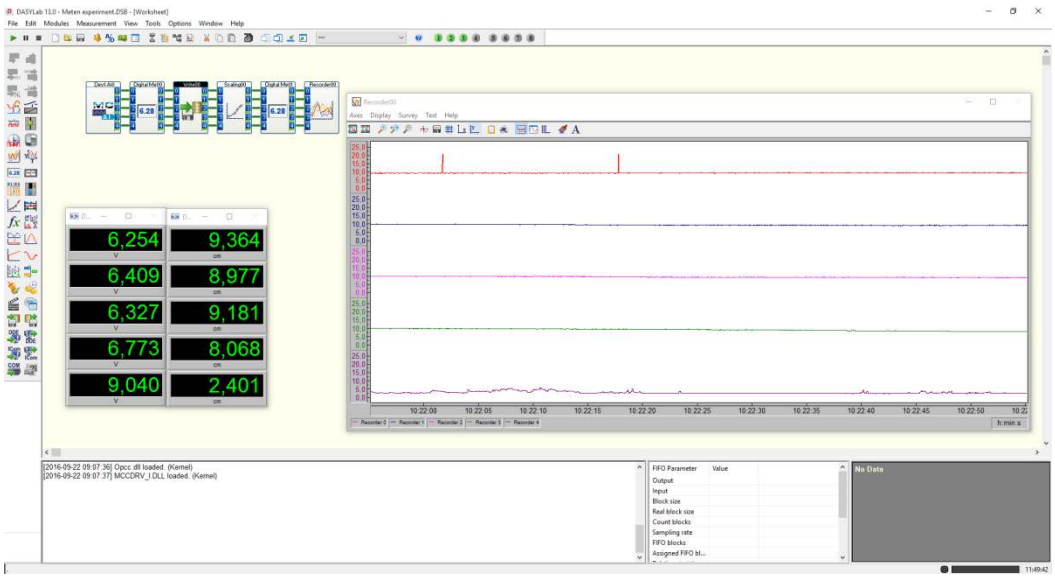


*Figure H.19 – Example of DASYLab 13.0 for data acquisition, graphics, control and analysis during an experiment. Each line in the graph represents a different laser in which on the vertical axis the bed elevation is shown and on the horizontal axis the distance in longitudinal direction. In the table each row represents a different laser. The left column shows the voltages and the right column the bed elevation in centimetres.*

*Figure H.20 - Sediment from feeder falls in small bowl*

*Figure H.21 –Sediment flowing out of the flume collected in a small sieve*

*Figure H.22 – Measuring erosion rate with tapeline*

*Figure H.23 – Dye in flask that is added to the water flowing in the main channel*